DOKUZ EYLÜL UNIVERSITY
GRADUATE SCHOOL OF NATURAL AND APPLIED SCIENCES

INVESTIGATION OF EXCESS PORE WATER PRESSURE GENERATION MECHANISM DUE SOIL-PILE INTERACTION UNDER INERTIAL LOADS

by
Hande YUMUK

October, 2022
İZMİR

INVESTIGATION OF EXCESS PORE WATER PRESSURE GENERATION MECHANISM DUE SOIL-PILE INTERACTION UNDER INERTIAL LOADS

A Thesis Submitted to the
Graduate School of Natural and Applied Sciences of Dokuz Eylül University
In Partial Fulfillment of the Requirements for the Degree of Master of Science
in Civil Engineering, Geotechnical Engineering Program

by
Hande YUMUK

October, 2022
İZMİR

M.Sc THESIS EXAMINATION RESULT FORM

We have read the thesis entitled **"INVESTIGATION OF EXCESS PORE WATER PRESSURE GENERATION MECHANISM DUE SOIL-PILE INTERACTION UNDER INERTIAL LOADS"** completed by **HANDE YUMUK** under supervision of **PROF. DR. GÜRKAN ÖZDEN** and we certify that in our opinion it is fully adequate, in scope and in quality, as a thesis for the degree of Master of Science.

Prof. Dr. Gürkan ÖZDEN

Supervisor

Assoc. Prof. Dr. Okan ÖNAL

(Jury Member)

Asst. Prof. Dr. Devrim ERDOĞAN

(Jury Member)

Prof. Dr. Okan FISTIKOĞLU

Director

Graduate School of Natural and Applied Sciences

ACKNOWLEDGMENTS

First and foremost, I want to express my profound appreciation and gratitude to my lecturer, Prof. Dr. Gürkan Özden. From the beginning till the end of my thesis study, his endless support, invaluable instruction, critical advice, gentle personality, and inspiration were indispensable. He kindled the torch of my thesis and guided me from beginning to end. I will be eternally grateful to him.

I would thank Dr. Özgür Bozdağ for his inspiration and advice during this thesis. His perceptive recommendations helped construct the road to the thesis.

I would like to express my deepest gratitude to my fiancee, Janberk Ceylan, for his support throughout this thesis. He has always been my role model with his hard work and determination. His visionary and disciplined personality has always made me a more hardworking person. I will always respect him as I will always love him.

I would like to thank my friends for their endless emotional support over the years. They were always there for me. I am forever grateful to them.

And finally, I would like to thank my family, my mother, Dilekhan Yumuk, my father Ali Yumuk, and my sister Dilay Yumuk. They have always supported me and believed in me. I wouldn't be the person I am today without their encouragement.

Hande YUMUK

INVESTIGATION OF EXCESS PORE WATER PRESSURE GENERATION MECHANISM DUE SOIL-PILE INTERACTION UNDER INERTIAL LOADS

ABSTRACT

The behavior of piles in submerged and liquefiable sandy soils under earthquake loads has attracted the attention of researchers since the 1980s. This study investigated the behavior of soil surrounding piles in such soils. In the study, the lateral response of the pile due to inertial and kinematic interaction was considered, and it was assumed that the soil was in passive terms during the earthquake. As a liquefiable soil layer, sandy soil whose liquefaction model parameters were determined at the California Wildlife Test Site was considered. In the inertial interaction analyses made under different horizontal loads and frequencies, it was determined that the stresses transferred from the pile to the soil could force the soil up to liquefaction by causing excess pore water pressure to change in the soil and its reflection on the horizontal load-displacement curves (p-y curves) is discussed. The analysis results revealed that the loading frequency had some effect on soil behavior, and the development of excess pore water pressure significantly affected the horizontal load-displacement curves. In kinematic analyses, the presence of inertial loading has been found to be less influential on excess pore pressure generation with depth than in the free-field case. It is detected that the influence of the pile on excess pore water pressure quickly diminishes with the horizontal distance for a particular depth. It is shown that Loading intensity affects the amount of induced pore pressures. The gap between the pile and free field displacements gradually developed as dynamic loading progresses.

Keywords: Liquefiable soils, laterally loaded pile, excess pore pressure, soil-pile interaction.

ATALET YÜKLERI ALTINDA ZEMIN-KAZIK ETKILEŞIMINE BAĞLI OLARAK AŞIRI BOŞLUK SUYU BASINCI GELIŞIMI MEKANIZMASININ İNCELENMESİ

ÖZ

Suya doygun ve sıvılaşabilen kumlu zeminlerde kazıkların deprem yükleri altındaki davranışı 1980'lerden beri araştırmacıların ilgisini çekmiştir. Bu çalışma, bu tür zeminlerde zemini çevreleyen kazıkların davranışını araştırmıştır. Çalışmada, kazıkların atalet ve kinematik etkileşime bağlı yanal tepkisi dikkate alınmış ve deprem sırasında zeminin pasif durumda olduğu varsayılmıştır. Sıvılaşabilir bir zemin tabakası olarak, California Yaban Hayatı Test Sahasında sıvılaşma modeli parametreleri belirlenen kumlu zemin dikkate alınmıştır. Farklı yatay yükler ve frekanslar altında yapılan atalet etkileşimi analizlerinde, kazıktan zemine aktarılan gerilmelerin zeminde fazla boşluk suyu basıncının değişmesine neden olarak zemini sıvılaşmaya ve bunun yataya yansımasına neden olarak zemini sıvılaşmaya zorlayabileceği belirlenmiştir. yük-deplasman eğrileri (p-y eğrileri) tartışılmıştır. Analiz sonuçları, yükleme frekansının zemin davranışı üzerinde bir miktar etkisi olduğunu ve aşırı boşluk suyu basıncının gelişiminin yatay yük-yer değiştirme eğrilerini önemli ölçüde etkilediğini ortaya koymuştur. Kinematik analizlerde, atalet yüklemesinin varlığının, derinlikle aşırı boşluk basıncı oluşumu üzerinde serbest alan durumuna göre daha az etkili olduğu bulunmuştur. Belirli bir derinlik için kazıkların fazla boşluk suyu basıncı üzerindeki etkisinin yatay mesafe ile hızla azaldığı tespit edilmiştir. Yükleme yoğunluğunun indüklenen boşluk basıncı miktarını etkilediği gösterilmiştir. Dinamik yükleme ilerledikçe kazık ve serbest alan yer değiştirmeleri arasındaki boşluk kademeli olarak gelişmiştir.

Anahtar kelimeler: Sıvılaşabilen zeminler, yatay yüklü kazık, boşluk suyu basıncı, zemin-kazık etkileşimi.

CONTENTS

Page

LIST OF FIGURES

LIST OF TABLES

Page

CHAPTER ONE

INTRODUCTION

1.1 Motivation of the Thesis

Earthquakes are considered the most destructive natural disasters because they are unpreventable and cause significant threats to human life by destroying the structures in the affected areas quickly, often to the level of destruction. Geological effects of earthquakes are evaluated in two groups as processor and subaltern effects. The initial effects are the formation of faults in the crust of earth and the resulting tectonic uplift and collapse. Secondary effects are ground behavior that develops at very shallow depths due to vibrations caused by earthquakes. These can be classified as liquefaction, compaction of soil particles, and different types of soil failure due to liquefaction or softening of cohesive soils. Repetitive stresses caused by earthquakes lead to unusual soil behavior in loose soils at shallow depths. After the 1998 Adana/Ceyhan and 1999 Kocaeli earthquakes, which occurred in our country and where soil liquefaction and related effects were widely observed, the liquefaction problem was examined more closely. This type of soil behavior, which develops due to characteristic properties of loose soils, groundwater level depth, and the magnitude of the ground acceleration caused by the earthquake, plays an essential role in structural damage in addition to the failure of foundation elements such as piles.

Liquefaction and related soil insensitivity, which is among the soil behavior caused by dynamic loads, play an active role in structural damages. The soil, which loses its bearing capacity by decreasing its strength due to liquefaction, cannot carry the structures on it, causing settlements, tilting or overturning the structures, and various damages to the buried infrastructure elements. In addition, due to lateral spreading and flow sliding behavior developed as a consequence of liquefaction phenomenon.

During an earthquake, in saturated cohesionless soils under dynamic loads, the effective stress decreases with the increase of pore water pressure and the soil act as a viscous liquid, and liquefaction occurs. Several methods are used to strengthen or by-pass such problematic soils. The most commonly used one is the pile foundation application.

Since earthquake records were being kept, damaged piles in submerged liquefied sand soils have been observed (Fukuoka, 1966; Kuribayashi and Tatsuoka, 1975; Youd and Hoose, 1978; Hamada and O'Rourke, 1992; O'Rourke and Hamada, 1992). However, research following the 1964 Niigata Earthquake has shown that this type of damage was encountered more frequently. In the 1964 Niigata earthquake, many structures were damaged due to liquefaction events, and it was revealed in the investigations that continued for more than twenty years after the earthquake. The infirmity of piles due to liquefaction was also confirmed in Kobe, where a detailed investigation of pile foundations was conducted following the 1995 Great Hanshin Earthquake (Ishihara, 1997; Nanjyo et al., 1998; Tokimatsu and Asaka, 1998. Recent reviews of pile damage case histories in lateral spreading areas (Yasuda and Berrill, 2002) show that this is a remarkable and big problem in earthquake engineering and that durable structural design should be a priority consideration in earthquakes.

In this thesis, soil behavior which placed surrounding the laterally loaded pile and the development of excess pore water mechanism in liquefiable submerged cohesionless soils were tried to be better understood by means of a series of numerical analyses where three dimensional finite element technique was employed. Studies on the liquefied soil model were completed with the analyses made for different frequencies and load amplitudes including inertial and kinematic loading conditions.

1.2 Statement of the Problem

In this thesis study, excess pore pressure field around a laterally deforming pile was examined. Although emphasis was given to inertial loading conditions, influence of kinematic loading was also studied. Several different loading amplitudes and frequencies were taken into consideration so that accordingly developing excess pore water pressure influence on soil resistance is better understood. One may note that there are already developed load-deformation relationships for piles in liquefied soils. However, effects of inertial loads on soil resistance still need further study since soils may undergo liquefaction provided that certain boundary conditions are met to cause undrained conditions. Besides, presence of piles alters soil response including excess pore water pressure development as compared with free-field conditions. The goal of this thesis is to gain more insight on understanding excess pore water pressure field around laterally displacing single pile by considering nonlinear undrained soil behavior.

1.3 Scope of the Thesis

The thesis commences with the first chapter, which describes the motivation and purpose of the thesis. The second section includes a review of the literature on liquefaction, liquefiable soil properties, liquefaction potential determination, inertial and kinematic soil-pile interaction in liquefiable soils, and current analysis methods. The numerical modeling is covered in the third section. The soil structure model employed, the numerical calculation model developed, and the approach underlying data collection and the generation of usable results are all explained. The results of the analyses and discussions about the achieved results are presented in the fourth section. Finally, in the fifth chapter, the observations and future research recommendations are presented.

CHAPTER TWO

SOIL-PILE INTERACTION IN LIQUEFIABLE SOILS

2.1 Liquefaction

The term liquefaction was coined in 1953 (Mogami & Kubo). Disasters that can be caused by liquefaction have been the subject of engineering research due to the Niigata and Good Friday earthquakes with magnitudes of 9.2 and 7.5 that occurred consecutively in 1964. Although the cause of earthquakes was revealed later, it has been seen a lot in examples such as slopes, bridges, buildings, and substructures caused by liquefaction. The subject of liquefaction has been studied by many researchers in different parts of the world in the last 30 years after these earthquakes (Kramer, 1996).

The term liquefaction is used where grain-to-grain contacts are lost as a result of excess pore water pressure generation leading to a permanent reduction in effective stress causing large plastic displacements on the order of several meters. This kind of deformation mechanism generally takes place in non-cohesive loose soils under earthquake excitation although liquefaction under static loads may also be possible for certain drainage conditions. Cyclic mobility, on the other hand, is temporary loss of effective stress, which is recovered in a short period of time with dilation taking place during dynamic loading in medium dense to dense non-cohesive soils. Albeit not producing as large permanent displacements as it is for full liquefaction case, cyclic mobility may also have severe consequences on pile foundations.

During an earthquake, seismic waves, especially shear waves, propagate through water-saturated loose sandy soils, causing displacement in soil grains by creating force pairs acting in opposite directions (shear forces). Under these conditions, loose sand particles tend to reorient themselves, and during this behavior, the tension stresses which transferred contact points of the grains is transmitted to the pore water. The precipitate movements caused by earthquakes prevent sufficient time for the water between the grains to drain out, thus increasing the pore water pressure, which cannot move away from the environment. This sudden increase in pore water pressure destroys the contact forces holding the soil grains together and pulls the grains away from each other, and thus the soil loses its strength (Figure 2.1). Under these conditions, the soil behaves as a viscous liquid substance instead of a solid material. The liquefaction phenomena that develop due to this process can be divided into two main groups: flow liquefaction and cyclical mobility as mentioned in the previous paragraph.

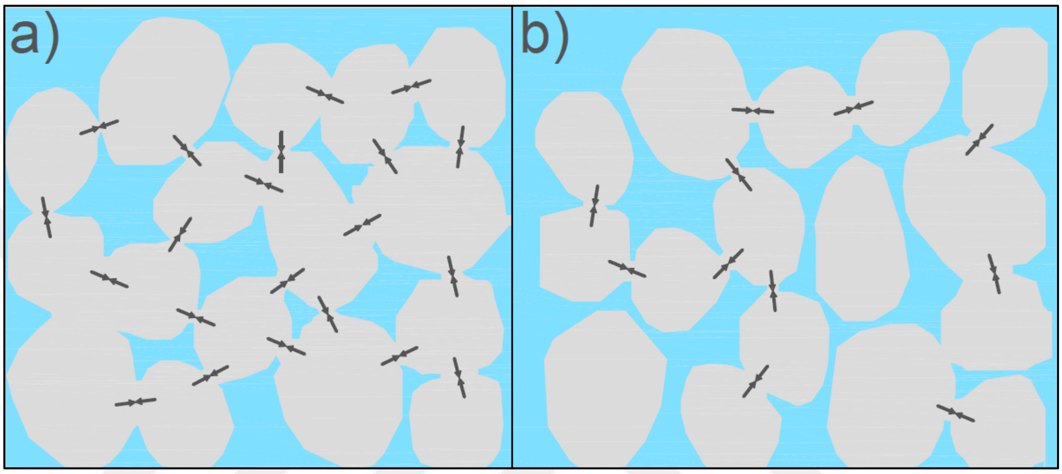

Figure 2.1 Soil grain contacts: (a) static conditions (b) earthquake loading (Özener, 2007)

Evidence of liquefaction at the surface are generally observed in terms of sand eruptions, solitary or cascading sand volcanoes, and fissures that appear as sand deposits along the neck. For example, in the 1999 Kocaeli Earthquake, the diameters of the sand cones developed in the Yalakdere Delta, east of Yalova, reached up to 50 cm. The high pore water pressure developed in soils during an earthquake tends to decrease with the movement of water towards the surface. Due to this movement, when the hydraulic slope reaches a critical value, the sand grains are transported to the surface along the cracks, fissures, and channels, and this process is called the "fast condition". The liquefied sand may reach the surface depending on the magnitude of the excess pore water pressure that develops, the thickness and density of the layer of the liquefied soil, and the thickness and permeability of the non-liquefiable soil that may be on the liquefied layer. In certain cases, liquefaction may not be observed on the surface. However, it does not mean that liquefaction does not occur. In the investigation pits dug in the soil after the earthquakes, it was observed that the liquefied sand was lined up along a dyke. It could rise to any depth below the surface.

In the 1999 Kocaeli Earthquake, in some parts of the Adapazarı region, liquefaction could not be observed on the surface. However, tilted buildings in the region may indicate that the liquefied sand could not reach the surface (Figure 2.2).

Figure 2.2 Liquefaction damage on buildings (Kocaeli Eartquake, Adapazari 1999, Photograph by Ömer Aydan)

There are examples of soil liquefaction effects in past earthquakes. These examples may be mentioned as 1920 California Calvers, 1938 Montana Fort Peck, 1948 Fukui, 1964 Niigata, 1964 Alaska, 1971 California San Fernando, 1976 Guatemala Earthquake, 1980 Mino-Owari, 1996 Ceyhan Earthquake, and 1999 Marmara Earthquake. Examples of buildings and bridges damaged in the 1964 Niigata Earthquake, where the harmful effects of liquefaction were seen, are shown in Figure 2.3 and Figure 2.4.

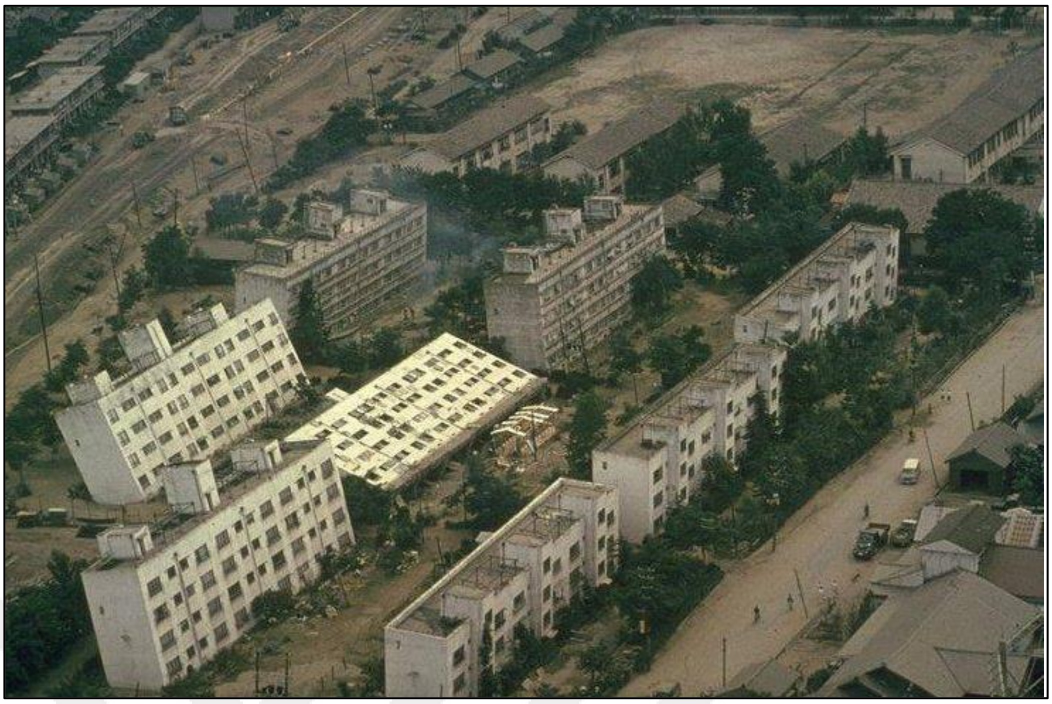

Figure 2.3 1964 Niigata Earthquake; Kawagishi-cho building (Jefferies and Been, 2016: 12)

Figure 2.4 1964 Niigata Earthquake; Showa Bridge (Kramer and Elgamal, 2001)

For assessments of liquefaction risk, the susceptibility of soil to liquefaction must be determined. There are three main headings in this context. The first is geological criteria. Liquefaction usually develops in environments where the groundwater level is shallow, where young and loose sediments, mainly sand and silt grain size material, are deposited. Holocene aged (less than 10000 years) delta, river, flood plain, terrace, coastal are highly sensitive to liquefaction because the dominant sediments in these environments were deposited in a uniform and loose state. It has been observed that the Pleistocene aged (0.1-1.8 million years) sediments have rarely liquefied in the earthquakes that took place in the last century. The liquefaction observed during earthquakes in our country is observed in Holocene aged very young alluvial sedimentary environments also supports this phenomenon. In addition, fine-grained and not well-compressed fills constructed in road and dam works, and delicate mine waste storage areas are also sensitive materials to liquefaction. Liquefaction occurs commonly in areas where the groundwater table is at a depth of up to 10 m from the surface. It is known that a limited amount of liquefaction occurs in places deeper than 20 m.

The second main factor is the criteria related to the composition of the soil. Uniformly graded soils have a much higher risk of liquefaction than well-graded soils with approximately the same size of grains. Excessive pore water pressure formation in well-graded soil is prevented during an earthquake. In addition to sands, liquefaction behaviour is observed in pebbles and non-plastic silts. Although clays were defined as insensitive to liquefaction until the early 2000s, it was determined that in the 1995 Kobe earthquake in Japan 1995, it was observed on the surface by mixing with the sand layer in the clays on the coast. The shape of the grains forming the soil also affects liquefaction susceptibility. Soils with rounded grains tend to compress more easily than soils containing angular grains, so the liquefaction potential of such soils is high.

Finally, the third element is the stress conditions and soil density criteria. Even if the criteria mentioned earlier and stipulated conditions are met, soils may not be susceptible to liquefaction. Because liquefaction sensitivity also depends on the tension conditions of the ground and the firmness of the ground. In soil that has been under the influence of long-term stress conditions, intergranular interlocking may deteriorate. Soils with a relative density below 47% are more prone to liquefaction as they will be in a looser position.

As a result, the main factors affecting liquefaction under earthquake loads are as follows: The physical properties of the soil, the drainage properties of the soil, the void ratio of the soil, its relative density, the loads that the soil has been exposed to in the past, the magnitude of the earthquake, the loading time and frequency of the earthquake. Whether a soil carries the risk of liquefaction or not can be understood by evaluating many factors together. These factors are grouped under two subheadings: the internal structure of the soil and the characteristics of the external factor causing liquefaction.

2.1.2 Liquefaction Mechanism

Various definitions for liquefaction have been made by Casagrande (1975) and Seed (1979). Apart from these, the definition made by the Committee on Soil Dynamics of the Geotechnical Engineering Division of the American Society of Civil Engineers in 1978 is: *"Liquefaction: The act or process of transforming any substance into a liquid. In cohesionless soil, the transformation is from a solid-state to a liquefied state as a consequence of increased pore pressure and reduced effective stress."*

In cohesionless soils, the shear resistance is directly proportional to the existing pressure and the coefficient of friction between soil particles, which is usually given relationship in Equation 2.1.

$$\tau = \sigma' tan\phi' = (\sigma - u) tan\phi' \tag{2.1}$$

Where τ_s is shear resistance: σ' and σ are effective and total normal pressures respectively; u is pore pressure; ϕ is angle of internal friction in terms of effective stress. The general stress condition in a saturated soil can be expressed in Equation 2.2 where σ_{ij} and σ'_{ij} are total and effective stress tensors respectively; δ_{ij} is Kronecker delta which represents pore water pressure change.

$$\sigma_{ij} = \sigma'_{ij} + \delta_{ij} u \tag{2.2}$$

When the soil becomes liquefied, the stress state changes as the effective vertical stress drops to zero and the pore water pressure rises to the effective stress level.

$$\left.\begin{aligned} q &= \frac{1}{2}(\sigma_1 - \sigma_3) = \frac{1}{2}(\sigma'_1 - \sigma'_3) \\ p &= \tfrac{1}{2}(\sigma_1 + \sigma_3) = p' + u \\ p' &= \frac{1}{2}(\sigma'_1 + \sigma'_3) \end{aligned}\right\} \tag{2.3}$$

In Equation 2.3 p and q can be defined dependent on maximum and minimum total-effective principal stresses. In liquefied soils, q becomes zero, p' becomes zero, and p becomes equal to pore water pressure.

2.1.2 Characteristics of Liquefiable Soils

Liquefaction event generally occurs in sands and non-plastic silts, and the probability of liquefaction in plate-shaped silts and clays with plastic properties is low. In addition, stiffness and strength loss may occur in sensitive clays with repeated shear stresses, and an effect similar to liquefaction occurs. Measures of liquefaction potential for soils with fine content were proposed by Wang (1979), which is known as the Chinese criterion. According to Wang (1979), liquefaction can be seen in soils where the percentage of clay in the ground is less than 20%, the liquid limit (LL) is between 21-35, the plastic limit (PL) is between 4-14 and the water content of the soil is greater than 0.9 times the liquid limit. Besides the Chinese criterion, some researchers have found new approaches to the liquefaction of soils. Some of them are as follows:

Andrews and Martin (2000) explained the soil liquefaction potential with soil indices; They suggested that liquefaction may occur when the 0.002 mm grains of the soil are less than 10%, and the LL value is less than 32. This situation is shown in Figure 2.5.

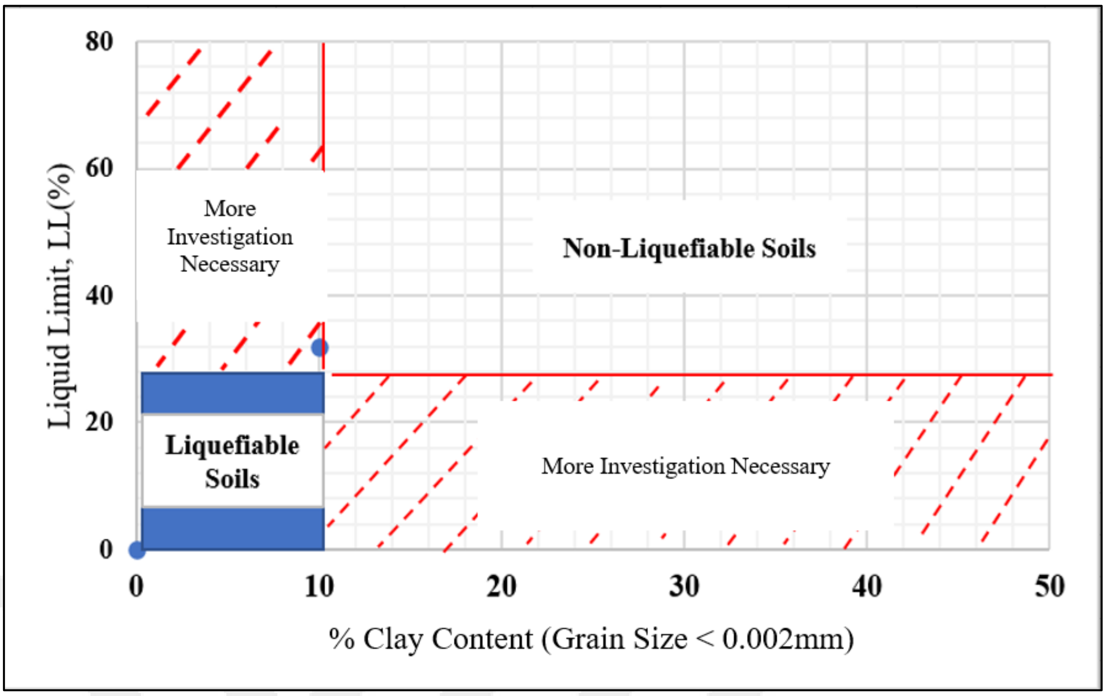

Figure 2.5 Suggested soil liquefaction susceptibility criteria (Andrews and Martin, 2000)

Seed et al. (2003) stated that the liquefaction of soils depends on soil index parameters, as shown in Figure 2.6:

i. If the soil index values are in the range of PI<12, LL<37, w/LL>0.8, the soil in zone A is liquefiable,

ii. if the soil index values are in the range of 12 <PI<20, 37 <LL<47, w/LL>0.85, the probability of liquefaction of the soil in zone B is moderate, but other tests should be performed,

iii. The ground outside these regions are defined as the C region, and it is stated that there is no risk of liquefaction.

In the studies of Chaudhary, Jawaid, and Zafar (2015), They stated that the method proposed by Seed et al. (2003) is more reliable than the Modified Chinese and Andrews-Martin (2000) criteria.

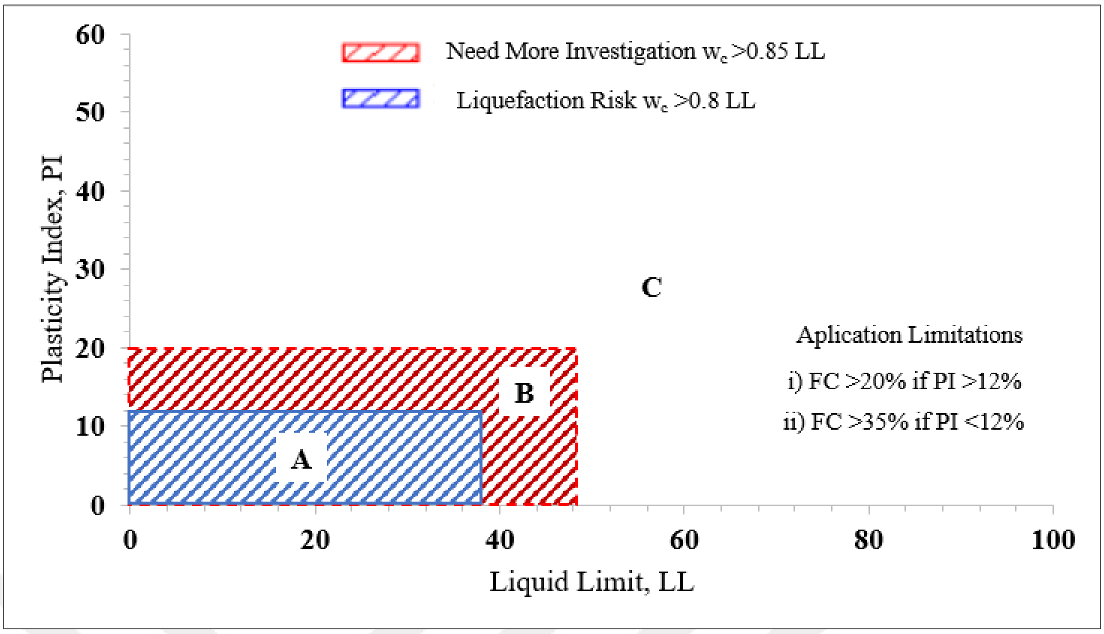

Figure 2.6 Recommended liquefaction limits values for fine-grained soils (Seed et al., 2003)

Boulanger and Idriss (2004, 2006) mentioned a subtle transition from sandy soil behavior to clayey soil behavior at Atterberg limits. They suggested that fine-grained soils exhibit clayey soil behavior when PI≥7 (PI≥5 for CL-ML soils). In addition, they mentioned that more laboratory tests should be done for soils in this range since it cannot be predicted exactly how fine-grained soils would behave if they had a plasticity index value between 3≤PI≤6. On the other hand, Boulanger and Idriss underlined that knowing the w/LL value would not give precise information about the sand or clayey soil behavior. Boulanger and Idriss schematically showed the cyclic shear strength ratio (CRR) used to define the liquefaction resistance corresponding to the PI value (Figure 2.7).

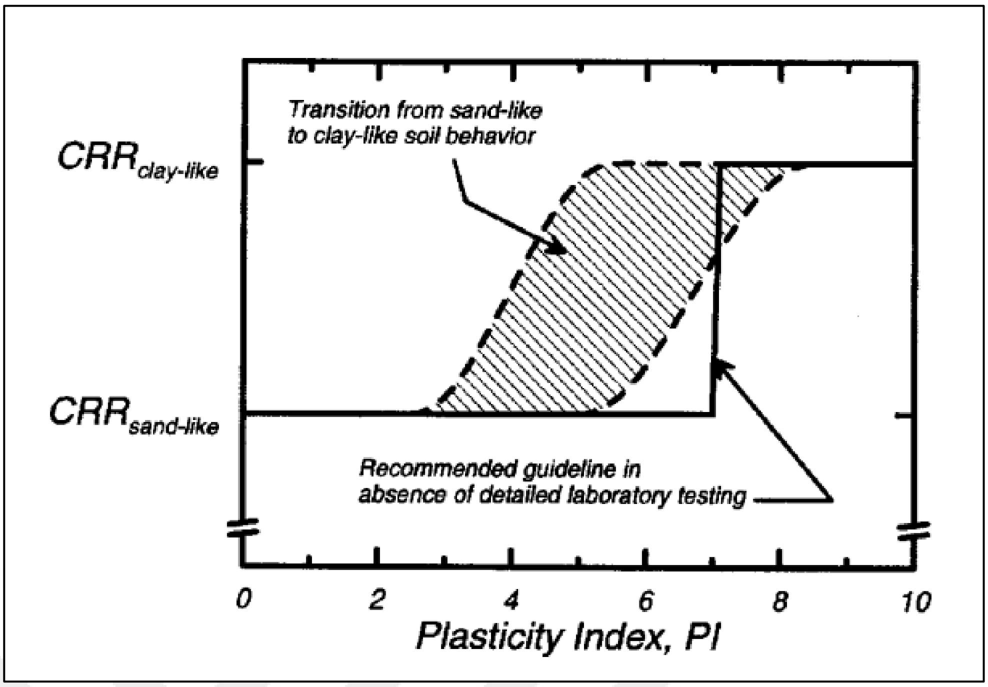

Figure 2.7 Recommended limit values for sand-like and clay-like soil behavior due to plasticity index (Bounlanger & Idriss, 2006)

2.1.3 Determination of Liquefaction Potential

Liquefaction potential may be determined either using field, laboratory, and case histories of liquefied soil sites in large-scale earthquakes, laboratory cyclic tests conducted on undisturbed soil samples or numerical analyses methods. Recovery or undisturbed liquefiable soil samples, however, is quite difficult and expensive making the first approach more feasible.

2.1.3.1 NCEER Method

According to the National Earthquake Engineering Research Center, assessing the liquefaction resistance of soils requires determining the seismic demand (CSR) on a soil layer and the soil's liquefaction resisting capacity (CRR). In 1971, Seed and Idriss formulated Equation 2.4 to determine the cyclic resistance ratio.

$$\mathrm{CSR} = (\tau_{\mathrm{ave}}/\sigma'_{\mathrm{v0}}) = 0.65(\mathrm{a_{max}}/\mathrm{g})(\sigma_{\mathrm{v0}}/\sigma'_{\mathrm{v0}})\mathrm{r_d} \qquad (2.4)$$

Where a_{max} = peak horizontal acceleration at the ground surface; g = acceleration of gravity; σ_{vo} and σ'_{vo} are total and effective vertical overburden stresses, respectively; and r_d = stress reduction coefficient. The latter coefficient accounts for flexibility of the soil profile.

In 1986, Liao and Whitman suggested some equations (Equation 2.5a, 2.5b) for estimating average values of r_d. Where z = depth below ground surface in meters.

$$r_d = 1.0 - 0.00765z \text{ for } z \leq 9.15 \text{ m} \quad (2.5a)$$

$$r_d = 1.174 - 0.0267z \text{ for } 9.15 \text{ m} < z \leq 23 \text{ m} \quad (2.5b)$$

There is considerable variability in the flexibility, and thus r_d at field sites, that r_d calculated from Equation 5 is the mean of a wide range of possible r_d, and that the range of r_d increases with depth (Golesorkhi 1989).

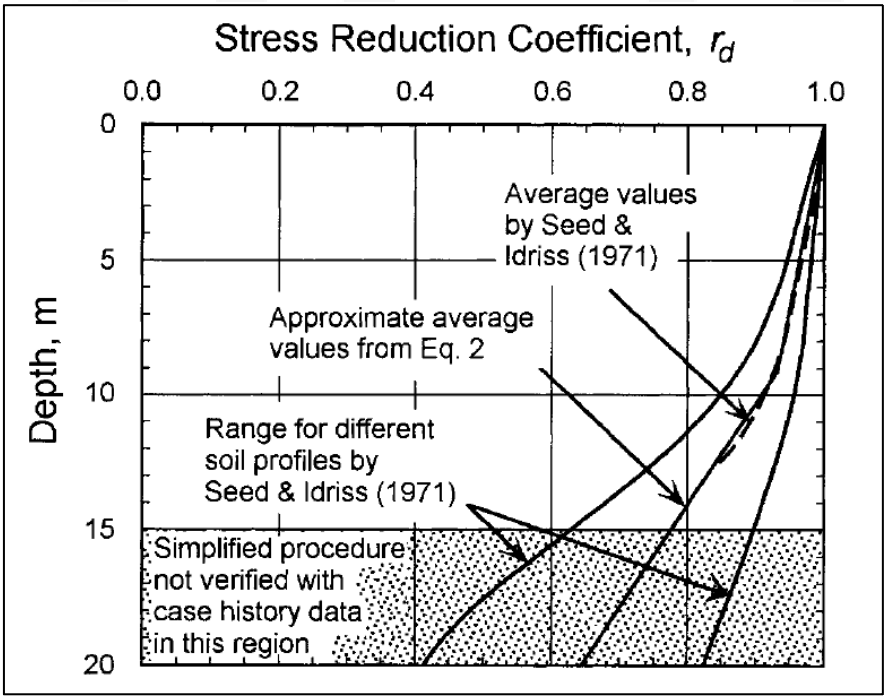

Figure 2.8 Stress reduction coefficient determination (Seed and Idriss, 1971)

In 1996, T.F. Blake estimated the mean curve plotted in Figure 2.8 for ease of computation by Equation 2.6.

$$r_d = (1.000 - 0.4113z^{0.5} + 0.04052z + 0.001753z^{1.5})/(1.000 - 0.4177z^{0.5} + 0.05729z - 0.006205z^{1.5} + 0.001210z^2) \tag{2.6}$$

Undisturbed soil samples in the laboratory can be used to evaluate the Cyclic Resistance Ratio. In situ stress conditions generally cannot be re-established in the laboratory, and sampling of granular soils with traditional methods does not yield meaningful results. In addition to these difficulties, several test methods are applied in the field to serve the purpose. Generally, two of them should be used in the same field, and the results should be compared and evaluated for engineering interpretation.

Field test methods commonly applied for assessing liquefaction resistance are summarized in Table 2.1. Methods can be preferred in terms of usage areas, advantages, and disadvantages. It is recommended to apply at least two of them for the same field in order to be able to verify. Frequently used tests are Standard Penetration Test, Cone Penetration Test (CPT), Shear Wave Velocity measurements (Vs), and Becker Penetration Test methods. The CPT test, which is applied in an exemplary way, provides a safe information flow as it is a test method with minimum discontinuity. SPT is a more standard test and allows taking samples of degraded soils from which characteristic features can be determined. Vs measurements provide valuable information about soil behavior where other test methods cannot be applied. BPT is a field test on granular soils. Liquefaction resistance curves based on SPT, CPT, Vs, and BPT data are given in Figures 2.9a~9d (Seed et al. (1985), Robertson and Wride (1998), Andrus and Stokoe (2000), Harder (1997)).

Table 2.1 Field test for liquefaction evaluation (NCEER,2001)

Feature	Test Type			
	SPT	CPT	V_s	BPT
Past measurements at liquefaction sites	Abundant	Abundant	Limited	Sparse
Type of stress-strain behavior influencing test	Partially drained, large strain	Drained, large strain	Small strain	Partially drained, large strain
Quality control and repeatability	Poor to good	Very good	Good	Poor
Detection of variability of soil deposits	Good for closely spaced tests	Very good	Fair	Fair
Soil types in which test is recommended	Nongravel	Nongravel	All	Primarily gravel
Soil sample retrieved	Yes	No	No	No
Test measures index or engineering property	Index	Index	Engineering	Index

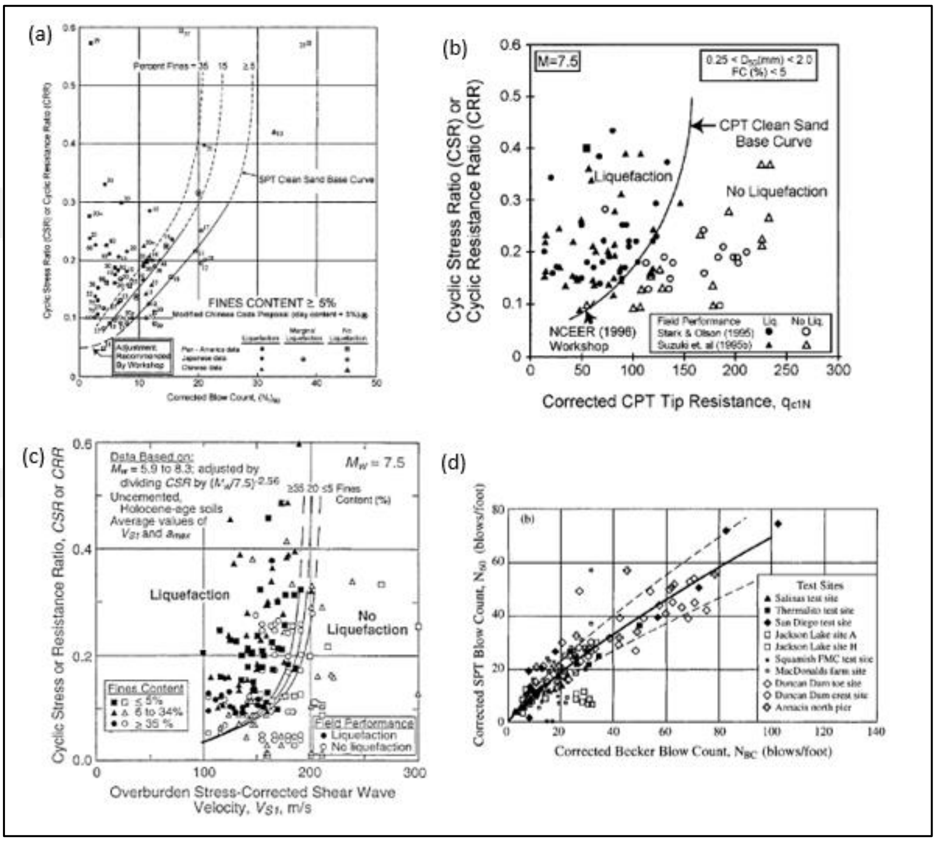

Figure 2.9 Cyclic resistance curves for liquefiable soils based on field tests data (a) SPT; (b) CPT; (c) V_s; (d) BPT

2.1.3.2 Numerical Methods

Numerical methods pertaining to liquefaction analyses are actually dynamic site response analyses approaches. They can be grouped in two broad categories: equivalent linear and nonlinear based algorithms. These approaches are briefly explained in below given sections.

2.1.3.2.1 Equivalent Linear Method. The equivalent linear model divides the earthquake motion into harmonic sine waves by means of fast Fourier transform (FFT) at first hand. The goal is to transmit the harmonics towards the ground surface using the appropriately defined transfer functions. Time dependent ground motion is then obtained at the desired depth via inverse fast Fourier transform (IFFT). The method itself is essentially linear since a constant shear modulus is utilized throughout the computation scheme and calculations are realized in the frequency domain for each harmonic (Figure 2.10). The nonlinear soil response, however, is taken into consideration in an approximate manner by performing the calculations iteratively (Schnabel et al., 1972). In this respect, the hysteresis loop is approximated using an average shear modulus in the calculation (Figure 2.11) (Seed et al., 1984). The calculation is repeated until the shear modulus converges on the modulus reduction curve points (Figure 2.12). This iterative approach can converge to equivalent linear material parameters ignoring the stress-strain history in previous steps. Because the model is linear, it cannot be used to calculate permanent displacements. The method is very efficient when the earthquake magnitude is small producing negligible displacements. The method cannot predict pore pressures since such a generation-dissipation model is not available and the effective stress is kept constant throughout the analysis scheme.

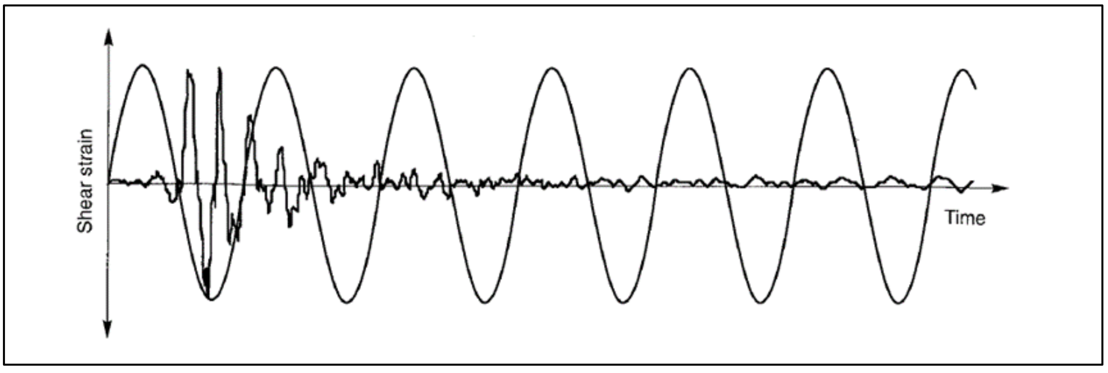

Figure 2.10 Harmonic sine waves representing earthquake waves

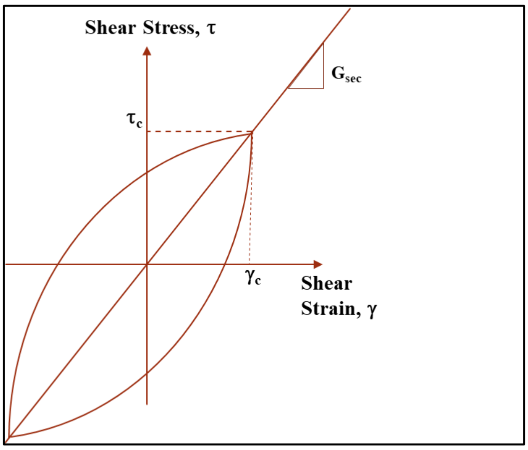

Figure 2.11 Average shear modulus, G_{sec}

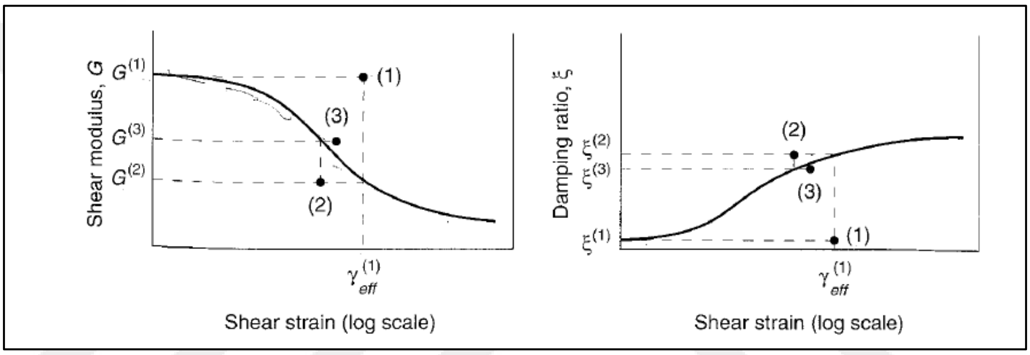

Figure 2.12 Iteration procedure for estimation of shear modulus and damping ratio in equivalent linear analysis (Kramer, 1996)

2.1.3.2.2 Nonlinear Methods. Nonlinear models' responses are determined by direct numerical integration of the equation of motion in small time steps (e.g., explicit finite difference technique) (Ramberg & Osgood, 1943). Using various constitutive soil models, nonlinear models can account for the nonlinear behavior of soil. The constitutive models used in various nonlinear model programs have various characteristics, such as using updated stress-strain relationships, pore-pressure generation, and cyclic modulus degradation. These features are not present in the corresponding linear model, allowing for more precise estimations of soil dynamics. Unlike similar linear models, nonlinear models can account for the build-up of porewater pressure, which can cause the soil to soften because they can be expressed in terms of effective stresses. Liquefaction hazard analysis is a significant application of nonlinear soil models.

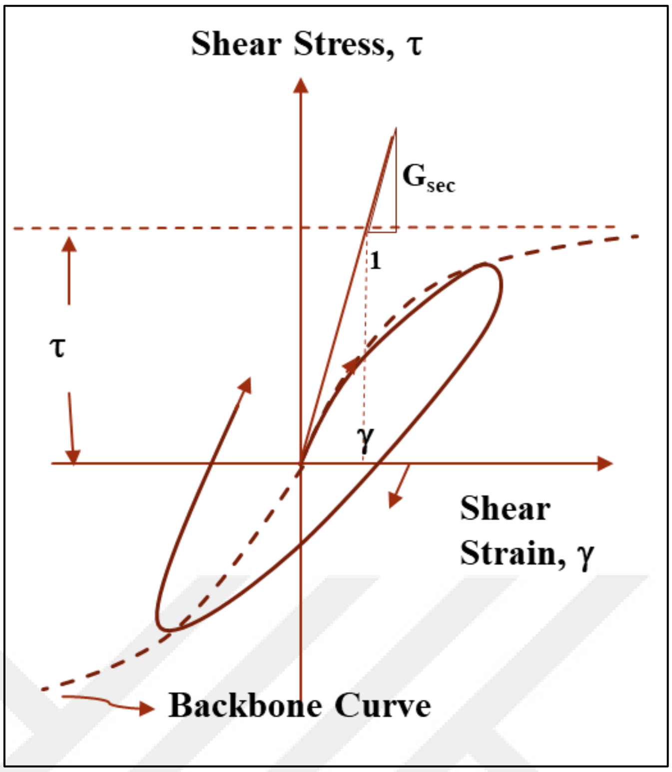

Figure 2.13 Hysteresis damping according to backbone curve

The soil performs hysteresis damping on the backbone curve according to the Masing Rules (Figure 2.13) (Masing, 1926). This hysteresis damping calculation can be made in the total stress-based method, assuming the effective stress is constant and the softening in the ground depends only on shear strain degradation. In the effective stress-based approach, if the pore pressure is calculated simultaneously and the effective stress is constantly modified, the backbone curve changes continuously, thus considering both excess pore pressure degradation and shear degradation.

2.2 Piles in Liquefiable Soils

Many researchers have done valuable work to understand the effects on pile foundations subjected to sudden horizontal loads such as earthquakes. There are studies in the literature on the movement of the pile exposed to inertial loads and the soil behavior adjacent to the pile in liquefiable soils, which are the subject of the thesis study. The literature research has been examined in two main elements to evaluate the problem elements better. The first chapter examines studies on laterally loaded pile response during earthquakes. Studies on horizontally modelling soil-pile interaction in liquefiable soils is examined in the second section.

Soil behavior around piles during earthquakes has been a topic of interest to researchers since the early 1980s.

Kagawa & Kraft (1980) presented a simple load-displacement curve relationship to study both inertial and kinematic soil-pile interactions under dynamic conditions. In the study, this relationship is expressed by the soil reaction coefficient as seen Equation 2.7). In the study, the concept of the average soil reaction coefficient is extended to develop a procedure for calculating the dynamic lateral load-deflection relationships of piles when the stress-strain response of the soil is non-linear and deteriorates due to cyclic loading and increased pore pressure.

$$\frac{p_1}{2\bar{f}B\bar{\delta_1}} = (1-r)^{0.5} G_{max} F(\gamma) \frac{(1+\nu)}{\bar{f}+B} y \qquad (2.7)$$

Brown, Reese, and O'Neill (1987) found that the deformations and bending moments in the pile group were higher than the results obtained from the single pile due to the experiment they conducted on the clay soil under cyclic and horizontal loads steel piles. Soil resistance measured in this study was higher in single piles than in pile groups.

Brown, Morrison, and Reese (1988) carried out lateral loading tests of pile groups and single piles in sandy soil under cyclic lateral load. As a result of the experiments, it was determined that the bending moment and displacement of the pile group increased due to the shading effect compared to the individual piles.

Dobry & Liu (1994) conducted a centrifugation test on a two-layer soil sample under seismic load. In this study, the results of two separate experiments were discussed according to the free field conditions and the presence of a foundation on it. The pore water pressures before, during, and after the shaking were compared in the experiment under free field conditions. It was observed that the pore water pressure increased rapidly during the earthquake (in the 2nd second of the earthquake), and the pore water pressure increased between the 2nd and 5th seconds of the earthquake, but the shear forces were prevented from passing due to the formation of a water layer between the sand and silty layer. At the 4th minute after the earthquake shaking, the pore water pressure was constant, but lateral spreading was observed. It was observed that the water layer disappeared after 4 minutes. In the second experimental setup, A foundation with a diameter of 10 cm was placed, and the centrifuge experiment was repeated. When the results of the pore water pressure under the free field and foundation at the same depth were compared, It was found that the pore water pressure was higher in free field conditions. It has been shown that the free field conditions of settlements after the earthquake are less than the case with the foundation.

Ishihara (1997) studied the failure conditions of piles. Pursuant to his study, the sandy soil had not yet softened at the beginning of the main earthquake shaking due to liquefaction. Accordingly, the relative displacement between the pile and the soil remained small. If the ground movement occurs enough to cause limit values of bending moments in piles, they will cause damage and collapse of piles. It has been observed that the inertial effects occasioned by the superstructure lead to damage near the pile heads, and these sections are exposed to maximum bending moments. He remarked that the time at which liquefaction occurs and the time during which the maximum acceleration occurs are approximately the same. After liquefaction, the sloping and loose sandy ground will start to move from the beginning of the liquefaction. In this case, the resulting lateral loads will act on the pile body in this soil and cause pile deformation in the slope direction.

Meanwhile, the seismic shaking passed the maximum acceleration value, and the shaking values decreased to smaller values. Thus, it is assumed that the inertial effects arising from the superstructure will lose their importance. The study stated that the maximum bending moment for this loading situation might occur at the bottom depths of the pile, not near the pile heads. In summary, Ishihara (1997) hypothesized that under dynamic loads, at the beginning of the main jolt, inertial effects from the superstructure will affect the pile and cause damage near the top of the pile. He indicates that at the end of the lateral soil movement due to liquefaction, the pile damages descend towards the middle parts due to kinematic effects.

Kagawa, Minova, and Abe (1998) conducted large-scale shaking table experiments for the first time in history with a real-size pile embedded in a moist sand layer depth of 5 m. The study aims to obtain experimental results that can be compared with existing numerical methods and better understand the dynamic soil-pile interaction. Consequently, they obtained that the stress-strain relations are consistent under relatively high vertical stresses when there is a vibration close to the natural frequency of the soil. The values measured and calculated in the evaluation of equivalent linear and nonlinear site response methods were compared, and a complete agreement could not be achieved. The reason for this is thought to be the high-frequency components included in the calculated values. The acceleration and moment values measured in the research for the pile behavior were found to be compatible when the gapping event was considered.

Cubrinovski, Ishihara, and Furukawazono (1999) analyzed the shaking table experiment and analytical method in order to show the cyclical stage of the structure-soil interaction and explained their findings as follows:

- Reinforced concrete and steel piles were placed in a laminar box with dimensions of 12×3 and 5×6 m, and earthquake loads were applied by forming sinus waves in two models. The maximum acceleration was 0.084 g in the first model and 0.21 g in the second model.
- In experimental data and the analysis results after liquefaction, cyclic lateral displacements were higher in test 2.
- In test 2, the bending moment values of pile heads limited to rotation and free-moving piles were higher than in test 1.
- Considering the test 1 and test 2 results, excessive pore water pressure formation, liquefaction test results, and damage distributions in the pile when the pile heads are limited or free to rotation were seen in both experiments.

Horikoshi, Tateishi, and Ohtsu (2000) evaluated 111 weak piles damaged by liquefaction in the 1995 Kobe earthquake. They stated that the cyclic displacement of the soil caused damage to the piles during the earthquake.

Their study stated that the most significant damage occurred in the transition zone of liquefied and non-liquefied soils, and the displacements at the pile heads varied between 25-42 cm.

In their studies, Finn and Fujita (2002) discussed the importance of pile design under earthquake loads on liquefiable soils. The study evaluation was conducted on a 14-story building and a 1.5 m diameter pile. They mentioned that critical regions would occur for the piles in the passage of liquefied non-liquified soils; due to pile heads being limited to dizziness, deformations would be high. There would be a loss of rigidity and strength in liquefied soils, and the bending moments and displacements of the pile would increase. The study mentioned that the most critical design for piles could be made under certain conditions. These conditions of analysis were determined as follows; the pile head is limited to displacement, the soil includes liquefiable and non-liquefiable layer transition, and loading would be with the earthquake.

Liyanapathirana & Poulos (2002) used an effective-based numerical model due to increased pore water pressure due to earthquake shaking, reducing the soil strength. They compared the experimental results and literature results with the new model. This study showed that shear deformations caused by pore water pressure at deep levels could be more than 0.01%.

Olson & Stark (2002) evaluated the shear strength of liquefied soils and the stresses due to yield failure during liquefaction by normalizing them with effective vertical stress. As a result, the strength ratio was obtained. They performed a retrospective analysis for 33 cases using the strength ratio in liquefied soils. They presented transition relations between the strength ratio and the (N1)60 and CPT value.

Bhattacharya & Bolton (2004) mentioned that buckling effects should be considered while designing piles under earthquake loading in liquefiable soils. It has been emphasized that the damaging effects of buckling on piles are different from the bending moment effects. They stated that the bending effect depends on the pile strength, and the buckling depends on the geometric rigidity of the pile. They mentioned that pile failures occur at the transition points of liquefiable and non-liquefiable soils and that the depth of embedding of piles in non-liquefied soil is essential. They concluded that while designing the pile, it is necessary to be careful about having sufficient strength and rigidity, having good pile sections, choosing the boundary conditions of the piles appropriately, and carrying the loads on them in the event of liquefaction without failing.

Klar, Baker, and Frydam (2004) used two types of models to analyze the pile-soil interaction in their article. The first model is a one-dimensional analysis in free field, and the second model is a three-dimensional analysis in which the pore water pressure changes. They made their analyses by changing the soil permeability coefficients, relative density values, and drainage conditions under different structural loadings in one and three dimensions and compared the moment-void water pressure results. In the one-dimensional and three-dimensional analyses, it was observed that the pore water pressure increased in the case with the same relative density but different permeability coefficient in the condition with a low permeability coefficient. One-dimensional and three-dimensional analyses showed that the moment distributions under the same loads were similar in soils with a high permeability coefficient (k=10-2 cm/sec). On the other hand, in soils with low permeability (k=10-3 cm/sec) coefficients, different moment distributions occurred in both models. In the study of the soil-pile behavior, it has been concluded that it is affected by the permeability coefficient, drainage status, earthquake impact time, and earthquake magnitude.

Maheshwari, Truman, Naggar, and Gould (2004) conducted a parametric study in the time domain under harmonic and discontinuous earthquake waves to show the existence of kinematic and inertial effects in soil-pile-structure interaction. They modeled the soil using a nonlinear material model. One-dimensional and three-dimensional numerical analyses were performed on a single pile and 2×2 pile groups, and the analysis results were compared. They divided the analysis into two situations;

The first case is the analysis under inertial forces from the structure, and the second case is the analysis for pile foundations by giving harmonic seismic waves in the bedrock under kinematic loads. At the end of the studies carried out on a single pile, it was observed that the nonlinearity of the soil was increased under low-frequency harmonic oscillations, and the pile heads and superstructure were more affected when high-frequency oscillations. For analyses where seismic waves are applied continuously, and the soil behaves non-linearly, the pile heads and superstructure response were greater in the solution with low-frequency loading. It has been observed that the effects of the pile head and superstructure are reduced in the analysis made of the harmonic and continuous earthquake motion in the pile groups.

Abdoun, Dobry, Zimmie, and Zeghal (2005) mentioned that damage occurred in deep foundations and support elements due to lateral spreading as a result of their case studies observations. In order to analyze these damages, centrifuge models have been created for individual piles and pile groups. The contribution of non-liquefied soil depth to the bending effects, soil improvement, and pile reinforcement strategies and results were evaluated. In their experiment, they tried to give the effect of lateral spreading by using a 2˚ inclined test setup on a single pile sample.

In the experiment, the effects of inertial loads, pile stiffness, and the height of the non-liquefied soil on lateral spreading. A rigid spring is used to describe the superstructure effect on the pile. According to the study results, it has been determined that the bending moments of the pile will increase over time and then will decrease with the resistance of the non-liquefiable soil part as a passive urge. Consequently, the upper part of the soil will be defeated and will be reflected in the pile and pile head. In other trials, a load representing the load from the superstructure was applied per pile, and inertial effects were activated. In this case, lateral spreading had a dominant effect. The inertial effect affected the 2-3 m upper part of the soil, but since the shallow depth is less than 2 m, the non-liquefiable soil was defeated, and the maximum moment occurred near the liquefiable soil parts.

Martin & Chen (2005) evaluated pile behavior under liquefiable or weak soil with the FLAC3D program. In their studies, they ignored the inertial loads and vertical loads from the superstructure. They evaluated the pile and pile groups considering that only the kinematic effects of soil movement (lateral spreading) affect the pile behavior. It has been featured in parametric and case studies articles. Their parametric studies investigated the pile-soil interaction during lateral spreading by changing the pile stiffnesses. The sensitivity analysis revealed that the difference in stiffness between the pile and the soil significantly affects the failure modes in a pile.

Takahashi & Takemura (2005) examined the pile-supported pier structure damaged in the Hyogo-ken Nambu earthquake in 1995 by performing a parametric study and centrifugation test. Analyses were made in the FLAC finite difference program, depending on whether existence is a deck on the pile, fill at the back of the structure, and changing the sand thickness under the stone fill. They used sine wave and Kobe earthquake recording in their analysis. At the end of the earthquake movement, it was observed that the caissons moved towards the seaside by making large displacements, and significant moments were formed. It has been observed that the piles prevent the movement of the stone fill, and the deck intercepts the movement of the caissons. It has been revealed that the change in the thickness of the liquefiable sand layer under the stone fill causes the displacement values of the soil and superstructure to change. In addition, it was observed that the improvement of the liquefiable sand layer under the filling contributed more to preventing lateral displacement and large deformations in the piles than the improvement of the filling behind the caisson.

Tokimatsu, Suzuki, and Sato (2005) conducted shaking table experiments on dry and saturated sand soil profiles to investigate the effects of inertial and kinematic forces on pile-structure behavior. In the ground profile, there is first 0.5 m of dry sand, 4 m of liquefied sand, and the next 1.5 m of dense gravel ground. The experiment was carried out in two ways, depending on the presence of the superstructure and the absence of the superstructure. For steel piles with a pile diameter of 165.2 mm and a wall thickness of 3.7 mm, the pile head is limited to rotation. At the end of this study, it was determined that if the natural period of the structure is smaller than the natural period of the soil, the displacement on the ground is in the same direction as the inertial effect caused by the superstructure and increases the shear force transmitted to the piles. On the contrary, if the structure's natural period is greater than the natural period of the soil, the ground displacement and the inertial effect are in the opposite direction. It has been determined that the stresses in the piles are inhibited.

Cubrinovski, Kokusho, and Ishihara (2006) conducted shake table experiments on single steel and concrete piles in liquefied soils. The 1 m section with the piles was formed from the non-liquefiable soil layer, and the 3.8 m section was formed from the liquefied soil profile. It has been observed that the reinforced concrete piles have more notable moments and more significant displacement, and the changes in pore-water pressures at different depths have been compared. They carried out an experimental study by changing the pile lengths and the thickness of the liquefied soil layers. They concluded that the flexible pile moves with the soil and makes the most displacement, while the rigid piles have less displacement.

Hwang, Kim, Chung, and Kim (2006) mentioned that cyclic displacement and lateral spreading due to liquefaction cause damage to structures on pile foundations. They compared liquefied soils to incomplete fluids. In order to analyze the pile behavior in soils that liquefy under lateral loads, they assumed the soil as a non-fluid liquid. The viscosity of the liquefied sand soil was determined by the "sinking ball test" and the "draw rod test." They stated that as the lateral effects of liquefied soil increased, the pile's shear force, bending moment, and lateral displacement increased.

Dash & Bhattacharya (2007) discussed the failure of piles in liquefied soils after major earthquakes and proposed design criteria for this. They mentioned that the piles must be socketed into the non-liquefiable soil, the shear strength of the piles should not exceed the allowable shear capacity, the axial load on the piles should be designed in such a way that buckling does not occur during liquefaction and that the settlements that may occur in the soil do not cause bending failures in the piles.

Erdoğan, Altun, Sezer, and Özden (2007) stated that inertial effects are effective at a depth of approximately 15 pile diameters from the beginning of the pile, and kinematic effects are effective at deeper depths. They stated that inertial and kinematic loading conditions, which occur due to the interaction of soil-pile-structure in pile foundations on liquefiable soils during an earthquake, might co-occur, depending on the liquefaction state, or they may occur independently of each other. They said that an effective loading state of inertial forces generally prevails during an earthquake before liquefaction begins. However, they underlined that inertia and kinematic loads arising from the displacement of soil layers began to act together on the pile foundation after the liquefaction started. They stated that in the phase where large lateral soil displacements occur after liquefaction, the effects of inertia force decreased while the kinematic loads increased significantly.

Forgetz & Çetin (2007) stated that although there is a consensus on determining the potential for liquefaction triggering under the influence of earthquakes in free field conditions, there is no agreement about the soil liquefaction of foundations with structures on it. For this purpose, three-dimensional dynamic analyses were performed using the finite-difference program (FLAC3D). In addition, in order to determine the liquefaction potential with a simple method without 3D analysis in their studies. The CSRSSI,mean value was defined, and this value is obtained by summing the shear stresses seen at the base of the structure and dividing by the total vertical effective stress at that point. At the end of the study, it was understood that the superstructure contributed to the liquefaction potential. As a result of the analysis, it was observed that the maximum values of CSRSSI in the sub-regions of the structure (x/B<0.5) were generally higher than the free-field CSR (CSRSS) values. Therefore, the regions with the highest value generally corresponded to the corners of the structures, increasing the liquefaction triggering potential of the structures. It is understood that the effect of the superstructure is almost absent in terms of liquefaction trigger potential at a distance of approximately as short as (B) from the structure. In some cases, it has been observed that the presence of the building can positively change the liquefaction potential of the foundation soils. It was observed that the contribution of the structures to liquefaction decreased along with the depth by about half the width of the building and almost disappeared when the depth was 1.5 times the width of the building.

Uzuoka et al. (2007) investigated the behavior of group piles in liquefied soils by performing numerical analysis. Damages in the pile group were tested using the soil-pile-building model using the soil-water coupled analysis method. They performed a numerical analysis of a five-story building that was damaged and tilted in the 1995 Kobe earthquake. At the end of the analysis, after complete liquefaction, large horizontal displacements occurred in the building, and it was stated that inertial effects from the superstructure on the pile were active during the liquefaction. They mentioned that kinematic forces act on the pile after the liquefaction process.

Bowen & Cubrinovski (2008) conducted a case study on the liquefiable soil profile. Within the scope of this analysis, the Fitzgerald Bridge over the Avon River in Christchurch is handled using the finite element method. The bridge was built with pile foundations on liquefiable soil. In their study, they compared the results of effective stress analysis and pseudo-static analysis. They examined the performance of pile foundations in the time history under seismic loads. In weak soil ((N1)60=10), pore water pressure started to increase suddenly in 13.5 seconds, and a liquefaction phenomenon was observed. In 14.5 seconds, the liquefaction event was completed in free field conditions. The pore water pressure increases, and displacement values were compared in free field conditions and the presence of piled foundations. While the maximum displacement on the soil is 0.2 m in the presence of piled foundations, it is observed that it is 0.3 m in free field conditions. The pore water pressure increases at 8 m depth were higher in free field conditions than in the presence of piled foundations. It has been observed that soil stiffnesses affect the pile behavior. It has been stated that the pile-soil interaction is affected by both soil and pile properties. They concluded that pile foundations increase soil stiffness and decrease their deformation capacity. Effective stress analysis is appropriate to determine the earthquake performance of piles under seismic loads.

Chenaf & Chazelas (2008) conducted a centrifuge test to understand the kinematic and inertial interactions. At the end of the study, it was seen that both kinematic and inertial effects were effective on the piles. It has been observed that the inertial effect contributes to the bending moment near the pile head. They stated that the inertial effect would affect deeper depths and ground displacement under seismic loads. They stated that If these two effects act in the same direction, it will affect the ground deformations.

Wei, Wang Q., and Wang J. (2008) mentioned the damage of pile foundations under the bridge due to the great earthquakes that occurred in the 1960s. In bridge piles after earthquakes. It has been observed that damages caused by crushing, settlement, shearing, and bending failures, liquefied and non-liquefied soil transitions due to kinematic effects.

Bhattacharya, Adhikari, and Alexander (2009) studied the effects of buckling, bending, and resonance in piles with a numerical example. According to the numerical analysis results, they stated that the natural frequency of the superstructure begins to decrease as soon as the soil begins to lose its stiffness. In designing the piles where liquefaction is observed, the natural frequency of the pile should not approach the earthquake frequency.

Dash, Govindaraju, and Bhattacharya (2009) discussed the damage caused by liquefaction and lateral spreading in piled raft foundations in Kandla Port and eccentrically loaded customs office damaged in the 2001 Bhuj earthquake. The analysis was carried out using the Winkler spring model under service loads and earthquake loads. At the end of the study, they concluded that the piles should be socketed into the non-liquefiable soil part and that the risk of failure and settlement of piles with sufficient strength raft and cap beams would be less.

Tang, Ling, Xu, Gao, and Wang (2009) determined the pile group behavior in liquefied soil by shaking table experiment using three different earthquake records. At the end of the study, they found that the extreme pore water pressure variation was related to the earthquake duration and soil depth. In addition, it was stated that the acceleration change in the sand layer changes according to the condition of the liquefied soil. It has been observed that in non-liquefiable soils, the acceleration decreases from the lower part to the upper part of the soil, and on the contrary, it increases in case of liquefaction. It has been observed that the maximum moment occurs at the pile heads with or without liquefaction.

Aydınoğlu (2011) explained a method for the structure-pile-soil interaction by using engineering software in his study. In the recommended method, It was stated that the non-linear three-dimensional dynamic behavior of the soil and piles should be taken into account. That analysis could be made for the superstructure under the reduced earthquake loads specified in the earthquake code. The dynamic interaction of soil and pile in the structure specified in the study is carried out in two stages: The first step, the kinematic interaction, is analyzed in the time history, taking into account the non-linear behavior of the soil and piles; In the second stage, the inertial interaction of the structure-soil-pile subsystem stiffness is shown with the equivalent dynamic stiffness matrix created by a different analysis. In the kinematic and inertial interaction stages, the effects occurring in the soil environment and piles are combined under appropriate conditions to obtain the design dimensions. These favorable conditions are stated in the study as follows:

i) In the case of linear analysis for the superstructure (building) under reduced earthquake loads according to the regulation within the scope of inertial interaction, the maximum displacement, and stress calculated in the soil-pile subsystem as a result of the calculation made separately for each of the average effective foundation acceleration spectrum components within the framework of the inertial interaction (The square root of the sum of the squares of the maximum values of the exact dimensions calculated within the framework of the kinematic interaction with the internal force (internal force in the piles) dimensions will be determined as the design-based dimensions. In the case of plastic deformation (plastic hinge rotation) in the piles during the kinematic interaction, the linear elastic is obtained from the inertial interaction. An approximate path can be followed since it will not be possible to combine directly with the size. In the inertial interaction, the differences in the relative translational ratios calculated between the neighboring nodes on the pile can be combined with the plastic hinge rotations obtained in the kinematic interaction, again according to the "square root of the sum of squares" rule.

ii) In the case of non-linear analysis in the time history of the superstructure within the scope of performance-based design for inertial interaction and non-linear analysis was also carried out within the scope of kinematic interaction. Consequently, the results of these two analyses that are compatible with each other in the time history can be directly collected in the pile-soil subsystem. Dimensions based on the design will be calculated by averaging for each dimension.

Abdrabbo & Gaaver (2012) presented a method for horizontally loaded pile groups in their study. They pointed out that although a reliable method for horizontal loading was presented in the study for single piles, this method was too complicated for groups of piles. Therefore, the multiplier factor has been applied to present a simple method for pile groups. At the end of the study, when the piles loaded horizontally on the sandy ground were analyzed, the result was; It has been revealed that there is a linear relationship between project load rates, lateral load, and lateral displacement at the pile heads. It has been observed that the moment and horizontal displacement of the bending pile cap decrease linearly as the P factor increases. It has been observed that the adequate depth of horizontally loaded flexible piles in cohesionless soils is approximately 16 times their diameter.

Ghosh, Mian, and Lubkowski (2012) presented comprehensive research for pile design in liquefiable soils under seismic loads. Two problems were addressed in this study; first, what should be the legal requirements in the design, and secondly, what the standards in national and international regulations should be when designing piles in liquefied and non-liquefied soils are summarized. They emphasized that the following items should be considered while designing piles:

1. Failure to fail should not occur in a pile, which is subjected to lateral and axial loads under the effect of earthquakes,
2. The permissible bending moment capacity should not be exceeded when designing the pile section,
3. Piles should be lowered to non-liquefiable soil (with sufficient socket depth),
4. It should be designed to carry sufficient axial load without buckling in the piles under the effect of an earthquake,
5. The settlements that will occur in the foundation with the loss of soil strength should remain within limits to be tolerated, and the piles should not be damaged due to settlements.

Mokhtar, Abdel-Motaal, and Wahidy (2014), pile behavior in liquefied soils was affected by soil properties, liquefiable soil depth, pile properties, earthquake instrument size-duration, and the stiffness ratio between pile and soil. Their study used the DIANA 9.3 finite element program to examine pile behavior in soils that liquefy under seismic loads. In the study, analyses were made by changing the pile diameters, earthquake duration-instrument size, and soil properties. They underlined that it is difficult for geotechnical and structural engineers to determine pile behavior before and after liquefaction. They stated that designs in which buckling of the piles and fractures due to plastic hinges may occur should be avoided.

Oral (2014) developed an effective stress-based soil-structure model working in FLAC software in order to determine the deformations that occur in liquefied soils. In order to confirm the accuracy of this body model, which was named METUSAND, he investigated the soil liquefactions in the "Imperial Valley" Wildlife area of the state of California during the "Superstition Hills" earthquake in 1987 and the "Port Island" area in Kobe during the "Hyogo-ken Nambu" earthquake in 1995. At the end of the analysis, the liquefaction in the case samples and the deformations that occurred after the liquefaction showed that it was compatible with the METUSAND model. In addition, numerical simulations were made to examine the horizontal deformations of the single pile sample under seismic loads. In these analyses, kinematic effects were taken into account.

Sextos, Mylonakis, and Mylona (2015) examined the behavior of reinforced concrete bridge pile groups under the influence of kinematic forces under cyclic and cyclical seismic movements of the pile heads on liquefied and soft soil. Analyses were made for uniform non-liquefiable and non-uniformly liquefied soil groups. It has been understood that there are non-linear movements of the piles and the pile in loose soils. Therefore, the cyclic and cyclic responses of the pile heads occur at high oscillations.

Hussien Tobita, Iai, and Karray (2016), seven different models on single piles and 3×3 pile groups supporting structures with one and two degrees of freedom on sand soil, acceleration of 40 g and 0.5-12 Hz. Centrifugation experiments were carried out under variable loading frequencies. Each model is exposed to 12 sinusoidal waves with constant acceleration amplitude and varying frequencies. As a result of the experiments, it was understood that two consecutive frequencies affect the movement of the pile heads. These are the low-frequency state in which the pile head motion increases and the high-frequency state where the pile head response decreases compared to the free field condition motion. In the experimental results, it was observed that the kinematic effect increased the bending moment in the piles when the resonance frequency of the soil was excited. In other words, when the excitation frequency approached the natural frequency of the soil-pile-structure system, the vibrations tended to produce significant bending moments on the piles. The bending moment distribution changed according to the frequency of the seismic effect and the pile characteristics. As a result of the experiments, it was stated that the kinematic effect caused the significant bending moments in the inner piles in the pile groups, and the inertial effect caused the bending moments in the outer piles. They mentioned that determining soil-pile-structure interaction in liquefied soils is a very complex phenomenon.

2.2.1 Pile Damage Mechanism in Liquefied Soils

Pile behavior is dominated by pile-soil interaction, failure mechanisms, and pile reaction in liquefiable soil. The depth and thickness of the liquefiable soil layer must be correctly calculated to design against collapse processes. The depth of liquefied soil affects more than just the horizontal pressures that cause the pile to shift and, consequently, the bending calculation. It also defines the length of the unsupported pile, which produces lateral instability. The deeper the liquefiable zone, the more likely pile foundations will collapse. As a result, accurately measuring the depth of the liquefiable soil layer is critical.

The primary concept of current approaches for liquefaction assessment, according to Idriss and Boulanger (2004), is to determine the liquefaction depth based on the peak ground acceleration, earthquake magnitude, and SPT. According to Abdoun et al. (2003), these depths are suitable for limit analysis. The pile may be unsafe against bending mode and buckling instability due to limit analysis. Furthermore, one cannot get a concept of the raid defeat mode.

The primary concept of current approaches for liquefaction assessment, according to Idriss and Boulanger (2004), is to determine the liquefaction depth based on the peak ground acceleration, earthquake magnitude, and SPT. According to Abdoun et al. (2003), these depths are suitable for limit analysis. The pile may be unsafe against bending mode and buckling instability due to limit analysis. Furthermore, one cannot get a concept of the raid defeat mode. On the other hand, the combined analysis of pile-soil interaction can help better understand the behavior of piles under earthquake loads.

2.2.2 Analysis of Piles in Liquefiable Soils

There has been a lot of interest in the analysis and design of pile foundations in liquefiable soil in recent years, for example, Finn and Fujita 2002; Abdoun and Dobry 2002; Bhattacharya 2003; and Boulanger and Tokimatsu 2005. Several pile design guidelines are frequently issued, including the Japanese Code of Practice JRA 1996; the European Committee for Standardization 1998; and the National Earthquake Hazards Reduction Program NEHRP 2000.

Loose cohesionless sands and silts below the water table cause significant porewater pressures or liquefy during strong earthquake shaking. High pore water pressures can degrade strength and stiffness significantly. In these liquefiable soils, seismic design of pile foundations provides exceptionally difficult analysis and design issues. The pile foundation may undergo severe shaking while the ground is completely liquefied and soil stiffness is at its lowest, depending on the incidence of liquefaction.

The pile is prone to significant cracking or breakage during this shaking phase. Liquefaction also causes significant increases in pile cap displacements over the non-liquefied scenario. Significant lateral spreading or downslope displacements may occur after liquefaction if the residual strength of the soil is less than the static shear stresses induced by a sloping site or a free surface such as a riverbank. Moving soil can put destructive forces on piles, causing them to break. Such failures were common during the Niigata earthquake in 1964 and the Kobe earthquake in 1995.

Lateral spreading is most harmful when a non-liquefied layer rides on top of liquefied soil. According to Finn and Fujita (2002), the profession has recently begun to deal adequately with these two significant design concerns. The advancement is due to advancements in analysis and results from centrifuge tests. Analysis improvement has also enabled more fundamental and extensive reviews of case histories, resulting in a better understanding of design issues.

Finn & Fujita (2002) conducted objectivity research to provide a general picture of the current state of the art and emerging technology for dealing effectively with the design and analysis of pile foundations in liquefiable soils, taking into account both earthquake shaking and lateral pressures from post-liquefaction displacements.

Large ground displacements can occur during liquefaction on sloping ground or towards an open area, such as a riverbank. The displacements induced by the Niigata earthquake's lateral spreading are depicted in the Figure 2.11. Displacements of up to ten meters in the direction of the Shinano River caused significant damage to the pile foundations and the collapse of two big bridges. A building's piles were moved nearly two meters in Niigata (Figure 2.12).

The pile built to support the warehouse was moved by around one and fifty centimeters during the 1995 Kobe Earthquake (Figure 2.13). Since the piles were meant to regulate settlement by meeting vertical loads, they could not withstand the shears and moments that could occur in the event of lateral spreading produced by intense earthquake shaking.

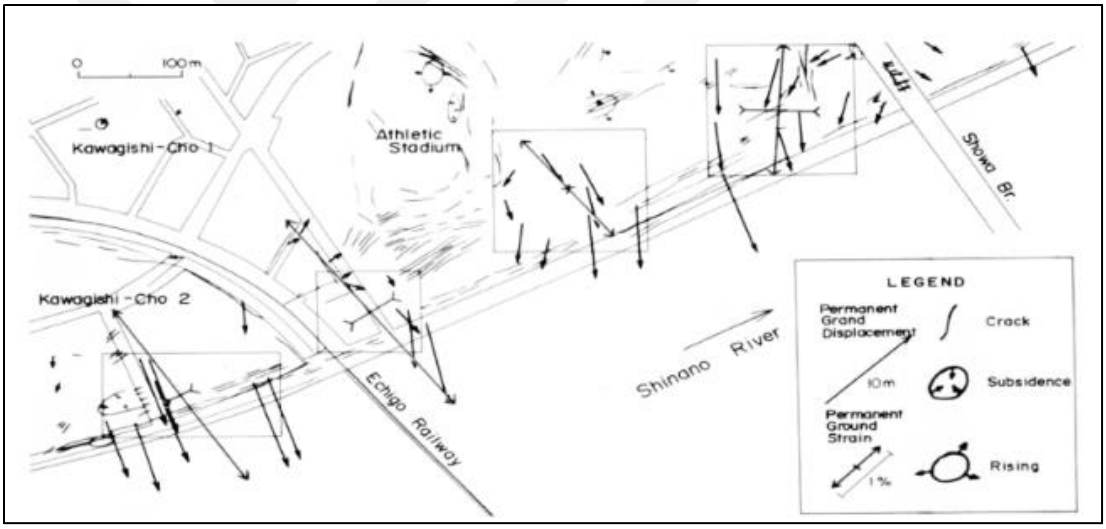

Figure 2.14 Lateral spreading in Niigata Earthquake (1964) (Hamada et al., 1986)

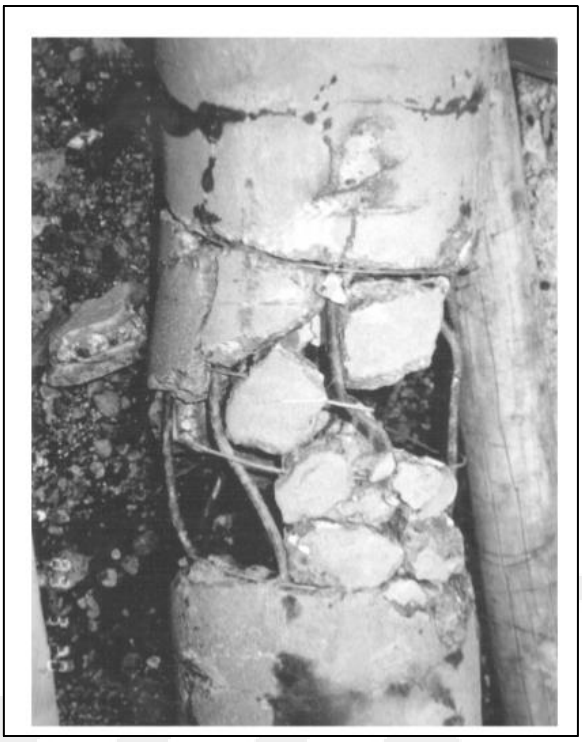

Figure 2.15 Damaged pile due to 2 meters ground displacement in Niigata Earthquake (1964)

Figure 2.16 Sheared pile due to lateral ground displacement in Kobe Earthquake (1995)

When piles are appropriately engineered to withstand lateral forces, they can survive without being harmed, like in the 1983 Nihon-Kai-Chubu Earthquake (Figure 2.14). A comparable example can be found on the piles that hold the crane rail on Port

Island near Kobe City. Despite the fact that the lateral spread exceeded one meter, it survived undamaged thanks to the construction of the piles (Figure 2.15).

Figure 2.17 Undamaged piles under the Bridge in Nihon-kai-chubu Earthquake (1983)

Figure 2.18 Crane rail undamaged piles regardless of the fact that ground lateral displacement more than 1 meter

A survey of case histories has clearly illustrated the design issues that pile foundations in liquefied soils provide. A reliable technique for assessing the effects of earthquake shaking and post-liquefaction displacements on pile foundations is required. An overview of the methods utilized in practice will be provided, emphasizing the benefits and limits of the various methods.

The pile foundation-structure system vibrates as a linked system during earthquake shaking. Logically, it should be evaluated as a connected system. This form of study, however, is not possible in engineering practice. Many typical structural analysis applications cannot directly incorporate the pile foundation into a computational model. When it is possible, the computational needs are high. As a result, numerous approximation methods of analysis are employed.

In pile foundation studies, Winkler springs and dashpots are widely employed to simulate soil stiffness and damping. It can be utilized with elastic or nonlinear springs. The American Petroleum Institute gives thorough instructions for creating nonlinear load-deflection (p- y) curves as a function of soil characteristics, which can be used to represent nonlinear springs. The most widely used API (p - y) curves in engineering practice are based on field data from static and slow cyclic loading tests.

The reliability of these (p –y) curves for the analysis of pile foundations, even under static and slow cyclic loading, is relatively low. Their performance under seismic loading is poorly established.

Figure 6 depicts a general Winkler model for seismic response analysis. Springs and dashpots simulate the near-field interaction between the pile and the soil. The seismic base and free field motions imparted at the end of each Winkler spring excite the near field pile-soil system and any structural mass included with the pile. 1-D dynamic analyses, such as SHAKE [5] or DESRA-2C, are used to compute the free field motions at the necessary altitudes in the soil layer.

A finite element continuum analysis based on actual soil characteristics is an alternative to the Winkler-type computer model. Because of the time required for computations, dynamic nonlinear finite element analysis in the time domain employing full 3-D wave equations is not now viable for engineering applications. However, by relaxing some of the boundary requirements associated with a complete 3-D analysis, accurate solutions for the nonlinear response of pile foundations can be obtained with far less computational effort.

There is very little quantitative data on the seismic reaction of pile foundations in the field, and what is available is difficult to access. Seismic loading of model pile foundations in centrifuge tests has recently produced data that allows for a more realistic evaluation of the reliability of various approaches for seismic analysis of pile foundations.

As a result, various streamlined techniques have been developed. Wu and Finn (1997) chose the Winkler spring and dashpot system over the semi-three-dimensional dynamic analysis system; the p-y technique was improved by Finn and Fujita (2002); the pseudo-static technique was employed by Liyanapathirana and Poulos (2005a). Several researchers conducted numerical studies of piles subjected to earthquake loading using linear/nonlinear dynamic finite element analysis, e.g., Finn and Fujita 2002; Liyanapathirana and Poulos 2005b; and Arduino et al. 2005. The research concluded that a thorough understanding of pile-soil interactions and the application of appropriate constitutive models is required.

2.2.2.1 Finite Element Approach

The finite element method stands out in the topic that soil-pile interaction can be determined by many approaches due to the existence of liquefiable test sites, creating test methodologies, data continuity, and the ability of this method to be developed. Many researchers will be able to validate analytical procedures using this strategy. The finite element approach offers good options for defining the soil found at a test site, selecting the appropriate and nonlinear constructive model, analyzing it at all drift ranges for an elastic pile and considering nonlinear soil and geometry. In addition to the mesh lock problem that should be considered in three-dimensional models, a model that correctly locates the water level of the soil layers can be constructed.

2.2.2.2 Load Deformation Curve Approach

This section presents calculation details and approaches to submerged pile behavior in saturated cohesionless soils. More than one concept has been put forward to analyze pile behavior, one of which is the p-y method. In a realistic approach, the stress-strain state around the pile affects the pile behavior, so it becomes difficult to express pile behavior under lateral loading. The soil reaction module is a fundamental concept for expressing buried structures and their strength. Soil reaction modulus is not a soil parameter but depends on pile deflection and soil resistance. The soil reaction modulus variables can be listed as pile type and geometry, bending stiffness of the pile, pile type on the pile, pile tip and pile cap conditions, pile installation procedure, pile batter, and curvature of the soil. The soil reaction modulus, influenced by many variables, is simple in analytical expression and is a case-study-validated approach. Studies on the soil reaction module are being developed daily to express the non-linear relationship between pile-soil.

This section will describe methods for determining p-y curves, including various approaches and loading situations on sandy soils.

Solving the lateral loading problem requires determining the number of soil properties. Considerable attention should be paid to the sample preparation and testing process in measuring the relevant properties of the soil. Assuming that a suitable sample represents the soil at the depth to be analyzed, tests should be repeated for each sample taken from each layer encountered to gain an idea of the strength of the soil. Field experiments should support test results. In laboratory tests, the sample is first exposed to ambient pressure and then to increased stress. The stress increase is maintained until parallelism to the horizontal axis is achieved. In the graph in Figure 2.16, the strain value in the bed axis is the strain rate found by dividing the shortening of the sample by the original length. In this graph, the slope of the line drawn from the point where the slope decreases considerably represents the soil's deformation modulus and stiffness.

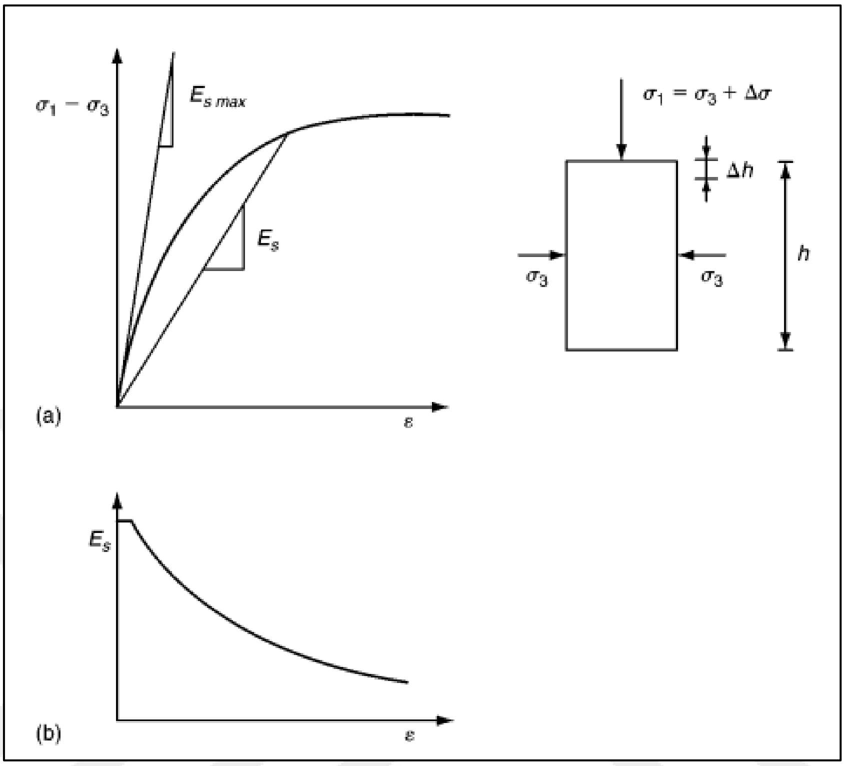

Figure 2.19 Results from testing soil specimens in the laboratory (Reese & Van Impe 2011)

2.2.2.2.1 Computation of values of Ultimate Soil Resistance. Two simplified models based on limit equilibrium theory are used in order not to calculate limit values that can be considered as ultimate resistance, P_{ult}, and carrying capacity. Expression of the final value of soil resistance as a function of the type of soil and its depth from the ground surface has been made by analytical methods, and the results can be compared with the test results.

The first of the methods, the wedge method, is shown in Figure 2.17. Here, the force Fp can be expressed as the weight of the wedge and the integral of the horizontal components of the resistances to the wedge. Pult is obtained by integrating Fp along the length of the pile depending on the depth. In addition to the simplicity of the model, it would be more appropriate to express a more realistic approach by considering the pile diameter, depth from the ground surface, soil properties variables, and the three-dimensional effect.

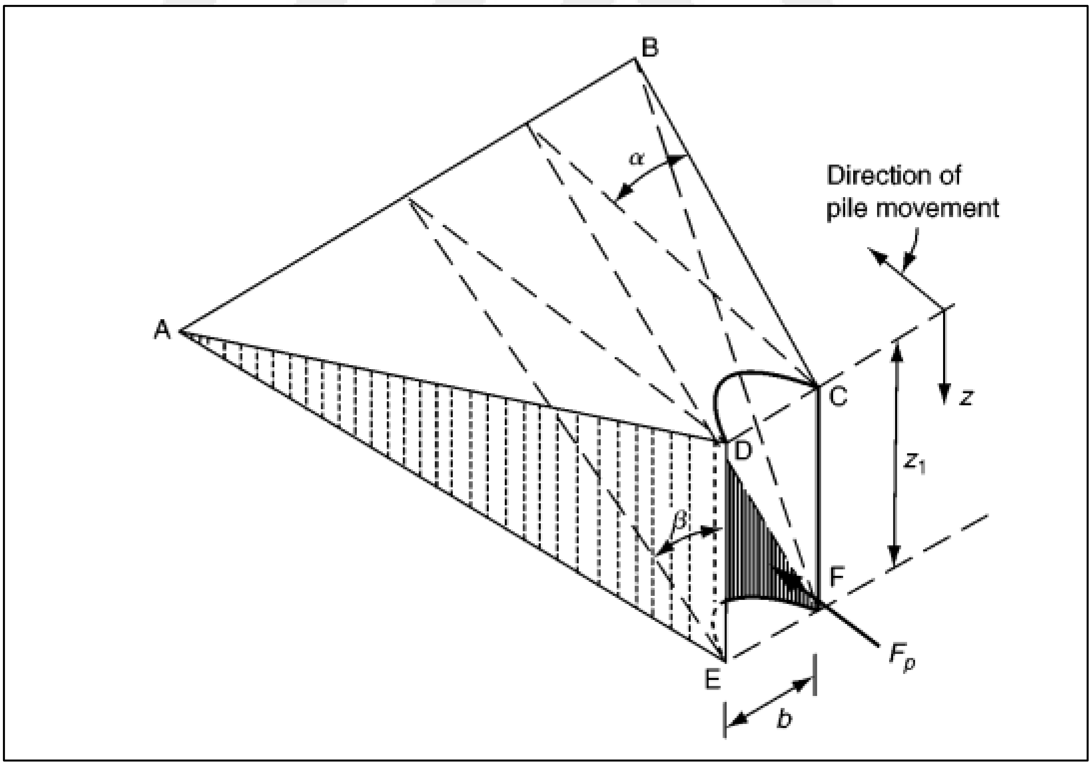

Figure 2.20 Passive wedge againts a laterally displacing pile (After Reese and Cox, 1974)

In Figure 2.18, the contours obtained as a result of the work done by Reese et al. in 1968 show the swelling of the ground surface in front of a 641 mm diameter steel pipe pile in overconsolidated clay. When a horizontal load of 596kN was applied, the swelling on the surface occurred 4m ahead of the pile, and when the load was removed, some lowering was observed on the surface.

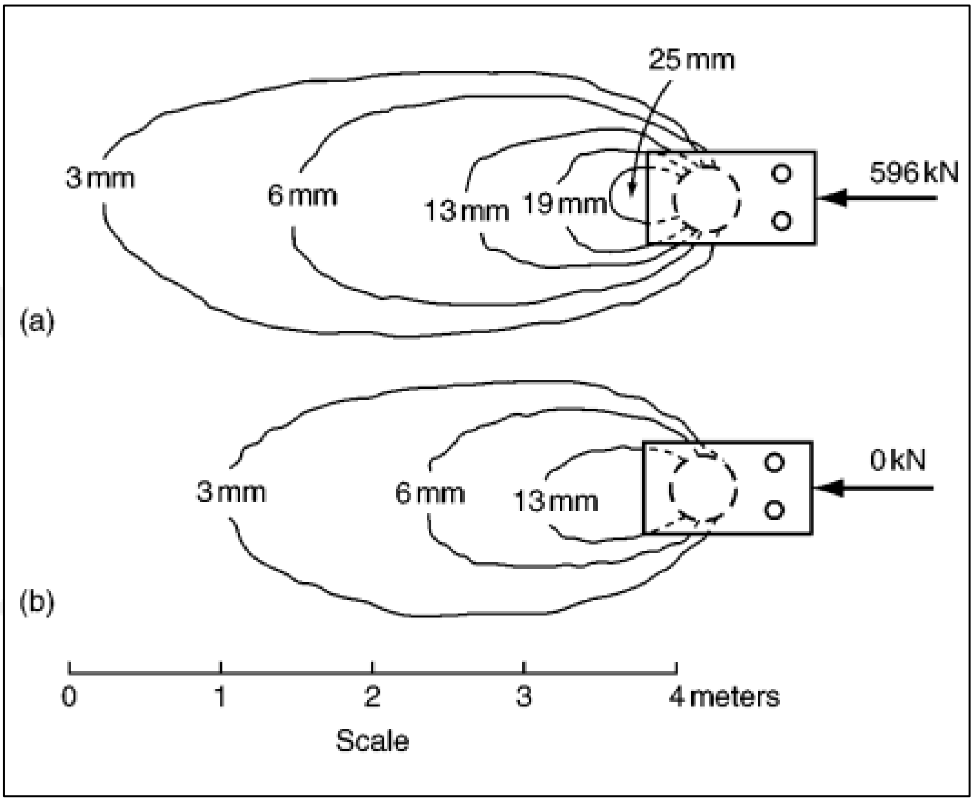

Figure 2.21 (a) Ground displacement contours due to static loading ; (b) Residual displacement contours

In the second model shown in Figure 2.19, a cylindrical pile and soil with five blocks are seen. Here it is assumed that the fifth block will fail against shear as a result of the pile movement. The ground movement is expected to cause the fourth, second, and first blocks to collapse with shear and the third block to slide. The ultimate resistance can be calculated as the difference between σ_6 and σ_1

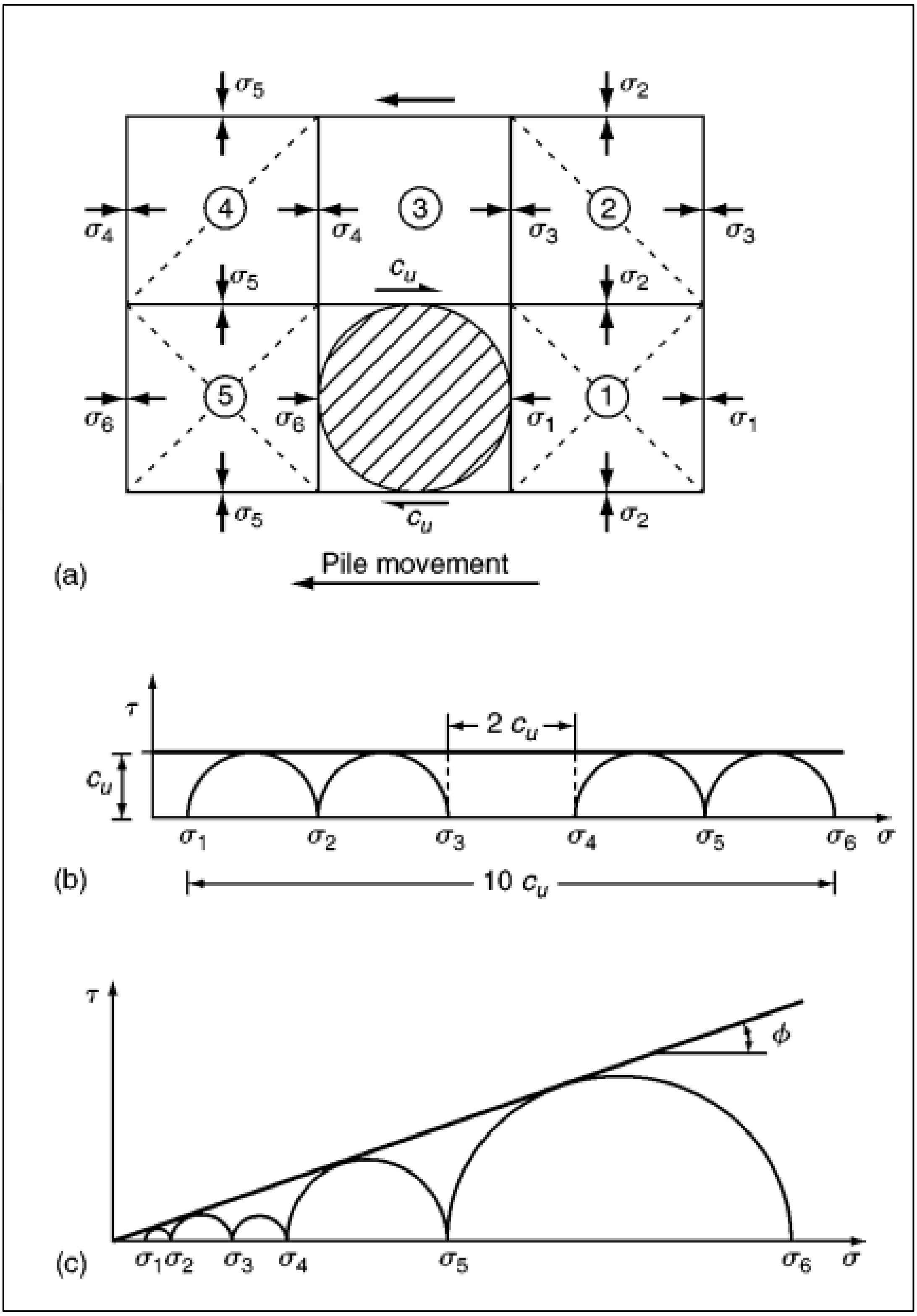

Figure 2.22 Expected failure of soil due to the lateral flow around a pile (a) plastic flow at deep depth; (b) Mohr-Coulomb diagram for pile in sand.

Analyses for sandy soils are assumed to be drained. The two previously presented models are used along the pile surface without considering any reduction factors. The ultimate soil resistance near the ground surface per unit length of the pile is obtained by finding the total opposing forces and differentiating the results concerning depth (Equation 2.7).

$$P_{ult} = \gamma z \left[\frac{K_0 z \tan\varphi \sin\beta}{\tan(\beta-\varphi)\cos\alpha_s} + \frac{\tan\beta}{tan(\beta-\varphi)}(b + z\tan\beta\tan\alpha_s)\right] + \gamma z[K_0 z \tan\beta(\tan\varphi\sin\beta - \tan\alpha_s) - K_a b] \tag{2.7}$$

Where K_0 = coefficient of earth pressure at rest; K_a = minimum coefficient of active earth pressure; and α_s = value of a for sand.

Bowman (1958) performed some laboratory experiments with careful measurements and suggested values of *as* from φ/2 to φ/3 for loose sand and up to *φ* for dense sand. The value of *β* is approximated by the following Equation 2.8.

$$\beta = 45 + \frac{\varphi}{2} \tag{2.8}$$

Studies on several large diameter piles to investigate the influence of pile diameter on p-y curves indicate that the diameter has no effect. Work on sands, on the other hand, is only done under static loads. Few pile tests with cyclic lateral loading have been documented. Because cyclic loading a pile in one direction causes permanent deformation when a sufficiently large load is applied, the pile head will significantly change direction. The movement of cohesionless soil particles during this time will prevent the pile from returning to its initial position. The hypothesis that the void ratio of the sand reaches a critical threshold, and the dense sand softens while the soft sand becomes denser is relatively frequent based on observations obtained during cyclic loading.

The API Method aims to estimate ultimate lateral earth resistance in a realistic manner. The API technique is empirical in nature, with several formulations available for shallow and deep foundations. The approach assumes that the deformation of the laterally loaded pile produces a passive wedge spanning from the ground surface to a particular depth. The ultimate estimate of earth pressure was backed by empirical evidence and was based on the work of Reese et al. in the 1970s. The passive wedge and plastic flow thought to occur below the critical depth are shown in the figure (Figure 2.17 and Figure 2.19a).

The soil-pile interaction occurs between ten and fifteen pile diameters from the pile head. The length of this section is referred to as the active or effective pile length. Passive wedge formation along the effective length is envisaged for piles of average size. In sandy soils softening due to the creation of positive pore water, passive wedges may form along the entire pile during seismic activity. The formula proposed by Reese et al. in 1974 has been changed.

The API technique is based on the procedures described by Reese et al. Reese documented the following processes in 1984.

1. Determine angle of internal friction (ϕ), soil density (γ), and pile width (b).
2. Perform the following calculations to be used in the ultimate soil resistance equations.

$$\alpha = \frac{\theta}{2}, \ \beta = 45 + \frac{\theta}{2}, \text{K}_0\text{=0.4}, K_\alpha = 45 - \frac{\theta}{2} \tag{2.9}$$

3

3. Use the following equations to compute ultimate soil resistance:

   (a)Near ground surface:

$$p_{ct} = \gamma z \left[\frac{K_0 z \tan\varphi \sin\beta}{\tan(\beta-\varphi)\cos\alpha} + \frac{\tan\beta}{tan(\beta-\varphi)}(b + z\tan\beta\tan\alpha)\right] + \gamma z[K_0 \tan\beta(\tan\varphi\sin\beta - \tan\alpha) - K_a b] \tag{2.10}$$

   (b)Well below the ground surface:

$$p_{cd} = K_a b\gamma z(\tan\beta - 1^8) + K_0 b\gamma z \tan\varphi \tan\beta^4 \tag{2.11}$$

   For submerged conditions, use the effective unit weight,$\bar{\gamma}$.

4. Determine the intersection point, x_f, of the equations of ultimate soil resistances. Above this depth, use the formulation for the near ground surface case and vice versa.
5. Decide for the depth at which the p-y curve is established.
6. Establish y_u as 3b/80. Calculate p_u using the following equation where $\bar{A}$ is found using Figure 2.20 for either static or cyclic loading case. Note that p_c is equal to the ultimate soil resistance of step 4.

$$p_u = \bar{A} p_c \tag{2.12}$$

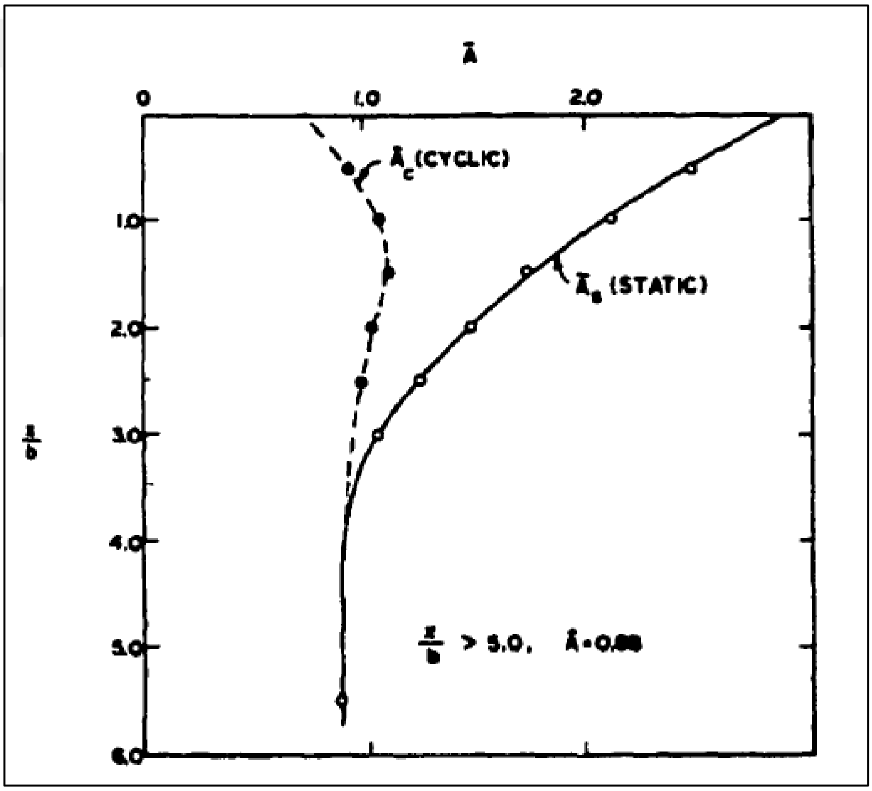

Figure 2.23 Nondimensional coefficient $\bar{A}$ for p_u versus depth (After Reese, 1984)

7. Similar to step 6, establish y_m as b/60. Use Figure 2.21 to choose the appropriate value for the coefficient B. The p_c is also equal to the ultimate soil resistance of step 4. Find out p_m using the following equations:

$$p_m = B p_c \tag{2.13}$$

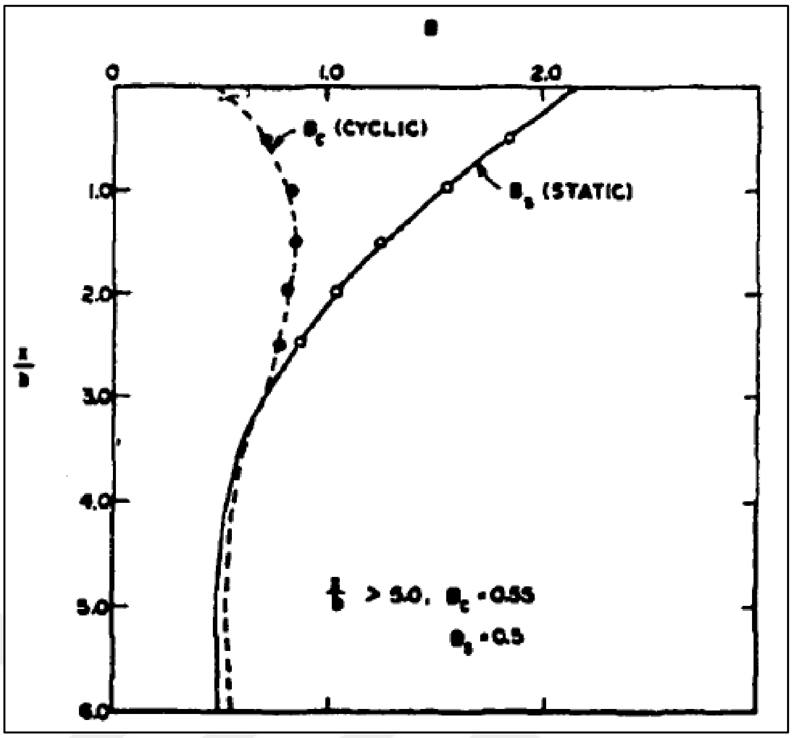

Figure 2. 24 Nondimensional coefficient B for p versus depth (After Reese, 1984)

8. Set the initial portion of the p-y curve by selecting a suitable value for k (Table 2.2).

Table 2. 2 Suggested k values under static or cyclic loading conditions (after Reese, 1984)

Relative Density, D_r	k (lb/in^3) for Submerged Sand	k (lb/in^3) for Sand above Water Table
Loose	20	25
Medium	60	90
Dense	125	225

1pci= 271.54 kN/m^3

9. Determine parameters of the following parabola to be fitted between the points k and m.

$$p = Cy^{1/n} \tag{2.14}$$

(a) Set the slope of the line between points m and u using

$$m = \frac{p_u - p_m}{y_u - y_m} \tag{2.15}$$

(b) The power of the parabolic equation is found by

$$n = \frac{p_m}{m y_m} \tag{2.16}$$

(c) The coefficient C is obtained by

$$C = \frac{p_m}{{y_m}^{1/n}} \tag{2.17}$$

(d) Determine the point k as

$$y_k = \left(\frac{C}{kx}\right)^{n(n-1)} \tag{2.18}$$

10. Compute enough number of points on the parabola using the equation of the step 9.

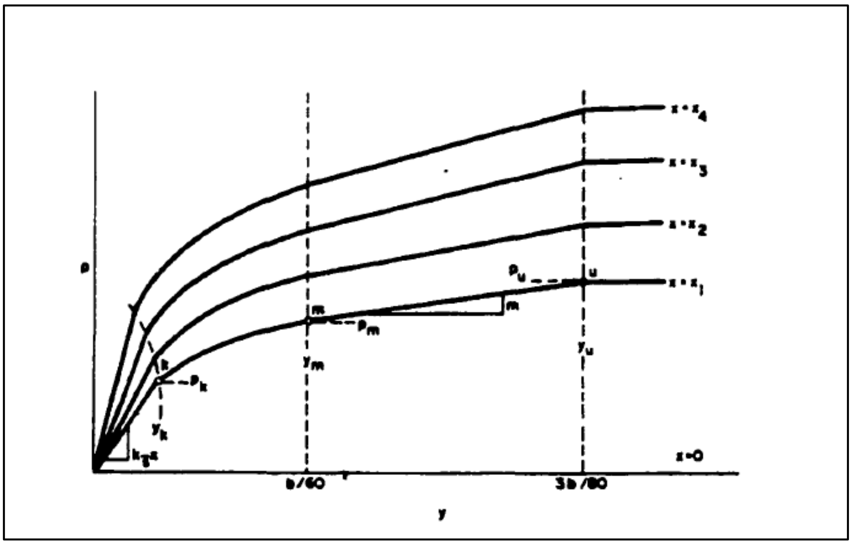

Figure 2. 25 p-y curves as established using API method

The p-y curves are created using the ten-step technique outlined above. It's worth noting that the original API method is based on the Mustang Island experiment (Cox et al., 1974). There is liberal use of empirical constants. Figure 2.22 summarizes the procedure.

Reese et al. (1974) were lateral loading tests on 24 in. diameter piles in sand and silty sand type of soil. Two types of loading were employed, static loading and cyclic loading. The data were analyzed, and families of curves were developed, which showed the soil resistance p as a function of pile deflection y. With theoretical studies as a basis, a method was devised for predicting the family of p-y curves based on the properties of sand and pile dimensions. Procedures are suggested, or both static loading and cyclic loading. Predicted p-y curves agreed with experimental results.

Kagawa & Kraft (1980) stated that to determine the realistic behavior of the pile-soil-structure interaction, three-dimensional analyses should be performed under free field deformations varying with depth and nonlinear stress-strain relations established in the light of soil parameters. They emphasized that the foundation spring model, which is one of the existing analysis approaches, remains simple, and although three-dimensional mathematical models are based on basic field research, these two models do not produce direct solutions to the problems encountered. They stated that the popular method was adopting the beam-on-Winkler foundation method with assumed discrete soil-pile springs and dashpots. They stated that soil-pile springs had been developed before, but additional research is needed to express the dynamic load-displacement relationships of pile-containing foundations in heterogeneous stratified soils. In their work, they developed FEM-based relationships to represent the p-y curves. The developed method represents complex soil conditions and stratification, so it reveals p-y relationships by taking into account the dynamic nonlinear behavior of the soil. They concluded that although the method they developed has multiple limitations, it can be used to develop more straightforward methods and present more rationally.

Boulanger, Curras, Kutter, Wilson, and Abghari (1998), using nine earthquake records with maximum accelerations between 0.02 and 0.7 g, performed a centrifugation test for two individual piles subjected to inertial loads in a soil profile with compacted sand on soft clay soil. Evaluating the dynamic beam foundation analysis results and test results, they concluded that with the maximum movement of the superstructure, 15%-20% deviation occurs in bending moments along with the pile. They concluded that this is related to equivalent linear soil behavior, structural and ground response, using the independent p-y spring model, and uncertain soil properties in free field conditions.

Humar, Bagchi, and Xia (1998) sought to find solutions in the frequency domain when considering the structure-ground interaction. For this, they took a five-story building. They modeled the building floor using springs, artificial dampers, and Ritz vectors. They recommended the use of the Ritz vector method.

Ishihara & Cubrinovski (1998) investigated the lateral spreading effects of liquefaction under earthquake loads on pile foundations. This study was done retrospectively, and the Winkler spring model was applied by reducing the soil stiffness in the liquefied parts by using the bearing coefficients. They examined large diameter pile foundations exposed to lateral spreading, slightly damaged and heavily damaged in the 1995 Kobe earthquake.

Fujii, Cubrinovski, Tokimatsu & Hayashi (1998) conducted field studies on damaged and undamaged pile foundations exposed to soil liquefaction during the 1995 Kobe Earthquake. The cause of the damage to the piles was investigated by dynamic response analyses of soil-pile construction systems using an effective stress finite element method. The effects of inertial force and soil deformation on pile stresses are discussed with parametric calculations. The applicability of a simplified pseudo-static numerical procedure using a beam model on Winkler-type soil springs for the evaluation of pile stresses is compared and discussed with the results of the dynamic analysis results and the observed damage. A method for evaluating Winkler-type soil springs from a 2D dynamic finite element analysis is also presented in the study. It was thought that the damages detected near the pile head in the examined buildings were caused by the inertial force coming from the building. However, the contribution of the soil's forced deformation and the significant constraint of the non-liquefied surface layer could not be ignored. As a result of the obtained results, it is understood that linear elastic modeling for a pile is not always suitable for the evaluation of the seismic safety of pile foundations. They concluded that by pseudo-static analysis of pile stresses using a model consisting of a beam on nonlinear Winkler-type springs, it could reasonably reproduce the damage caused by the observed inertial loads.

Tokimatsu & Asaka (1998) conducted a study explaining the failure modes of pile foundations and liquefied-non-liquefied soil interface and failure modes for coastal piles after the 1995 Hyogoken-Nambu earthquake. They explained the process of liquefaction phenomena and the cyclical phase and permanent ground displacement cases after the liquefaction event. They mentioned using the p-y curves method for pseudo-static analysis of pile foundations.They expressed SPT-N values of cyclic and permanent shear strength occurring during an earthquake. They observed the damages in the pile head and liquefied non-liquefied soil interface thanks to the cameras placed in the boreholes and slope indicators. They stated that the lateral soil movement affects the pile deformations.

Wang & Reese (1998), presented a practical method for design of pile foundations in deposits containing liquefiable soils during earthquake. An analytical solution to take into account the effect of the soil movement on the behaviour of piles during the post liquefaction period was developed.The models of the pile and the soil presented herein may be used, along with the appropriate computer code, to gain considerable insight into the interaction of piles and liquefiable soil.

Ashour & Norris (1998), presented the undrained formulation of saturated sand is used to assess the response of an isolated pile under undrained lateral loading. The technique presented yields the undrained p-y curves along the deflected length of the pile showing a distinctive variation from the drained response. Compared to pile response under drained conditions, the approach proposed showed that a dramatic reduction in pile head capacity could occur due to developing liquefaction under inertial loads.

Budkowska & Elmarakbi (2001) researched the determination of the subgrade reaction modulus in the sandy and clayey soils with laterally loaded short piles in their work. They put forward two scenarios. In the first scenario, when deciding on the subgrade reaction modulus, horizontal displacement was considered equal in the laboratory and numerical conditions. In the second approach, when the piles were loaded laterally, they evaluated the lateral soil strength and the effect of shear force on the pile.

Dutta & Roy (2002) have carried out a study in which past studies were collected to solve the soil-pile-structure interaction. They mentioned that it should be solved under both static and dynamic loads while solving soil-structure interaction problems. Although the Winkler hypothesis contained limited information, it has given good results. They were mentioned that non-linear soil constitutive models should be used to determine the soil-structure interaction on clayey soils. The study aims to propose a suitable method for the correct analysis of the soil-structure interaction.

Liyanapathirana & Poulos (2003) investigated the effect of the superstructure on the pile and the pile-soil interaction in liquefiable soils using the pseudo-static analysis method. They took two approaches in the method they used. In the first approach, effective stress-based response analysis, including maximum soil displacement along with the pile and reduced soil modules were applied, and in the second, static loading analyses were performed at the pile heads depending on the soil displacement and maximum soil surface acceleration in free field conditions. This new method they developed is independent of dynamic analysis. The effective-based response analysis in free field conditions includes soil displacement, reduced soil stiffness, and inertial effects at the pile head. The Winkler spring coefficients used in the pseudo-static analysis were extracted from the Mindlin equation. They compared the centrifuge model study in the literature with the new method they used in their study and the bending moments in Ishihara and Cubrinovski's (1998) study. They have seen that the values are close to each other. Comparing the analysis and literature data, they concluded that the bending moment value is maximum at the pile heads and at the liquefiable and non-liquefiable soil transition points.

Rollins, Gerber, Lane, and Ashford (2005) evaluated the pile-soil-pile interaction state by performing the laterally loaded pile group test in liquefied soil. For comparison, they have also considered single piles. They stated that the pile group interaction lost its importance after liquefaction. They said that the P-y curves become rigid with depth, and the excess pore water pressure increases. As a result of their tests, they showed that the p-y curve equations they developed also depend on the diameter of the pile.

Lombardi & Bhattacharya (2016) performed numerical analyses on four pile models (single piles and pile groups) with shaking table experiments and SAP2000 computer program for short-term liquefaction and full liquefaction situations. They made use of the proposed p-y curves and the p-multiplier method. At the end of the analysis, moment and displacement values were compared for both experimental and numerical methods. In the case of short-term liquefaction, the moment values in the experimental study were higher than the moment values in the numerical study. It has been observed that the displacement values in the proposed p-y curves method and the values in the p-multiplier method differ in the case of total liquefaction. They took the P-factors as 0.3 and 0.1.

2.3 Methodology of the Thesis

In this thesis the goal is to investigate the influence of piles on excess pore water pressure generation in liquefiable soils. In this respect emphasis is given to inertial soil-pile interaction. Since presence of a pile may alter excess pore pressure field with respect to free field conditions, a limited number of kinematic soil-pile interaction analyses were also made. The complexity of boundary conditions necessitated use of three dimensional finite element method. The goal was to study excess pore water pressure mechanisms and acquire data to develop a pore pressure model similar to those of Kagawa and Kraft (1981). The following assumptions were made while establishing thesis methodology:

i. Firstly, a single pile with a deformation modulus and Poisson's ratio similar to concrete was chosen as the pile type. Influence of pile flexibility was also investigated by assuming other deformation moduli.

ii. The soil type was a loose to medium dense silty sand from Wildlife Instrumentation Site. This assumption is made due to the fact that UBCSand model, one of the preferred liquefiable soil models, parameters are well studied by means of field measurements and laboratory soil dynamics tests.

iii. Three dimensional dynamic finite element model was established for inertial and kinematic interaction analyses.

iv. Cyclic loading conditions were assumed with constant amplitude and frequency.

v. Monotonic undrained and drained FEM analyses were also made to check the accuracy of the model by comparing achieved p-y curves with that of the literature.

CHAPTER THREE

NUMERICAL MODELLING

3.1 Constitutive Model Utilized for Liquefiable Soil

Puebla et al. first described the University of British Columbia Sand (UBCSAND) model in 1997, and Beaty and Byrne first applied it in 1998. An efficient stress-based elastoplastic constitutive model called UBCSAND was created to forecast how sands and silty sands will behave when subjected to seismic loads like earthquakes.

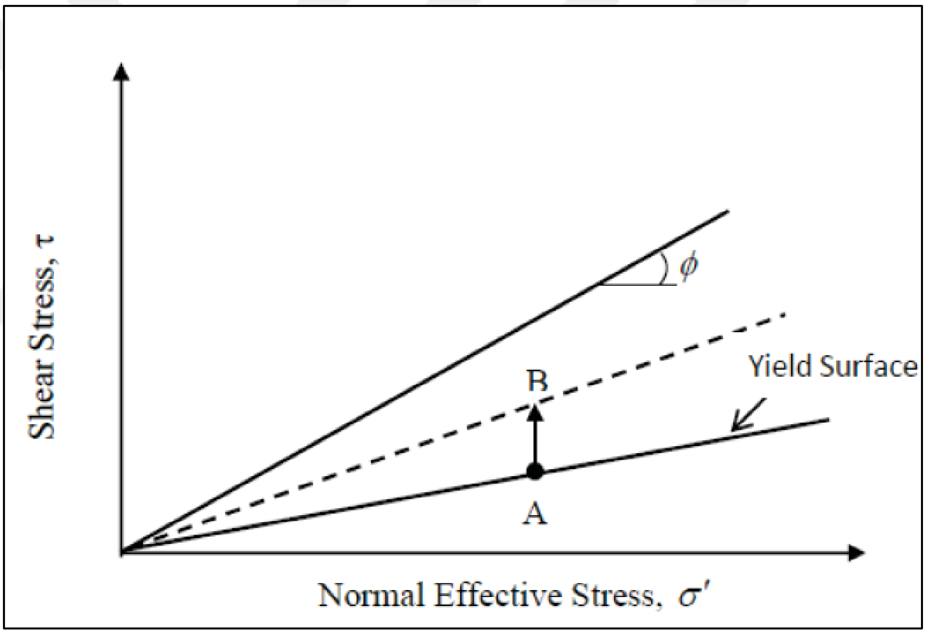

Figure 3.1 Yield surface for UBCSAND (Bryne, 2009)

A Mohr-Coulomb yield function and a matching unrelated plastic potential function are used in the original 2D model. A model's yield surface determines where elastic and plastic behavior diverge. The yield surface for the UBCSAND model can be described as radial lines spreading from the origin at a specific stress ratio. For first-time shear loading, the yield surface, point A in Figure 3.1, is controlled by the current stress state. As shear stress increases, the stress ratio rises, causing the stress point to shift to point B. The well-known Rowe's modified strain-expansion formulation provides the basis for the flow rule (Rowe, 1962).

The yield surface with a condensed kinematic hardening rule and the Mohr-Coulomb failure criterion are the two main components of the UBC3D-PLM model (Tsegaye, 2010). It has been discovered that the yield function-based unrelated plastic potential, which uses mobilized dilatancy angle instead of moving friction angle, enters non-coaxially between stress and strain in the deviatoric plane.

The UBC3D-PLM code for use with Plaxis was introduced in 2013 by Alexandros Petalas and Vahid Galavi. Non-permanent strains in this model are a consequence of shear or normal effective stress increases. The deformations become permanent when the plastic response stress ratio exceeds the yield surface. The model's plastic strains are computed using hyperbolic relationships from the available stress ratio, and their direction is independent of the yield surface (Figure 3.2).

The elastic strains in this model vary as the shear or normal effective stress changes. The shear and bulk moduli govern the relationship between stresses and strain. Both moduli are isotropic and non-linear, which means they depend on the current mean stress:

$$G = K_G^e P_A \left(\frac{\sigma'}{P_A}\right)^{n_e} \tag{3.19}$$

$$B = \alpha\, K_G^e \tag{3.20}$$

$$B = K_B^e P_A \left(\frac{P'}{P_A}\right)^{m_e} \tag{3.21}$$

Where G is shear modulus, B is bulk modulus, K_B^e, K_G^e bulk and shear modulus which are dependent on relative density respectively. P_A is atmospheric pressure and σ' is mean effective stress and m_e and n_e are rate of stress dependency.

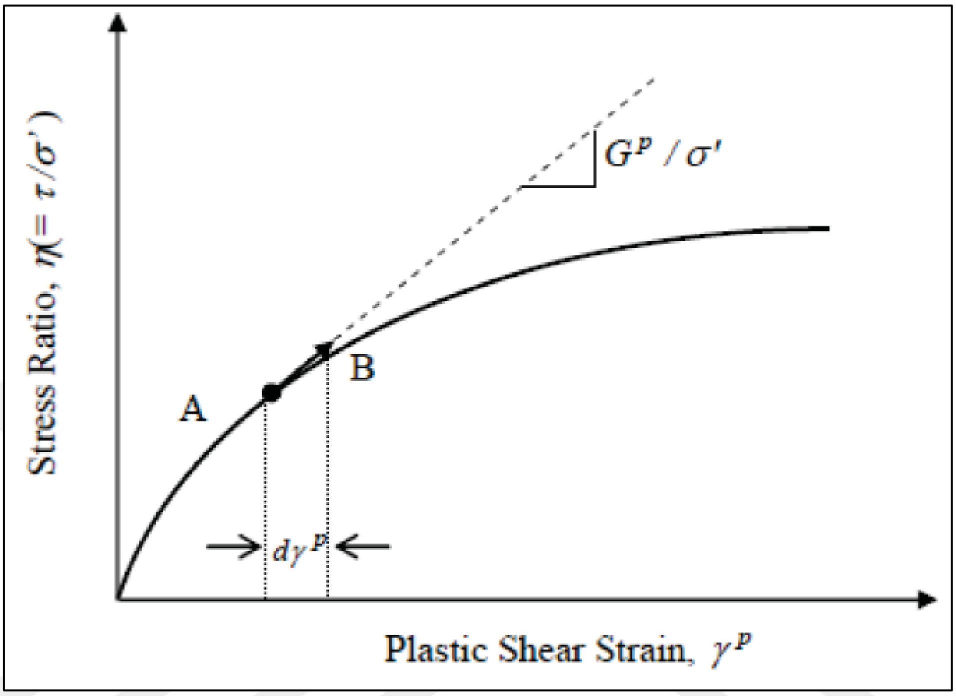

Figure 3. 2 Plastic strain increment and plastic modulus (Bryne, 2009)

The plastic shear strain increment, $d\gamma^p$ can be expressed using the Equation 3.22.

$$d\gamma_p = \frac{1}{G^p/_{\sigma'}}\, d\eta \tag{3.22}$$

Where G^p is the plastic shear modulus, σ' is the shear and normal effective stresses on the plane of maximum shear stress, dη is shear stress ratio increment. The G^P is assuming a hyperbolic relationship between shear stress ratio and plastic shear strain, is given by Equation 3.23.

$$G^p = G_{\mathrm{i}}^P.(1 - \frac{\eta}{\eta f} R_f)^2 \tag{3.23}$$

Where G_i^p is the plastic modulus at a low level of stress ratio (η=0), η_{peak} is the stress ratio at failure and equals $\sin\varphi_{peak}$, R_f is the failure ratio (generally decreases with increasing relative density).

Through the angle of dilation, the magnitude of the plastic volumetric strains is connected to the shear strain. Volumetric strains can be contractive or dilative. This is governed by the soil's proximity to the critical state line, which is specified by the constant volume friction angle. Soils with a stress ratio less than the constant volume friction angle contract, and soils with a stress ratio more significant than the constant volume friction angle dilate. Volumetric stresses will not occur in soils at the critical state line. Figure 3.3 depicts this tendency, which is consistent with critical state theory.

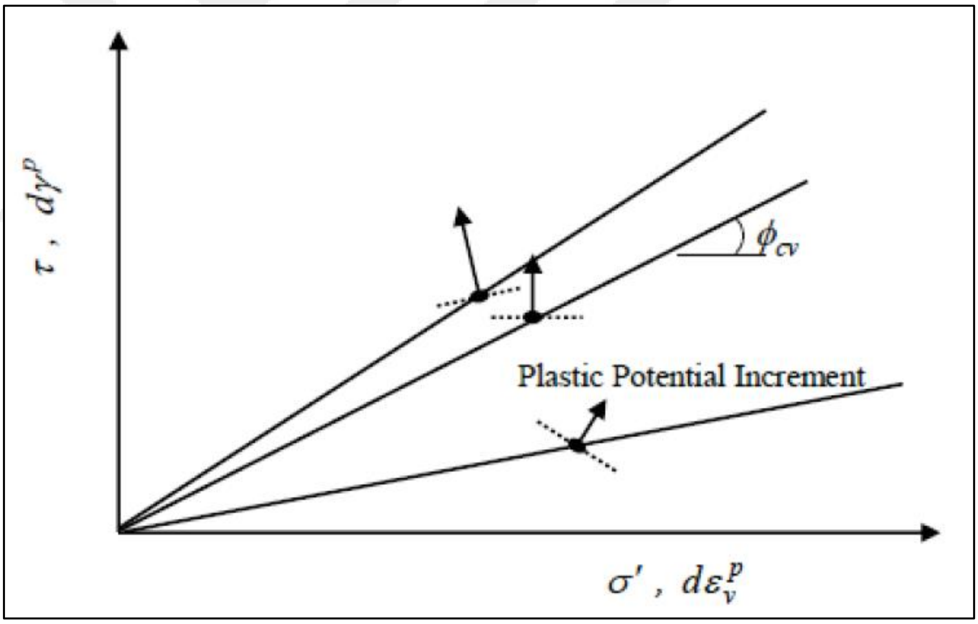

Figure 3. 3 Plastic strains tendency due to yield surface of soil (Bryne, 2009)

The yield surface starts as a tiny radial line stretching from the origin but "opens" when the soil is plastically sheared. Because the maximum and minimum stress ratios observed in the soil are monitored separately, the hardening law is tracked separately for positive and negative stress ratios. Unloaded soil behaves elastically until the sign of the shear stress reverses. The soil will "reload" until it returns to its last maximum or lowest stress ratio. Plastic strains are generated during reloading but with a shear modulus that is substantially stiffer than during the first or virgin loading.

The UBC3D model differs from the UBCSAND model, primarily including its generalized 3-D formulation. In 3-D principal stress space, the UBC3D model utilizes the Mohr-Coulomb yield condition (Figure 3.4). Furthermore, for a stress path beginning from the isotropic line, a modified non-associated plastic potential function based on Drucker-Prager's criterion is used to preserve the assumption of stress-strain coaxially in the deviatoric plane (Tsegaye, 2010).

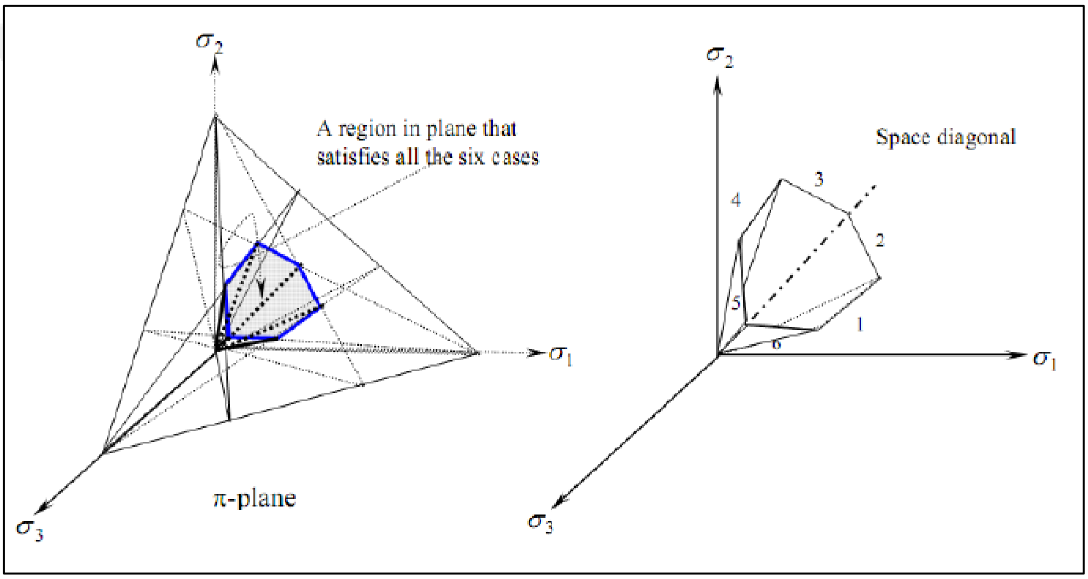

Figure 3. 4 The yield surface in three dimensional stress space (Tsegaye, 2010)

Volumetric locking is an essential aspect of cyclic liquefaction modeling in sands. After the stress path reaches the yield surface given by the peak friction angle, the evolution of the volumetric strains becomes constant due to the flow rule formulation. Because of this limitation, the soil stiffness degradation described in experimental studies due to the post-liquefaction behavior of loose non-cohesive soils or cyclic mobility of dense non-cohesive sands cannot be predicted. The UBC3D-PLM formulation addresses this issue by employing an equation that gradually decreases the plastic shear modulus as a function of the generated plastic deviatoric strain during soil element dilation.

Comprehensive in situ and laboratory testing is required better to interpret the soil's mechanical and dynamic properties. For these reasons, the UBC3D-PLM model performs a custom formulation with input parameters based on these tests.

Table 3.1 UBC3D-PLM Parameters, symbols, determining methods, and default values.

Name	Symbol	Unit	Method	Default
Constant volume friction angle	φ_{cv}	(°)	CD TxC or DSS	-
Peak friction angle	φ_p	(°)	CD TxC or DSS	-
Cohesion	c	kPa	CD TxC or DSS	0
Elastic Shear Modulus	K_G^e	-	Curve Fitting	-
Plastic Shear Modulus	K_G^p	-	Curve Fitting	-
Elastic Bulk Modulus	K_B^e	-	Curve Fitting	-
Elastic Shear Modulus Index	n_e	-	Curve Fitting	0.5
Elastic Bulk Modulus Index	m_e	-	Curve Fitting	0.5
Plastic Shear Modulus Index	n_p	-	Curve Fitting	0.5
Failure Ratio	R_f	-	Curve Fitting	0.9
Atmospheric pressure	P_A	kPa	Standard Value	100
Tension Cut-off	σ_t	kPa	-	0
Densification Factor	fac_{hard}	-	Curve Fitting	1
SPT Value	$N1_{60}$	-	In-Situ Testing	-
Post Liquefaction Factor	fac_{post}	-	Curve Fitting	0.2-1

Table 3.1 summarizes the UBC3D-PLM input parameters. The UBC3D-PLM model is descriptive, with model parameters determined by curve fitting using the cyclic undrained direct (CD), simple shear (DSS) test. Although, these tests are not available in many domains, and data from in situ testing such as the Standard Penetration Test (SPT) or Cone Penetration Test (CPT) exist. As a result, Beaty and Byrne presented some correlations for model input parameters in the UBCSAND model (Beaty & Byrne, 2011). This relationship was discovered by measurements of clean sand equivalent SPT blow-count. These relationships are as follows (Equation 3.24-3.28):

$$K_G^{e*} = 21.7 \times 20 \times (N_1)_{60}{}^{0.3333} \tag{3.24}$$

$$K_B^{e*} = 0.7 \times K_G^{e*} \tag{3.25}$$

$$K_G^{P*} = K_G^{e*} \times (N_1)_{60}{}^2 \times 0.003 + 100 \tag{3.26}$$

$$\varphi_{cv} = 20^{\circ} + \sqrt{15.4 \times (N_1)_{60}} \tag{3.27}$$

$$\varphi_p = \varphi_{cv} + \frac{(N_1)_{60}}{10} + \max(0; \frac{(N_1)_{60} - 15}{5}) \tag{3.28}$$

In this study, UBCSAND parameters obtained from field studies in Wildlife National Geotechnical Instrumentation Site, California/USA were used for a realistic approximation of liquefiable soil model parameters.

The wildlife site is in the Imperial Valley. This site became of seismic interest after the 1981 Westmorland earthquake (M_s = 5.9), which seemed to have caused liquefaction in the area. The site was then instrumented in 1982 by the U.S Geological Service (USGS), with the primary objective of recording ground and pore-pressure response data during earthquakes (Holtzer et al., 1989). Between November 23 and 24, 1987, two earthquakes occurred in the Imperial Valley within 12 hours. The first had its epicenter in Elmore Ranch, 23 km west of the Wildlife Site, with a magnitude of M_s = 6.2. At the ground surface, the peak ground acceleration measured was 0.13 g. The second event, thought to have caused liquefaction, was the Superstition Hills earthquake, with an epicenter 31 km southwest of the Wildlife Site, a moment magnitude of M_s = 6.6, and measured peak ground acceleration of 0.20 g. Figure 3.5 shows the map locating the epicenters of the three earthquakes in the Wildlife Site area.

Figure 3. 5 Past earthquakes in the Wildlife area (Holtzer et al., 1989)

Shallower deposits, according to Holzer et al. 1989's description, are saturated floodplain sediments that fill a historic Alamo River incised channel. The deposits are most likely the result of catastrophic river flooding between 1905 and 1907. The Alamo River flows via a 3.7-meter-deep channel 23 meters east of the Wildlife Site, controlling the groundwater table depth of roughly 1.2 meters. Generally, the stream is used for drainage and irrigation. The highest layer is a 2.5 m thick flat-lying silt bed that sits on top of a 3.3 m thick silty sand layer. The uppermost unit of a dense, widespread, sedimentary deposit is a 5-thick clayey silt layer discovered underneath these two layers of floodplain deposits.

Several researchers present a description of the instrumentation installed at the Wildlife Site. On-site, six pore-water pressure transducers, or piezometers, were installed. Five are in the liquefiable layer, or inside the silty sand unit. These piezometers have depths ranging from 2.9 to 6.6 m, as indicated in Table 3.2. During the 1987 incidents, Piezometer P4 failed to function (Holzer et al., 1989).

Table 3.2 Piezometer identifications and depths in Wildlife Site area

Identification	Depth (m)	Layer
P1	5	Silty Sand
P2	3	Silty Sand
P3	6.6	Silty Sand
P4	3.5	Silty Sand
P5	2.9	Silty Sand
P6	12	Silt

The analyses planned to be carried out on loose water-saturated sand soil samples were carried out on the sample taken from the depth where the piezometer 3 was placed. The soil parameters used are given in Table 3.3.

As the study essentially targets pile response in saturated cohesionless soils Wildlife National Geotechnical Instrumentation Site was chosen as the parent site to obtain material model parameters pertaining to liquefaction analysis. University of British Columbia sand model was the preferred material model due to the availability of calibrated UBC3D-PLM and soil profile parameters for the Wildlife Site in the literature (Youd et al., 2004). Soil parameters assigned to the FEM model are given in Table 3.3. Petelas and Galavi (2012) explained the physical meanings of the parameters and details of the model. The pile was modeled as an elastic volume element using a non-porous material model.

Table 3.3 UBC3D-PLM model and volumetric pile parameters

UBC-PLM PARAMETERS IN WILDLIFE					
Name	Symbol	Unit	II	Pile	Plate
Model			UBC3D-PLM	Elastic	Elastic
Type			Undrained (A)	Drained	
Depth		m	2.5-3.5	0-15	
Young Modulus	E	MPa	72.8	30000	30000
Poisson's ratio	ν	-	0.3	0.2	0.2
Unit weight phreatic level	γ	kN/m^3	19.7	25	25
Unit weight below phreatic level	γ_{sat}	kN/m^3	21.8	25	25
Void Ratio	e	-	0.74	0.25	0.20
Shear Modulus	G_0^{ref}	MPa			
Strain	$\gamma_{0.7}$	-			
Constant volume friction angle	φ_{cv}	(°)	22		
Peak friction angle	φ_p	(°)	22.765		
Cohesion		kPa	0		
Elastic Shear Modulus	K_G^e	-	854.6		
Plastic Shear Modulus	K_G^p	-	250		
Elastic Bulk Modulus	K_B^e	-	598.2		
Elastic Shear Modulus Index	n_e	-	0.5		
Elastic Bulk Modulus Index	m_e	-	0.5		
Plastic Shear Modulus Index	n_p	-	0.5		
Failure Ratio	R_f	-	0.811		
Atmospheric pressure	P_A	kPa	100		
Tension Cut-off	σ_t	kPa	0		
Densification Factor	fac_{hard}	-	0.2		
SPT Value	$N1_{60}$	-	7.65		
Post Liquefaction Factor	fac_{post}	-	0.02		
Permeability	k	m/s	5.00E-07		
Tangent stiffness for oedometer		kPa	98000		
Dilatancy angle		(°)	19.00		

3.2 Establishment of Finite Element Model

Two separate finite element analysis models were established to investigate lateral load displacement and excess pore pressure pattern around a pile on which cyclic lateral load was applied. The pile diameter was set as 60 cm with an assigned elasticity modulus of 30x10^6 kPa. The first model (Figure 3.6a) has 10 m length, 10 m width and 30 m deep. It has consisted of a slender pile with a length to diameter ratio of L/B=15/0.6=25 (Figure 3.7). The second model, on the other hand, involved a 1.0 m long pile section where the influence of effective stress was taken care of uniform applied vertical stress on the surface of the model, which was consolidated before the application of the cyclic load (Figure 3.8). The lateral load was applied as traction on pile heads along the y-axis. Viscous absorbent boundaries were provided on the sides of both models. The fine mesh was applied while discretizing the models with 32771 ten node wedge elements provided for the long pile model and 82358 elements for the pile section one Figure 3.6a and 3.6b. A mesh quality check revealed that over 99% of the elements had Quality Sphere or Quality SICN values larger than 0.5.

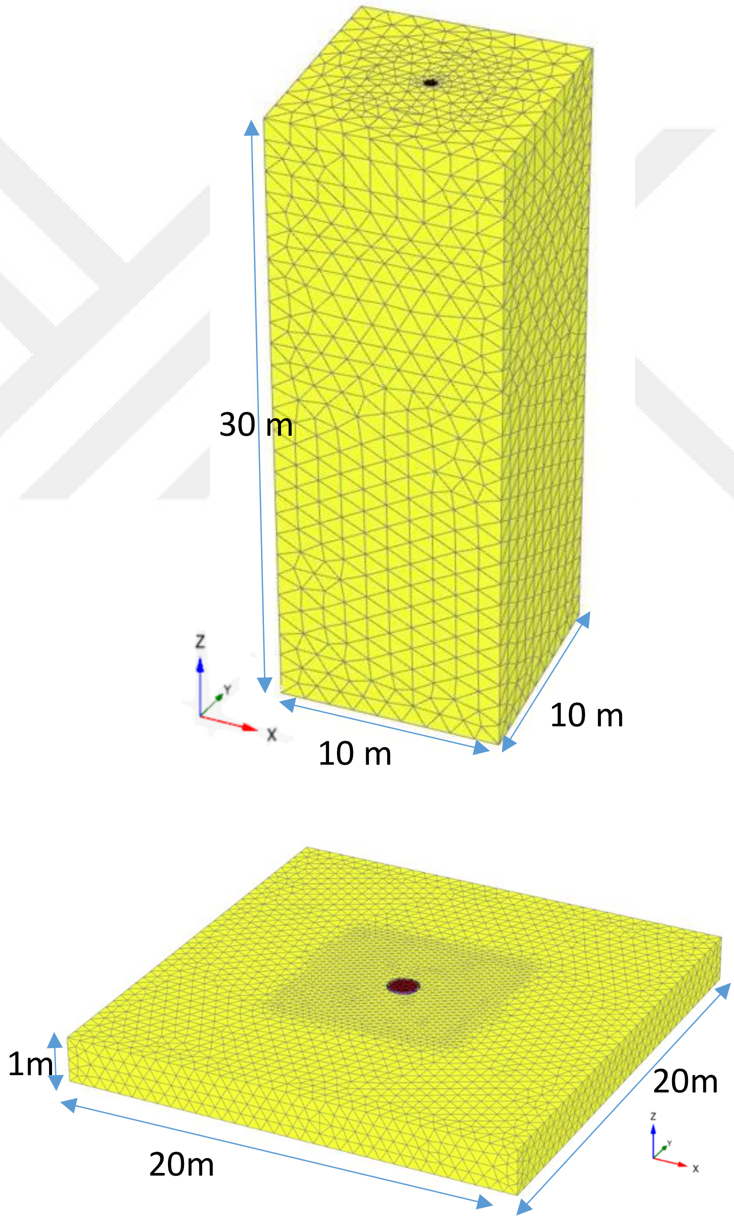

Figure 3.6 Finite element model connectivity plots (a) L/B=25 pile (b) 1.0 m long pile section

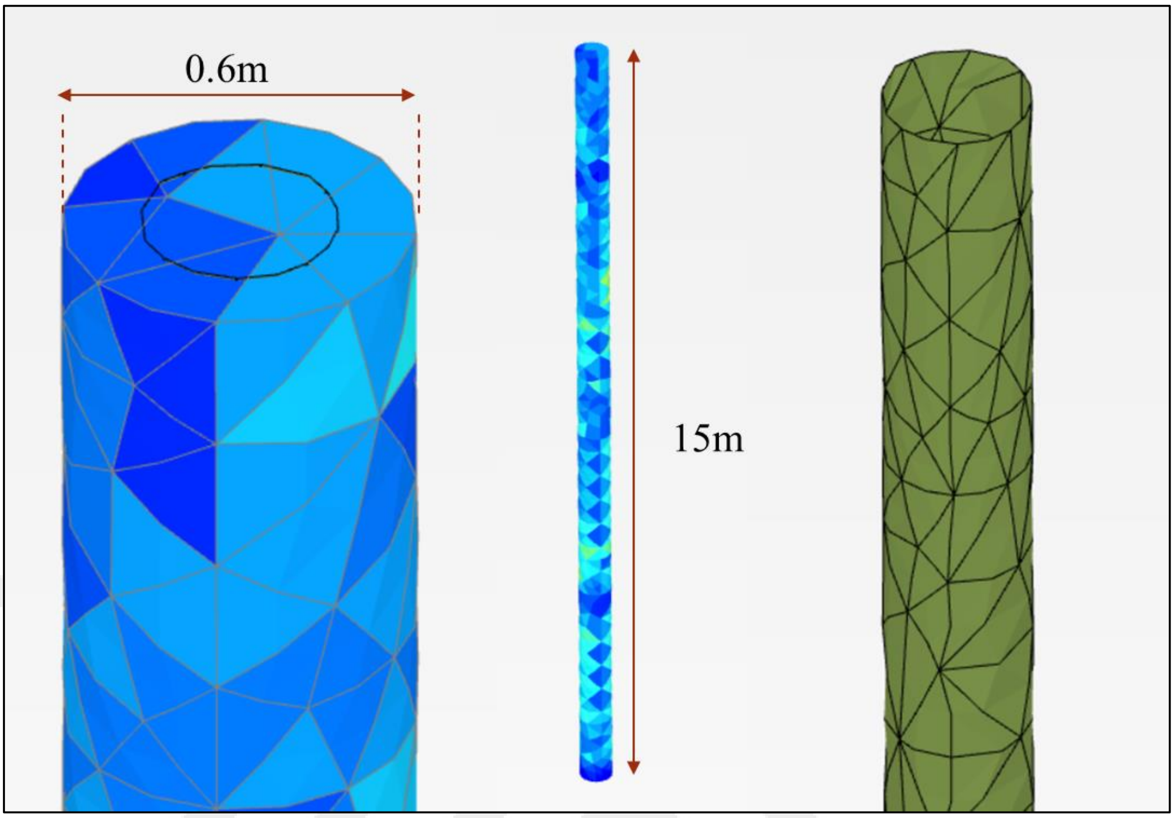

Figure 3.7 3D finite element analyses volume pile modelling and dimensions

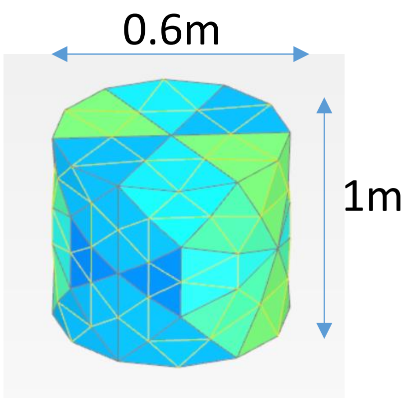

Figure 3.8 Section finite element analyses volume 1-meter-thick pile model and dimensions

3.3 Data Reduction Approach

3.3.1 Computed Excess Pore Water Pressure

The excess pore water pressure values, which are caused by inertial effects around the pile, were examined in the analyses. Dynamic analyses were repeated and consolidated, considering the higher-than-expected excess pore pressure gradients observed when the analyses were performed under undrained conditions. As a result, active and passive pressure situations created by the forced pile in the direction of loading and the opposite direction were examined under repeated strains. In the oscillating pile, starting from just in front of the pile in the direction of loading, the excess pore water pressures developed at stress points selected in one diameter, two diameters, three diameters, four diameters, and five diameters are given below for a depth of three meters where the change is observed steadily. Accordingly, it has been observed that the soil gradually approaches liquefaction as the load is increased. It was observed that the increases observed at the point in the immediate vicinity of the pile dampen away from the pile.

3.3.2 Derivation of Lateral Load Deformation Curves

As a result of the analyses made, several previous approaches have been considered to determine the soil resistance around the pile subjected to lateral load. Wolf et al. (2013) stated that interface or soil stresses could determine soil resistance. In this study, the method of determining the soil resistance over interface stresses is emphasized. This method has been successfully applied under static loading conditions. The method aims to obtain average normal stress in the loading direction in which the pile enters the active and passive state and vice versa. For this, the stresses produced by all interface stress points are taken and filtered at a certain depth. Based on the point coordinates, the points remaining in the active and passive directions are separated from each other. Sudden maximums and minimums due to numerical error are discarded from this data collection, and average normal stress is obtained. Below are the interface and stress contours around the pile divided into elements (Figure 3.9).

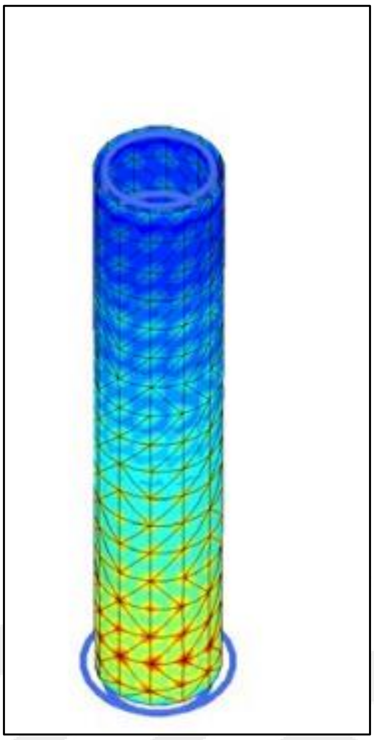

Figure 3.9 Pile interface normal stress concentrations

The dynamic analyses carried out were found inefficient during the modeling experiment due to the lack of computer performance and the length of the analysis period. Inspired by Wolf et al. (2013), it was concluded that the studies for a certain depth of an elastic pile could be obtained by modeling it on a sliced pile-soil model to represent that depth (Figure 3.10). It has been observed that the section analyses carried out on this result in a shorter time than the cyclic analyses carried out on the three-dimensional model and are compatible with the literature. In the inspired approach, the reading of the average soil stresses by considering the thickness of about one meter at a certain depth of the pile was obtained by creating a section model.

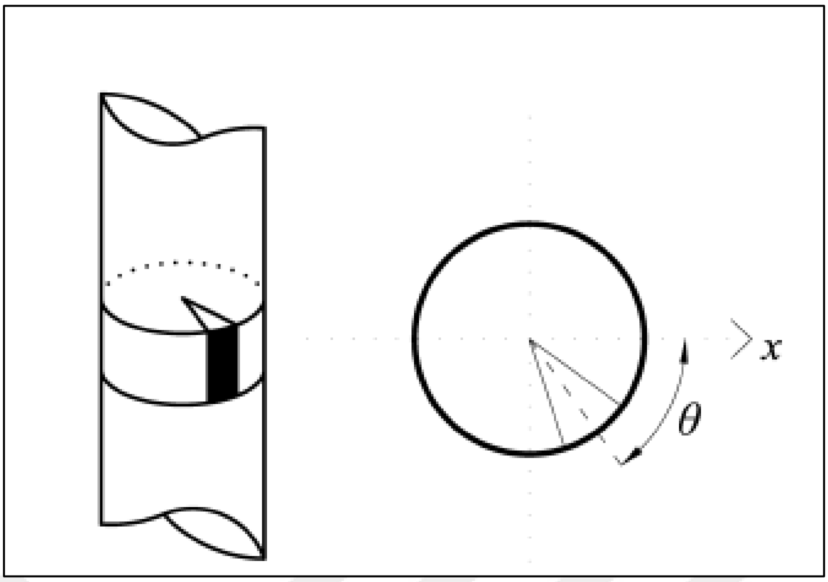

Figure 3.10 A pile section at specific depth and the angle of stress points area for examination

In the analyses performed under dynamic conditions in the three-dimensional models made later, the values read from the interface stresses could not be changed with the optimum mesh fineness settings, so the soil resistance was determined with the values read from the points in the soil. Here, the soil response method was applied precisely as a result of the finite element analysis by Kim and Jeong (2011).

In their study, Kim and Jeong (2011) determined an effective zone around the pile, deduced the soil stresses in the direction of the applied load, and stated that the average of the stresses at the points along a certain arc length constitutes the stress representing this arc length (Figure 3.11).

The soil resistance of a pile subjected to lateral loads is readily determined by integrating the stresses in the soil elements around the pile's circumference. According to Fan and Long (2005), using soil elements around the pile is an excellent technique to estimate lateral soil resistance (p). The stresses in the soil elements at the Gauss points nearest to the pile are taken as the soil stresses between the pile and soil based on this notion. Figure 3.12 depicts a cross-section of a pile-soil system with a lateral load applied in the x-direction. The dashed circumference shows the nearest Gauss points to the pile in the soil elements.

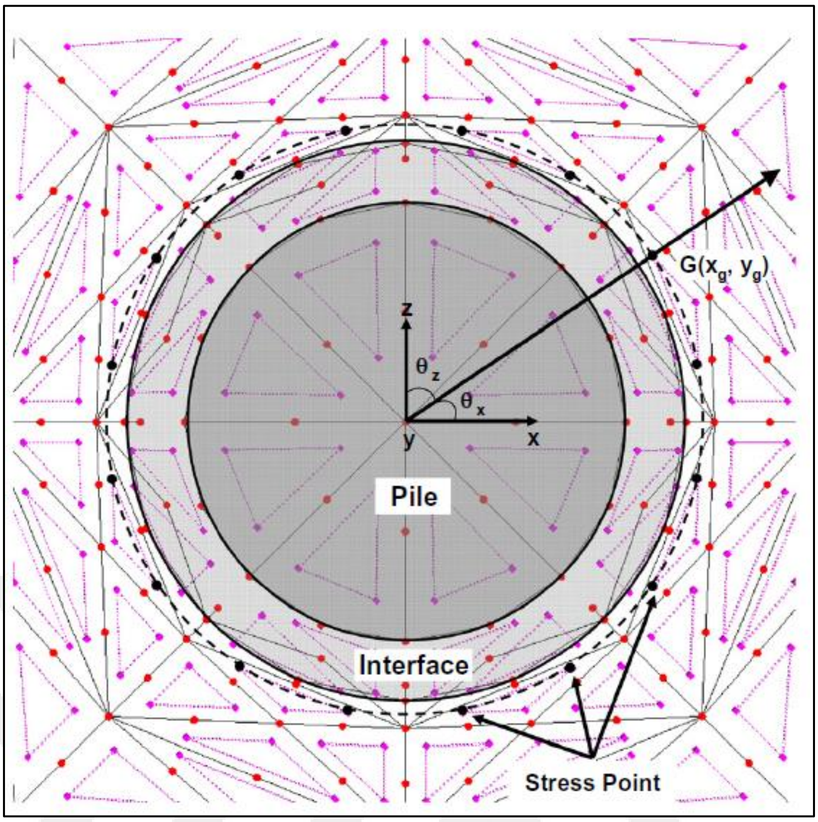

Figure 3.11 Horizontal cross-section of a three-dimensional model

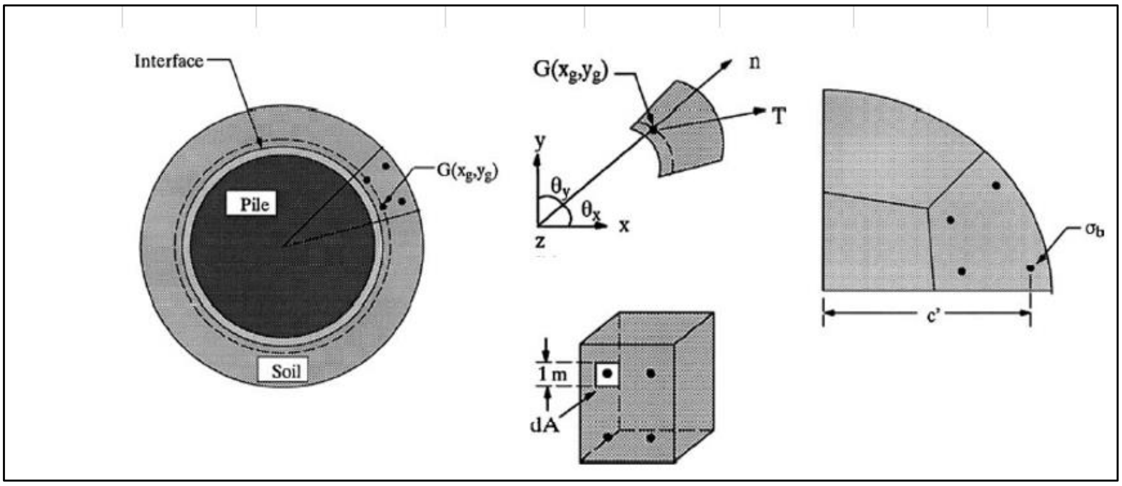

Figure 3. 12 Determination of lateral normal stress for examination area

The x-component of the total tension acting on the dashed circumference is the soil resistance per unit length along the pile. The x-component stresses at a point in a soil element can be represented by the following traction vector, Tx:

$$T_X = \sigma'_{XX} n_x + \sigma'_{xy} n_y + \sigma'_{xz} n_z \tag{3.29}$$

$$n_x = \cos\theta_x \tag{3.30}$$

$$n_y = \cos\theta_y \tag{3.31}$$

$$n_z = \cos\theta_z = 0 \tag{3.32}$$

Where $n_{x,}$ n_y and n_z are components of unit normal along the x, y, and z directions respectively.

The conventional p-y curves approach used to express the soil-pile interaction was evaluated over the varying soil stresses and pile deformations at constant depth as a result of the analyses. While determining the soil stress, the selected contour points between the investigation diameter determined around the pile and the pile wall are integrated separately for the front and back of the pile as potential stress points. This approach aims to evaluate the stresses at the points selected from the area between the pile wall swept by an angle of 30 degrees and the inspection circle formed according to the inspection diameter. In this way, it is aimed to eliminate instant maximums and minimums caused by numerical errors and obtain an average. This calculation is continued by subtracting the components of the mean lateral stresses in the load's application direction and adding the appropriate shear stresses. Then, repeated calculations for each thirty-degree slice were integrated for the front and back of the pile. In order to obtain the resistance responsible for the pile strength and, therefore, the pile movement, the net stresses were obtained by taking the difference in the soil strengths formed at the front and the rear. These stresses were removed from the horizontal strengths formed in the geostatic condition, and strength changes were noted. The pile movements resulting from this change were obtained as average for the volumetric modeled pile at a constant depth.

CHAPTER FOUR

RESULTS AND DISCUSSIONS

4.1 Inertial Soil-Pile Interaction Analyses

Finite element analyses were performed for full pile length and pile section models (Table 4.1). In this context, it has already been mentioned that the general trend is to model the pile at its entire length and either drive the p-y curves along the pile length along the interface or analyze the stresses induced in the soil in the immediate vicinity of the pile.

Some researchers (Pradhan, 2012) state that the soil resistance is affected by the rotation and flexibility of the pile. Limiting the pile displacement along the loading direction is recommended to achieve pure lateral displacement. It was thought that the pile section model, in which 100 cm pile portion is allowed to be displaced only in the y direction, would serve this purpose. An applied surface load represents the effective stress level acting along the length of a pile. Here, we aimed to limit the interface deformations by keeping the interface strength parameter very low. Soil resistance was obtained against the laterally deformed piles along the interface stress points. Monotonic and cyclic surface traction was applied at the pile head (Figure 4.6).

In order to examine the inertial interaction in the three-dimensional finite element analysis, a rigid plate element was placed on the pile head, and the cyclic load was applied to the entire surface of this plate element along the pile head. Here, the dynamic surface load is loaded with a uniformly distributed harmonic signal. Various analyses were made by changing the amplitude (A) and frequency (f) of the given cyclic load signal. The purpose of the analysis is to monitor the trend of pore water pressures and stresses in the soil surrounding the pile in the soil towards liquefaction. As a result, soil strength-displacement curves and stress changes were observed at depths where changes are expected.

Table 4. 1 Analyses schedule of investigation for soil-pile inertial interaction

Analyses Schedule of Soil-Pile Inertial Interaction					
Name	**Loading Type**	**Amplitude**	**Frequency**	**Drainage Type**	**N (num. of cycles)**
Reprensenting 3 meters depth					
Section	Dynamic	25~200 kPa (Δp=50)	1 Hz	Undrained	2
Section	Dynamic	150-200 kPa	1-2 Hz	Undrained	2
Section	Monotonic	25~300 kPa (Δp=25-50)		Undrained	
Section	Monotonic	25~375 kPa (Δp=25-50)		Drained	
Section	Monotonic	25~600 kPa (Δp=25-50)		Drained	
Reprensenting 5 meters depth					
Section	Monotonic	25~225~-225 Δp=25 and -25		Undrained	
3D-Model	Dynamic	150 kPa	1-2 Hz	Undrained	2
3D-Model	Dynamic	50~200 kPa (Δp=50)	1 Hz	Undrained	2
3D-Model	Dynamic with consolidation	50~650 kPa (Δp=varies)	1 Hz	Undrained	4
3D-Model	Dynamic with consolidation	50~650 kPa (Δp=varies)	2 Hz	Undrained	2
3D-Model	Monotonic	50~1000 kPa (Δp=50)		Drained	
3D-Model	Monotonic	100~700 kPa (Δp=100)		Undrained	

4.1.1 Monotonic Loading

Monotonic loading analyses progressed up to 300 kPa (i.e. 25~300 kPa corresponding to a lateral point load of 7~85 kN at the pile head), beyond which the soil body collapsed due to excessive pore water pressure and plastic point development (i.e. H=113 & 141 kN). UBCSAND material model parameters in Table 3.3 were used in the analyses made in this section.

4.1.1.1 Drained Analyses

It is seen in Table 4.1 that the drained monotonic analyses were made using pile sections and 3D full-length pile models. As a result of section analysis, p-y curves were derived under drained conditions. The results are compared with the p-y curves obtained via the API method described in the second chapter (Figure 4.1). One may note that API p-y curve fits the drained p-y curve if API model parameters are adjusted accordingly. The parameters assigned to the API curve are shown in Table 4.2. This shows us that the methodology considered for section analyses and explained in detail in the third section is correct.

Table 4.2 Determination of API curve

API Curve Parameters		Curve Values	
		y (m)	p (kN/m)
C_3	11	0	0
C_1	0.7	0.00023	4.20
C_2	1.5	0.00050	9.01
$\gamma'(kN/m^3)$	11.8	0.00074	13.31
h (m)	3	0.00109	19.30
D (m)	0.6	0.00209	35.73
A_c	0.9	0.00323	51.88
A_s	-1	0.00488	69.30
k (kN/m^3)	6000	0.00761	85.28
		0.01392	94.58
p_u (kN/m)	106.2	0.02409	95.56

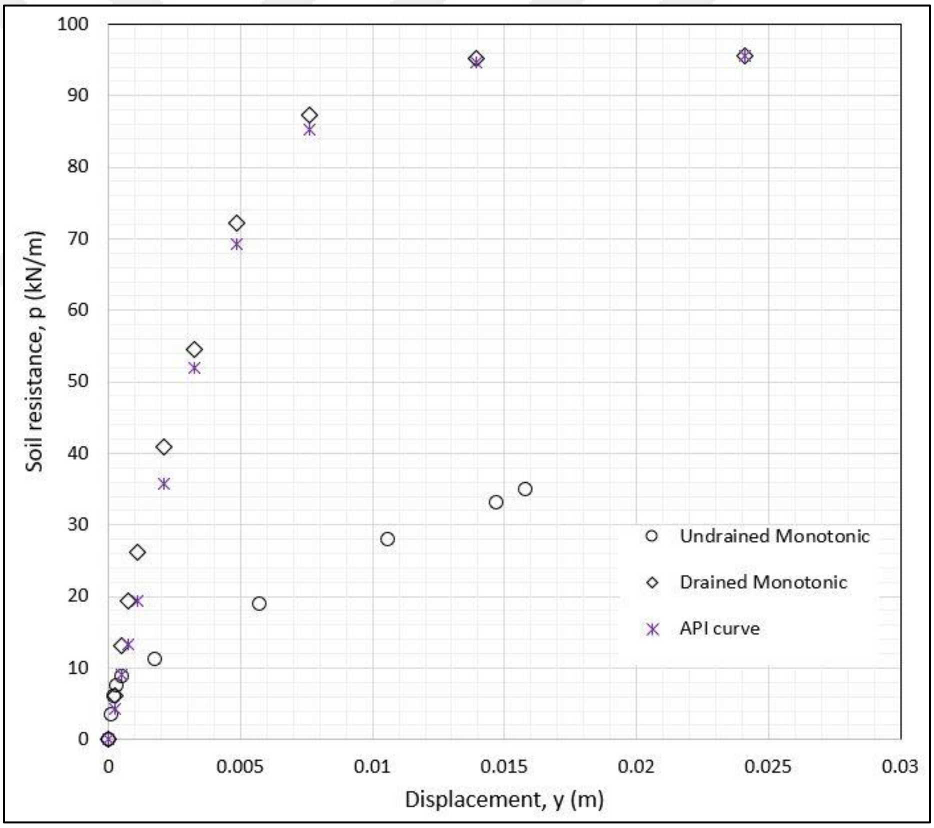

Figure 4.1 p-y curves for monotonic drained and undrained loading cases (pile section analyses that correspond to a depth of 3m below the surface)

4.1.1.2 Undrained Analyses

When we evaluated the results of the undrained analyses, it became apparent that computational time required for the completion of pile section model analyses was much shorter. Because of that, monotonic undrained analyses were performed on this model. Although results are given for an effective stress level corresponding to 3 m depth, it is quite easy to adjust the depth by arranging the vertical surface traction applied at the surface of the model. The p-y curve deduced from undrained analyses is presented on Figure 4.1 along with the drained curve. The influence of excess pore water pressure is obvious when the two curves are compared.

Excess pore water pressure (Δu_e) field because of the lateral displacement of the pile towards and away from the surrounding saturated loose sand is one of the expected outcomes of undrained analyses. Results of monotonic loading tests are presented in Figure 4.3~4.5 for a depth of 3m below the ground surface. In these figures, variation of Δu_e with horizontal strain, e_{yy} is plotted for stress points selected adjacent to the pile, 1B, and 3.8B away from the pile axis parallel to the loading direction. It may be followed in Figure 4.3 that pore pressure development adjacent to the pile is associated with dilative soil response. In contrast, it is almost entirely positive for all loading levels 3.8B away from the pile. It is noteworthy that excess pore pressure generation is not the highest for larger loads. This trend is related to dilation taking place as the loading level increases. However, at H=113 and 141 kN, negative pressure development ceases at about e_{yy}=4.5x10-3 and 7.8x10-3, respectively, due to soil body collapse. The influence of head loads less than 42 kN is negligible on excess pore water pressure development. The excess pore pressure field is also given in Figure 4.2, which is plotted in terms of coloured contours.

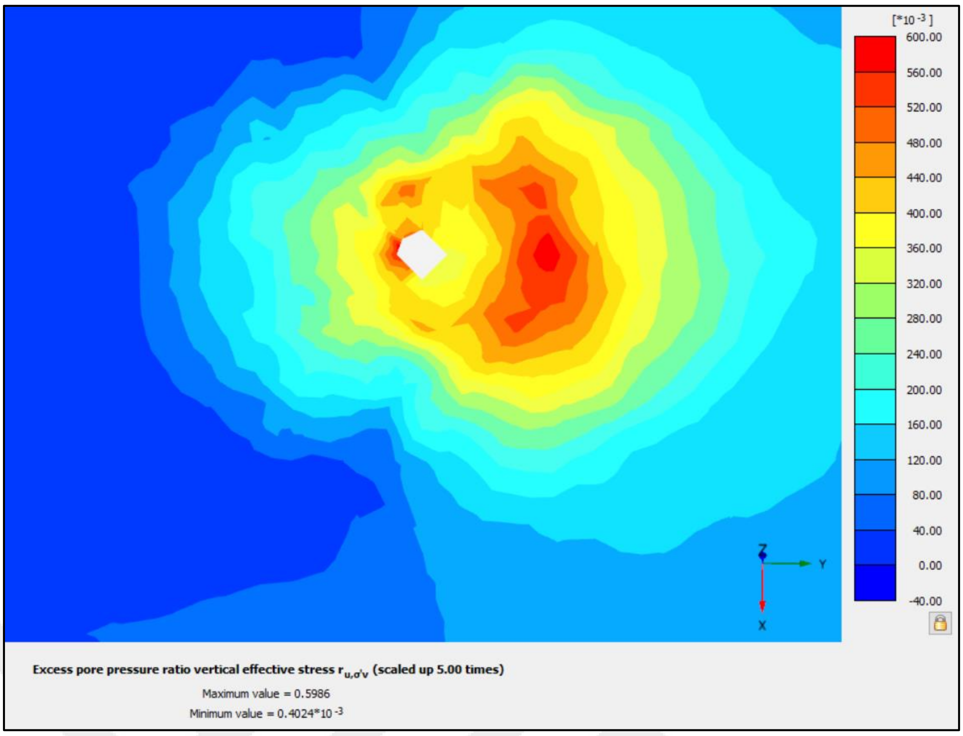

Figure 4. 2 Excess pore pressure ratio (r_u) at 3 meters depth under undrained and monotonic loading condition

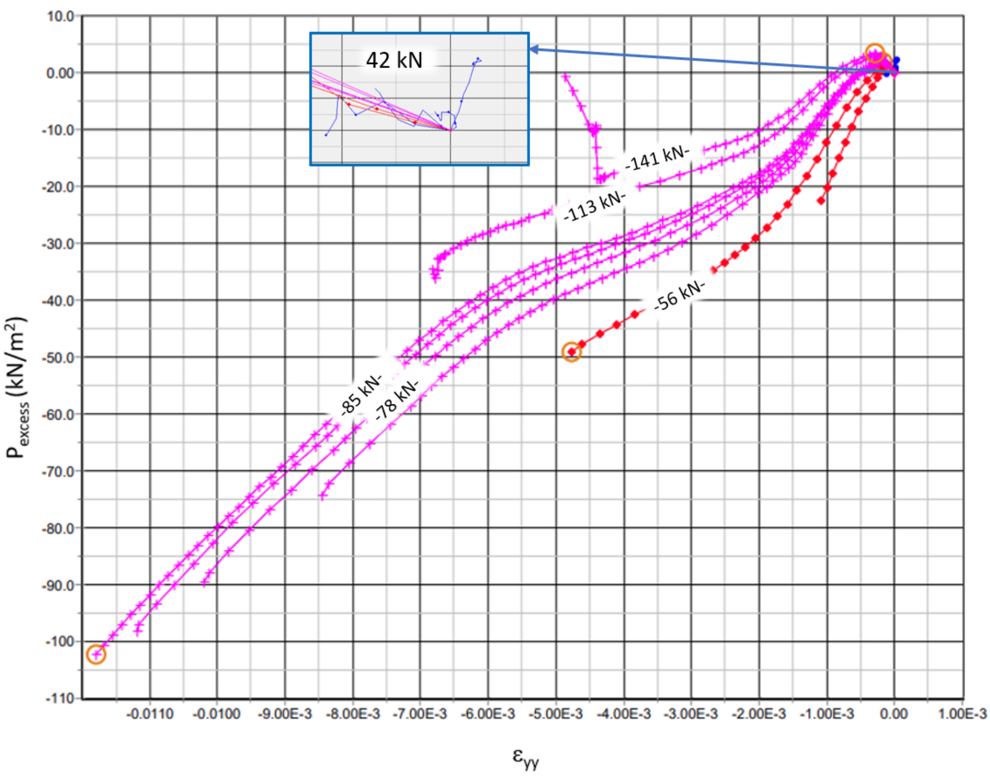

Figure 4.3 Excess pore water pressure with respect to horizontal strain adjacent to the pile surface

The figures obtained via undrained monotonic analyses demonstrate excess pore pressure generation potential due to pile displacement. Both dilative and compressive soil response-related pressure development tendency increases with loading intensity. Higher positive excess pore pressures are generated 1B away from the pile section surface, and they quickly diminish at 3.8B distance. At the pile-soil interface, dilative soil response is observed as a result of passive wedge development. Maximum induced pore pressure, however, did not induce liquefaction at 1B distance since initial effective vertical stress was σ'_{v0}=37.3 kPa as opposed to Δu_{max}=27.8 kPa.

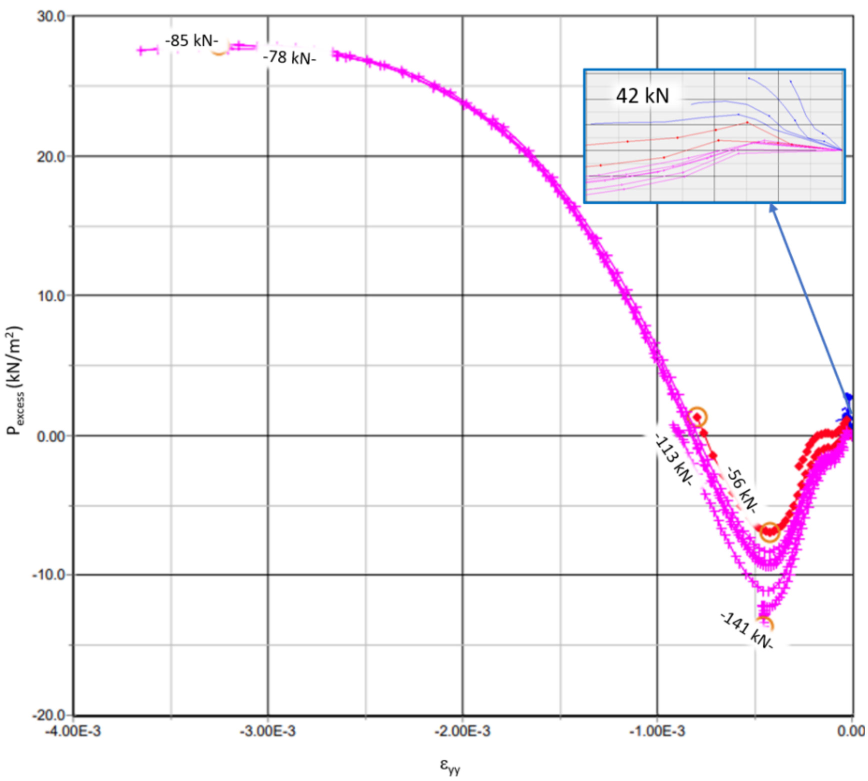

Figure 4.4 Excess pore water pressure with respect to horizontal strain 1B away from the pile surface

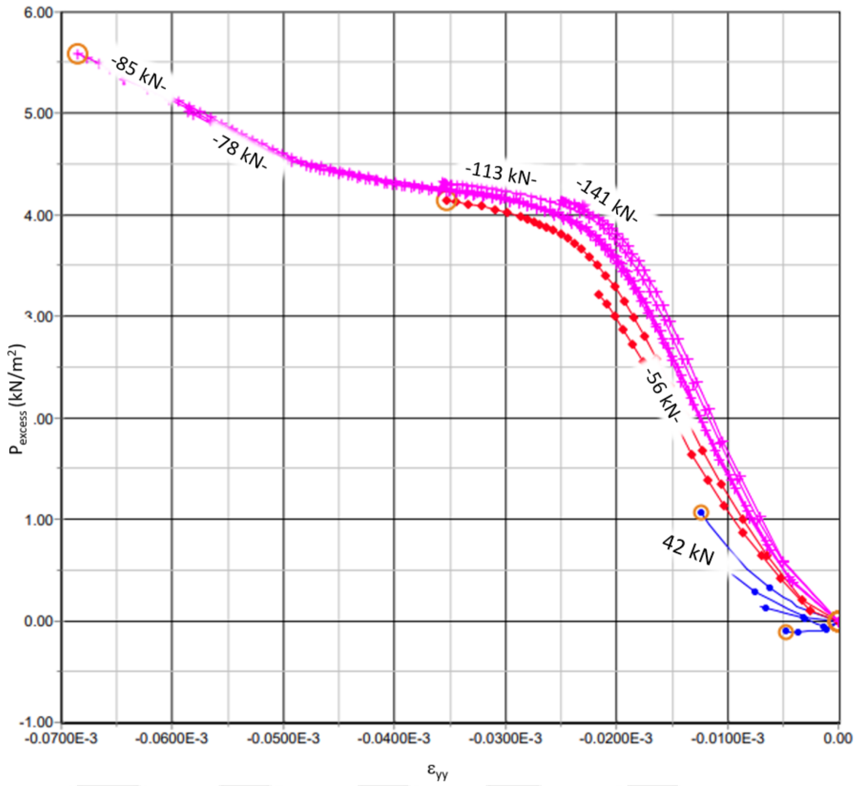

Figure 4.5 Excess pore water pressure with respect to horizontal strain 3.8B from away the pile surface

4.1.2 Cyclic Loading

Loading intensity varies between 25 kPa and 200 kPa in cyclic loading and undrained analyses. The cyclic loading frequency was set to 1 and 2 Hz. The influence of loading frequency and intensity on the achieved results are presented in terms of p′-q plots at a depth of 3m below the model surface. It may be followed in Figure 4.7 that a slight influence of loading frequency (1 Hz and 2 Hz) on deviatoric stress is pronounced in three-dimensional full-length pile analysis. A two-cycle analyses showed that 2 Hz cyclic loading with an amplitude of 42 kN (i.e. 150 kPa pile head cyclic traction) resulted in more than 30% decrease in deviatoric stress as compared with the 1Hz case. Although loading intensities are not the same with the full pile length analyses (Figure 4.5a), pile section (Figure 4.5b) runs at 1 Hz and 2 Hz cyclic loading with a magnitude of yielded a similar trend. It is interesting to note that deviatoric stresses are comparable for both cases probably because same initial effective stresses are achieved in pile section analyses (Fig. 4.8). A better insight might be captured by applying head loading as a cyclic displacement pattern with a magnitude equal to full pile length analyses. Loading intensity effects on deviatoric and mean effective stress levels are observed in Fig. 4.9. It is clear that excess pore water pressure generation reduces shear strength especially with lower loading intensities (i.e. 25 kPa and 75 kPa) where a steady decrease towards failure takes place. At larger loading levels, however, dilation takes place at a certain level and shear strength recovery occurs. Dilative tendency quickly disappears with the distance from the pile surface.

,

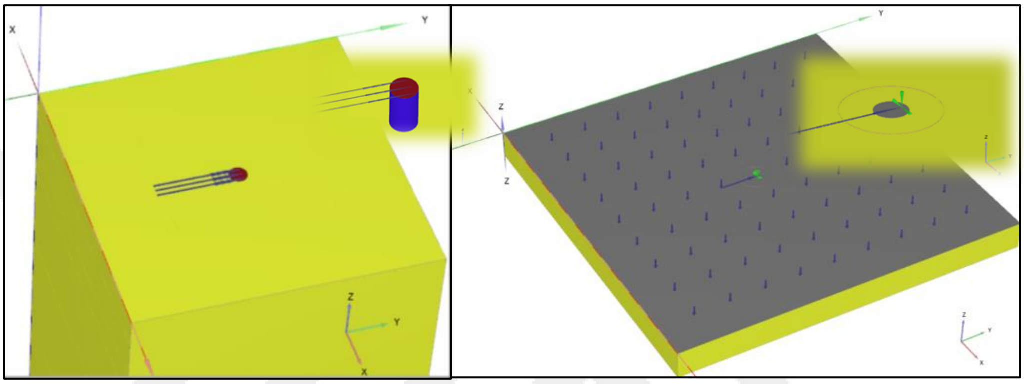

Figure 4.6 (a) Full - length pile cyclic head loading (b) section pile head loading

Cyclic inertial loading analyses continued at 1 Hz loading frequency on full pile length model this time applying the harmonic signal at 0.1 second intervals so that the passive and active wedge formations on the front and rear faces with respect to loading direction could be better traced with the consequent excess pore pressure field as well. The 3D dynamic analysis's loading density is 50-650 kPa. Analyzes were performed at 1Hz and 2Hz loading frequencies. Results from repeated analyses for different load densities are given in Figure 4.11-4.22. In Figure 4.14, we see that the displacements increase considerably for the 650 kPa load amplitude at which the pile is defeated. In Figures 4.13, 4.14, and 4.15, pore water pressure ratios taken from the sections in accordance with the examinations made for 1m, 3m, and 5m depths, respectively, higher gradients were obtained for the soil behind the pile due to loosening after the initial loading. The behavior in the analyses was idealized and evaluated (Figure 4.30). It was observed that the soil resistance remained constant during unloading. Then lower soil response was encountered during the reloading compared to the first loading. This behavior was also checked for monotonic analysis in the section model, and similar behavior was obtained (Figure 4.23). Here, it should not be overlooked that the soil is failed when the reloading is started, which is tried to be repeated for different load levels.

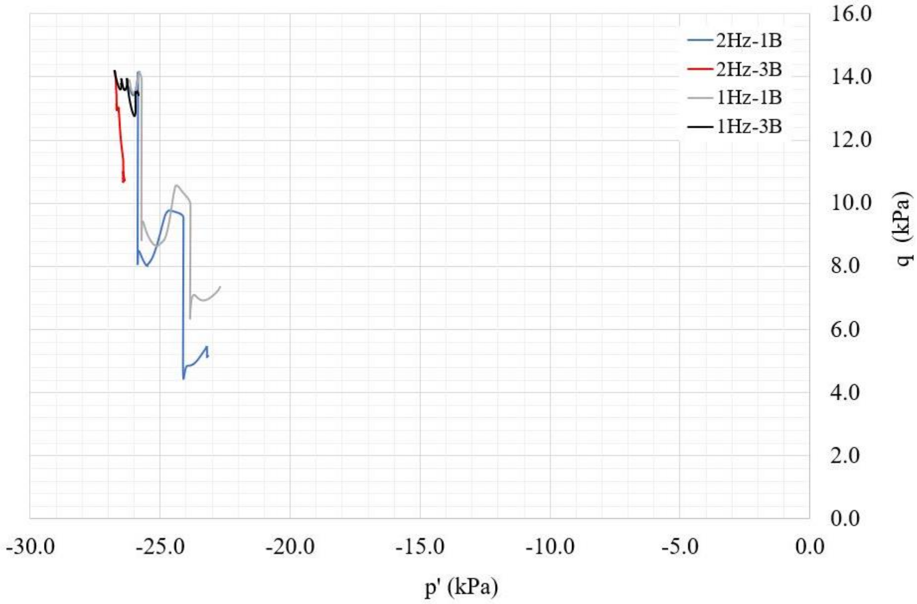

Figure 4.7 Variation of deviatoric stress versus mean effective stress in full pile length analyses

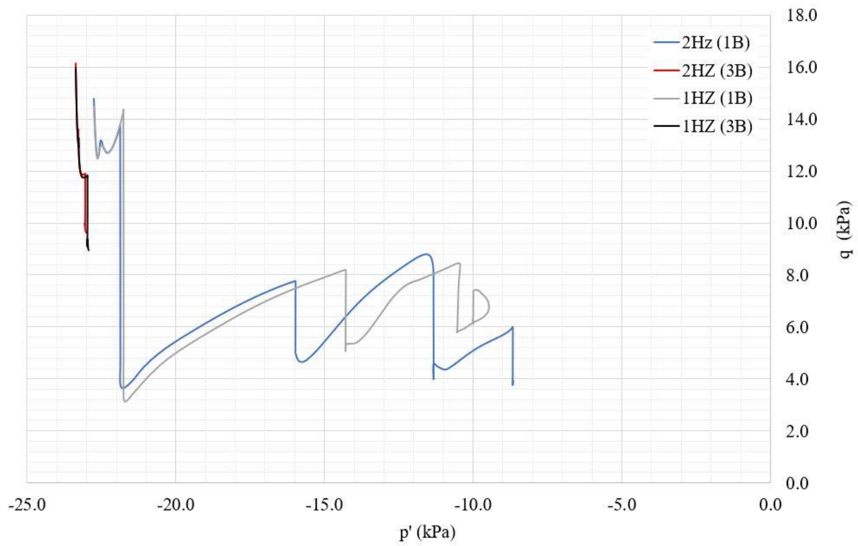

Figure 4.8 Variation of deviatoric stress versus mean effective stress in pile section analyses

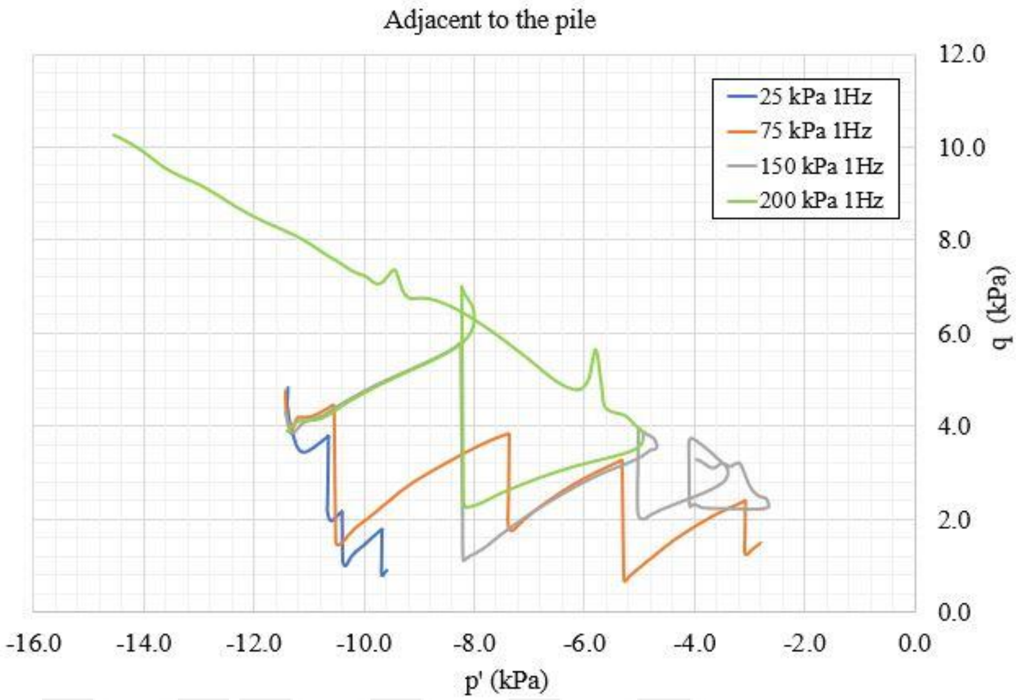

Figure 4.9 Influence of loading intensity on variation of deviatoric stress versus mean effective stress in pile section analyses (stress points adjacent to the pile)

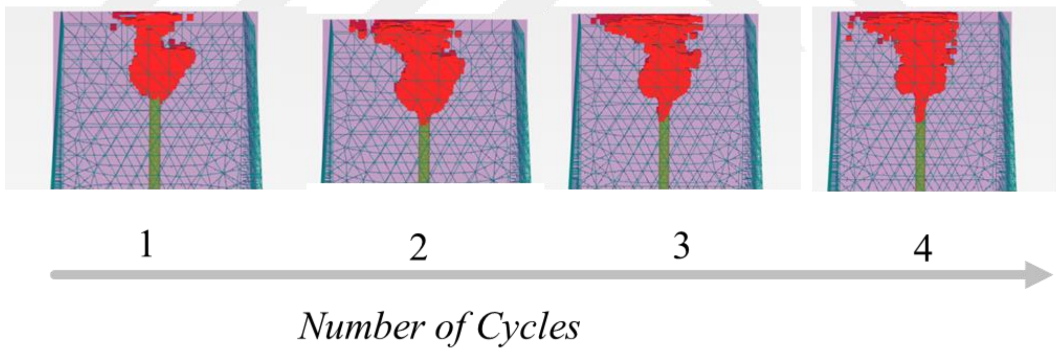

Figure 4.10 Plastic points at soil around displaced pile under cyclic loading conditions (with an amplitude of 650 kPa and 1Hz frequency at the ends of cycles (1-4))

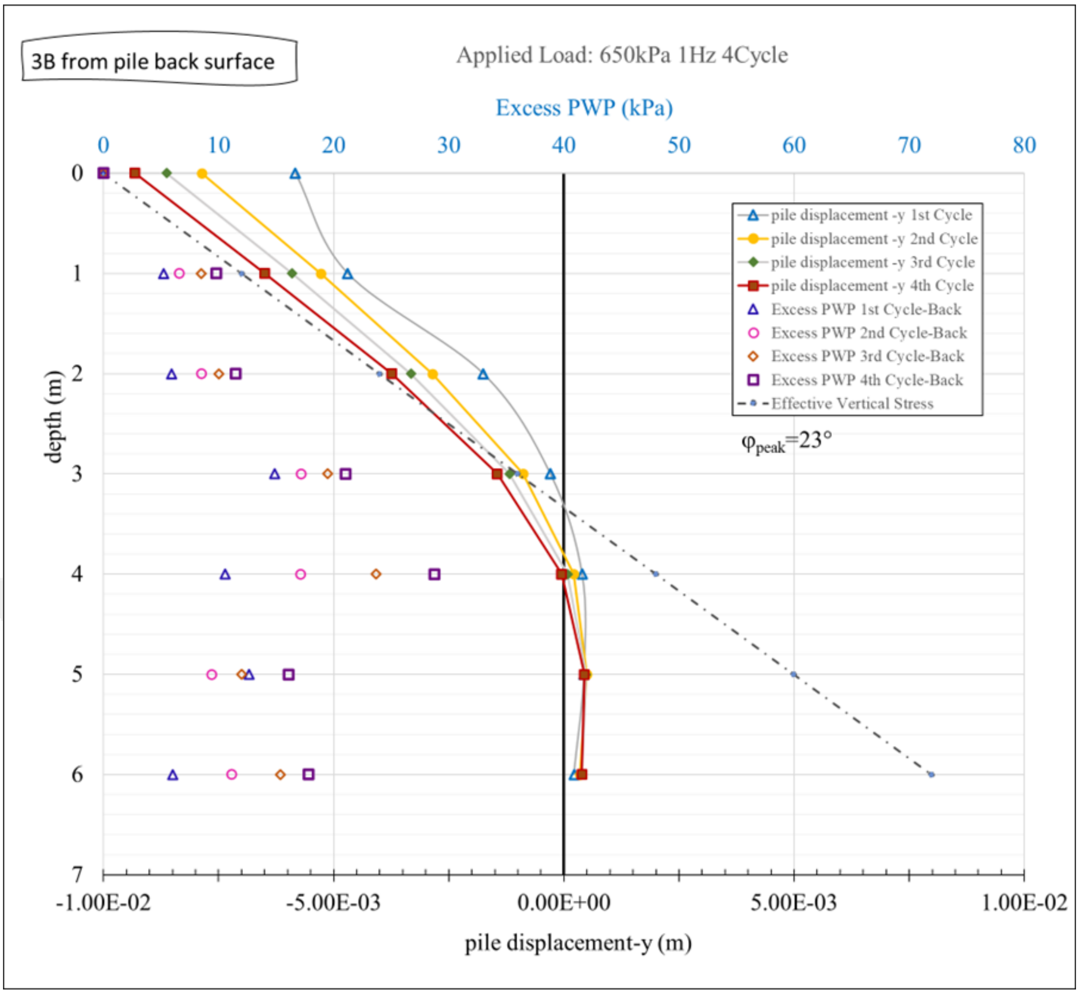

Figure 4.11 Excess pore pressure generation 3B from pile back and pile displacement along depth of full-pile length model under cyclic loading (with an amplitude 650 kPa and 1Hz frequency at the end of cycles

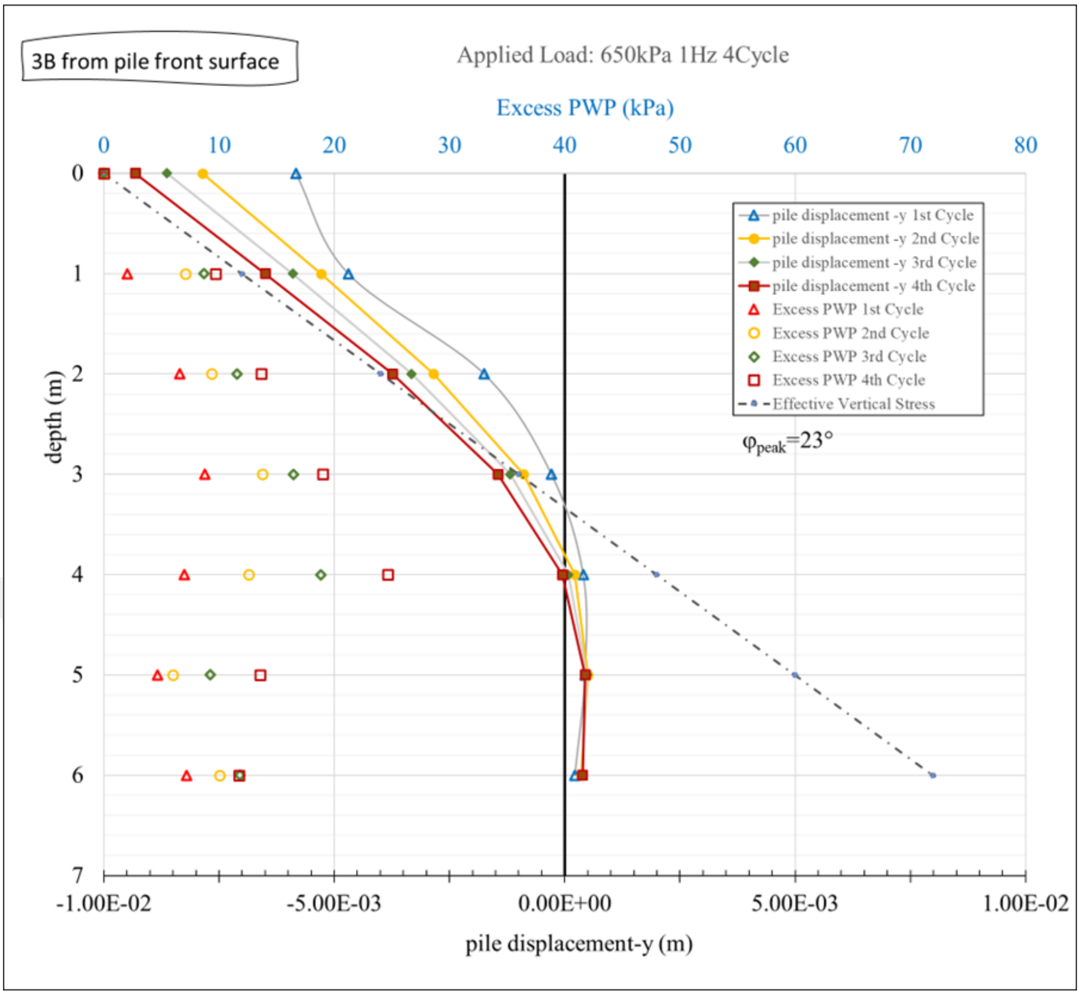

Figure 4.12 Excess pore pressure generation at 3B from pile front and pile displacement along depth of full-pile length model under cyclic loading (with an amplitude 650 kPa and 1Hz frequency at the end of cycles)

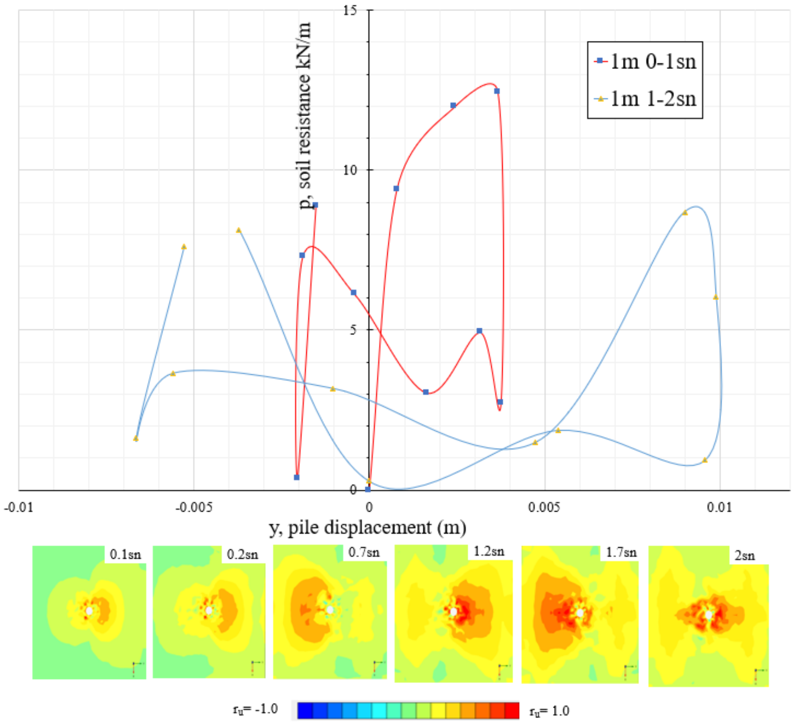

Figure 4.13 Soil resistance versus pile displacement at 1 meter depth under the cyclic loading with an amplitude 650 kPa and loading frequency is 1Hz

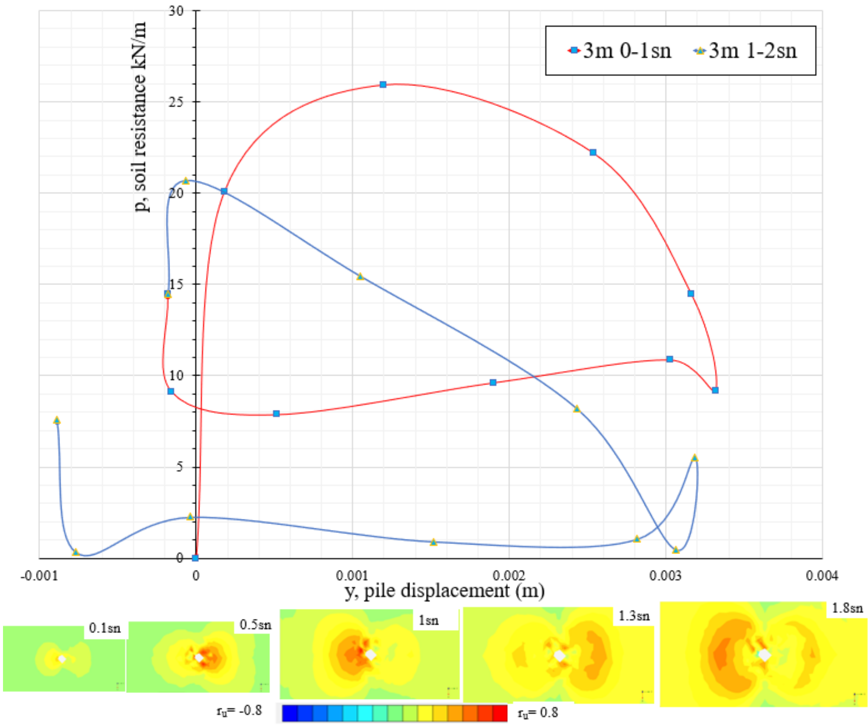

Figure 4.14 Soil resistance versus pile displacement at 3 meters depth under the cyclic loading with an amplitude 650 kPa and loading frequency is 1Hz

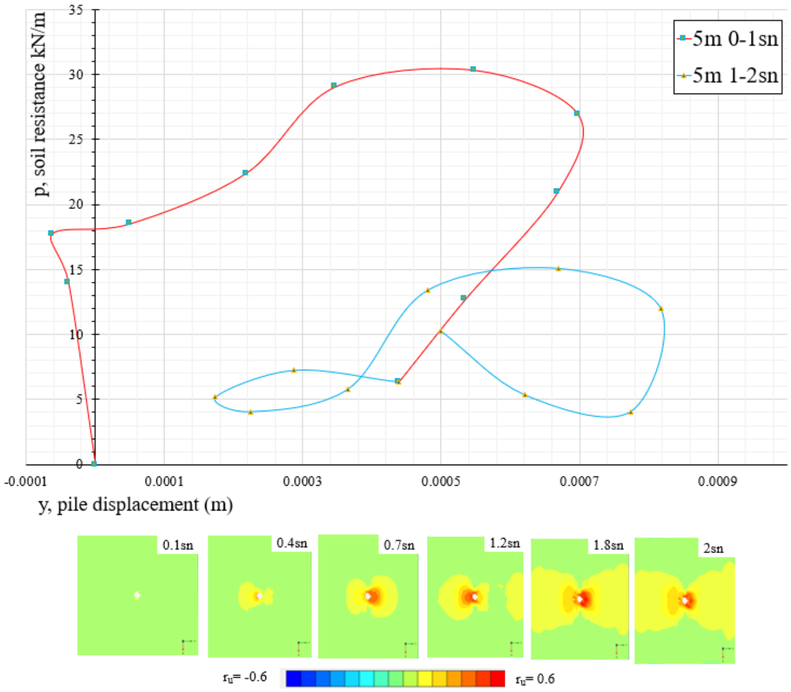

Figure 4.15 Soil resistance versus pile displacement at 5 meters depth under the cyclic loading with an amplitude 650 kPa and loading frequency is 1Hz

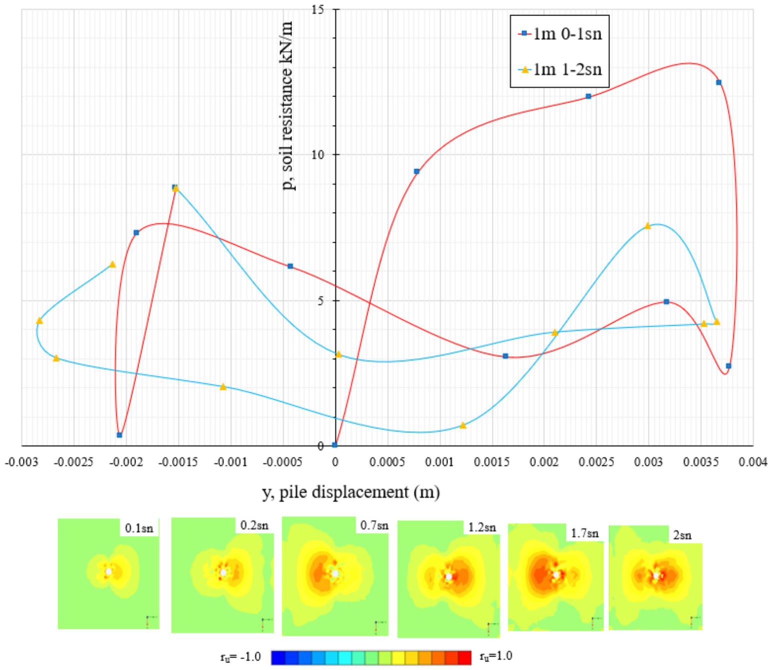

Figure 4.16 Soil resistance versus pile displacement at 1 meter depth under the cyclic loading with an amplitude 325 kPa and loading frequency is 1Hz

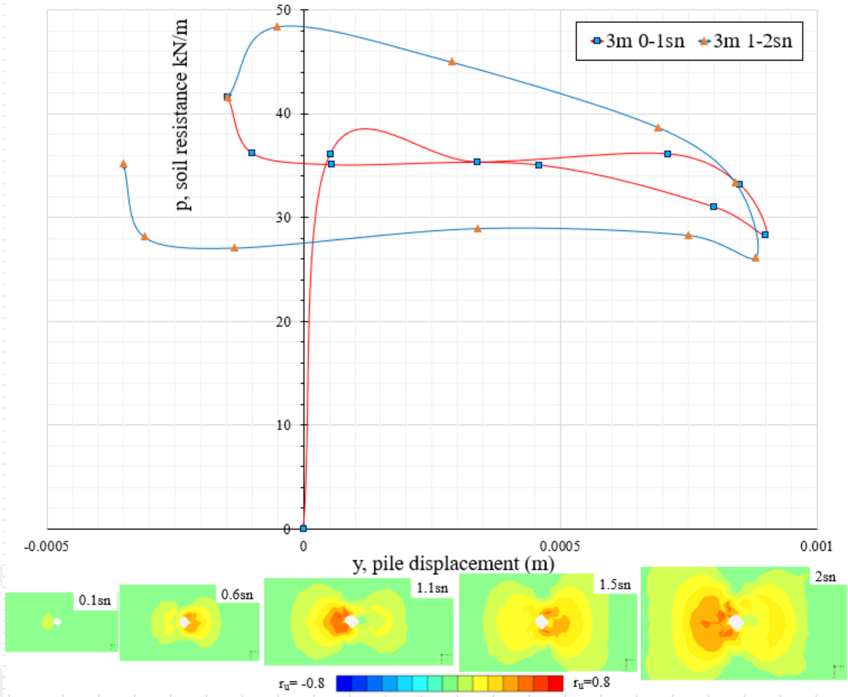

Figure 4.17 Soil resistance versus pile displacement at 3 meters depth under the cyclic loading with an amplitude 325 kPa and loading frequency is 1Hz

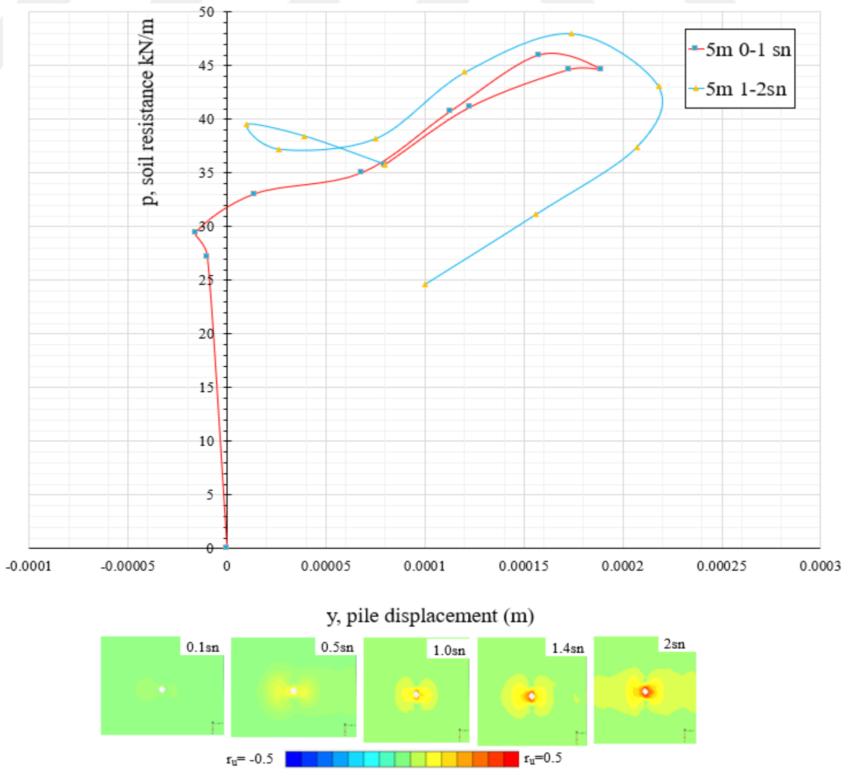

Figure 4.18 Soil resistance versus pile displacement at 5 meters depth under the cyclic loading with an amplitude 325 kPa and loading frequency is 1Hz

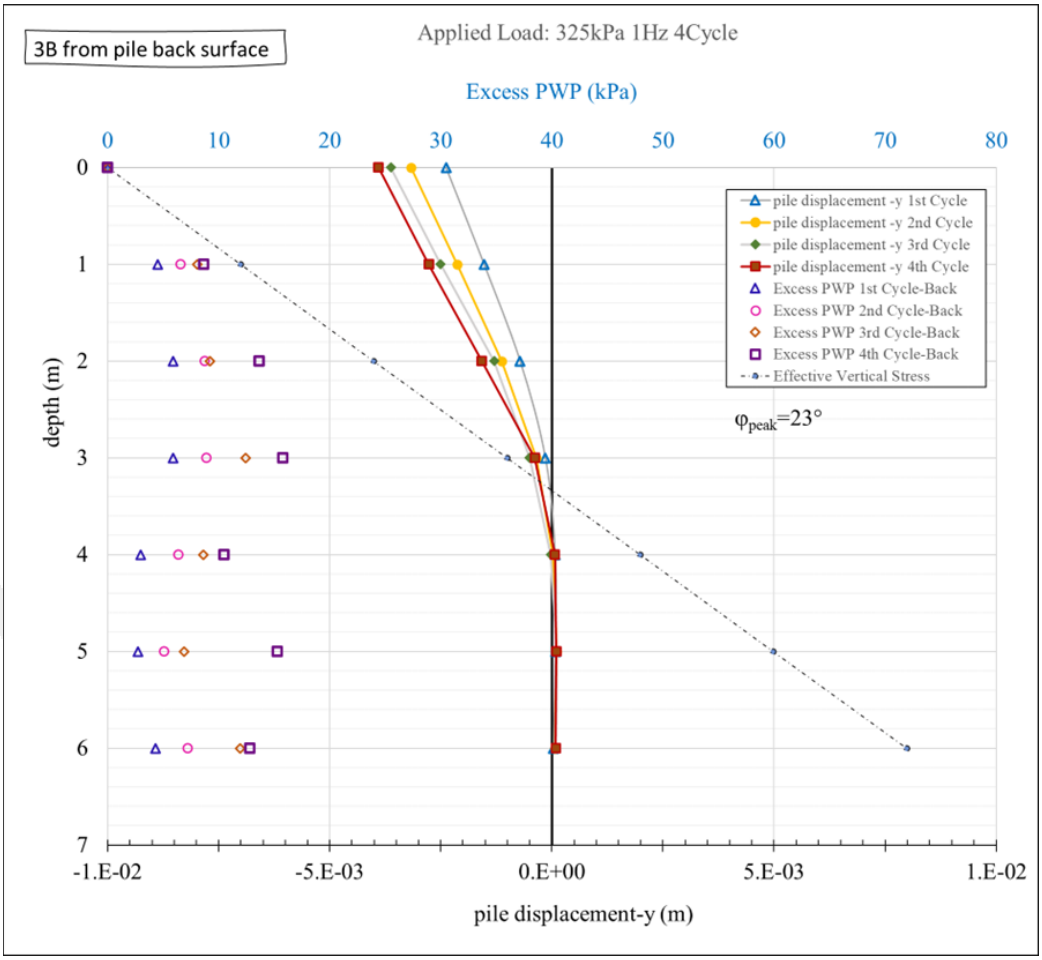

Figure 4.19 Excess pore pressure generation at 3B from pile back and pile displacement along depth of full-pile length model under cyclic loading (with an amplitude 325 kPa and 1Hz frequency at the end of cycles)

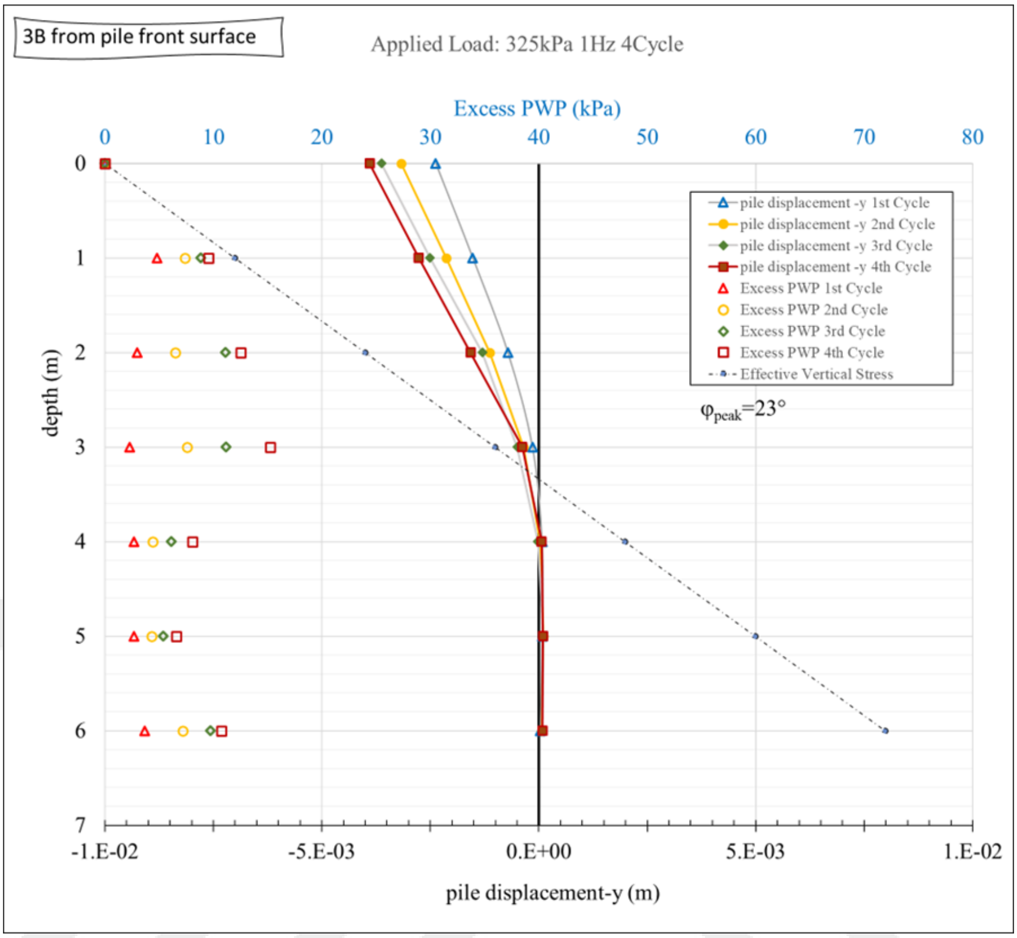

Figure 4.20 Excess pore pressure generation at 3B from pile front and pile displacement along depth of full-pile length model under cyclic loading (with an amplitude 325 kPa and 1Hz frequency at the end of cycles)

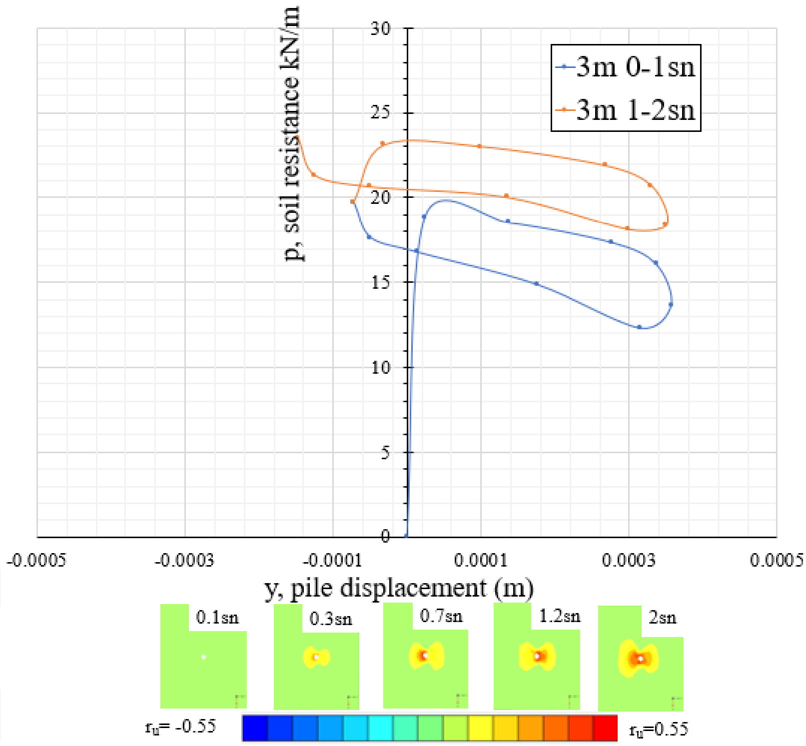

Figure 4.21 Soil resistance versus pile displacement at 3 meters depth under the cyclic loading with an amplitude 200 kPa and loading frequency is 1Hz

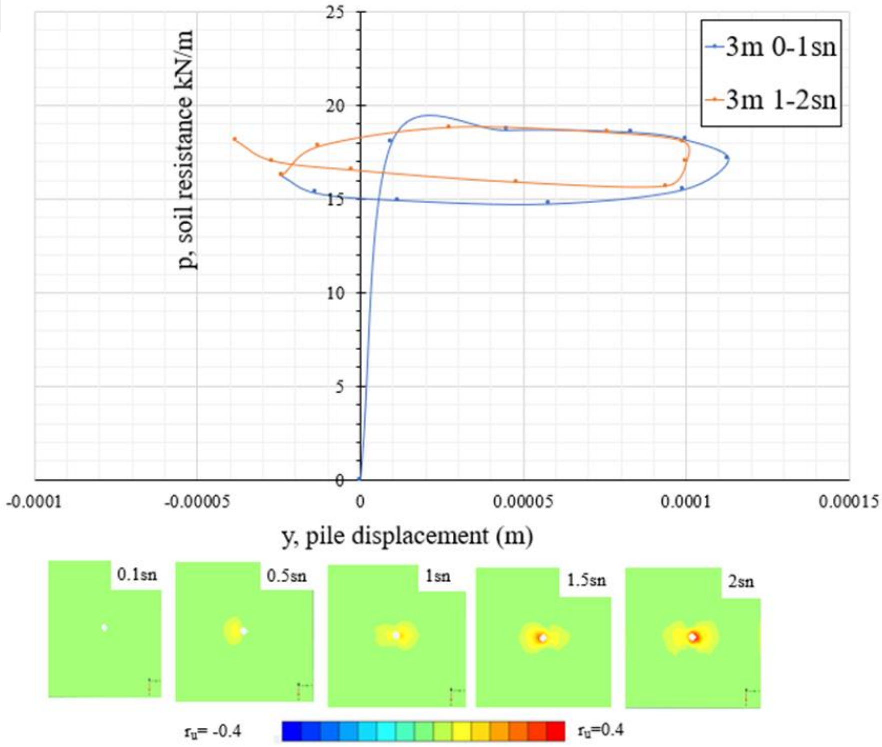

Figure 4.22 Soil resistance versus pile displacement at 3 meters depth under the cyclic loading with an amplitude 100 kPa and loading frequency is 1Hz

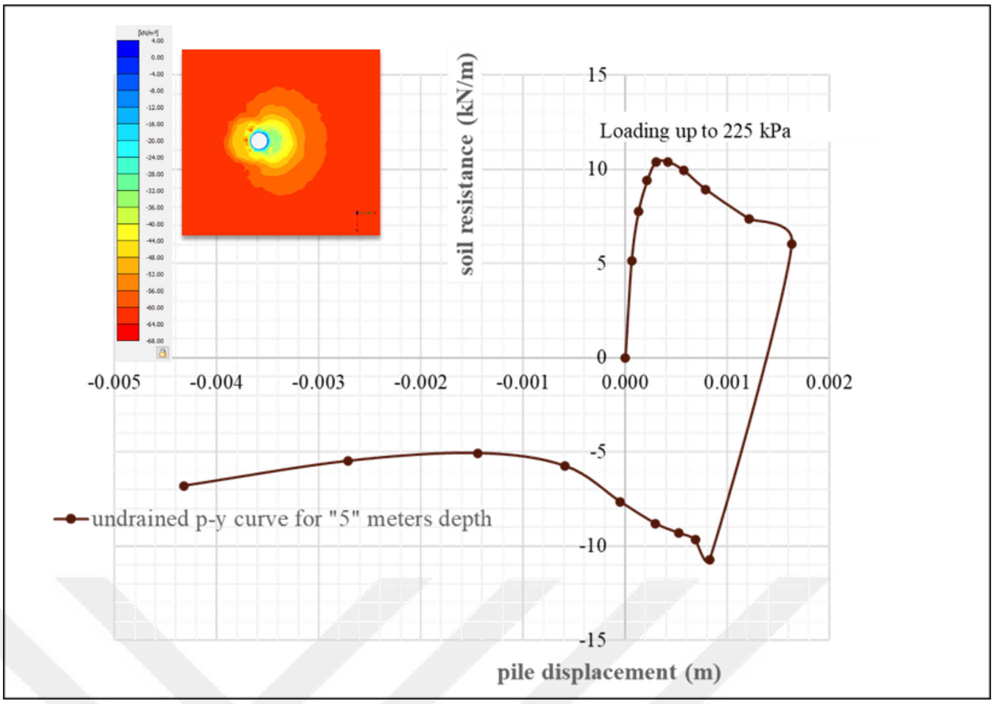

Figure 4.23 Soil resistance versus pile displacement at 5 meters depth under the monotonic loading up to 225 kPa

In the analyses made, the graphs obtained from the gradual monitoring of the cyclic loading showed us that the excess pore water pressure generation follows the average pile displacement calculated at the same depth. Since this trend, which we observed in our study investigating the inertial effects on excess pore pressure, includes findings that a relationship can be established between pile displacement and excess pore pressure ratio, these relationships are shed light on by using the curve fitting method. In the graph shown in Figure 4.24, the relationship between excess pore pressure ratio and pile displacement is plotted for undrained analyses performed under cyclic loading with an amplitude of 650 kPa and frequency of 1Hz with a fixed number of cycles. Here, besides the effects such as the number of cycles and depth, we obtained the excess pore water pressure ratio that could be expressed in pile displacement with second-order polynomial relationships where the correlation coefficient is above 0.9 (Figure 4.25). Kagawa and Kraft tried to shed light on the dynamic load-displacement curves for the soil going towards liquefaction in 1981. The relations obtained as a result of the analyses showed that the pore water pressure ratio in Equation 2.7 could be expressed in terms of pile displacement.

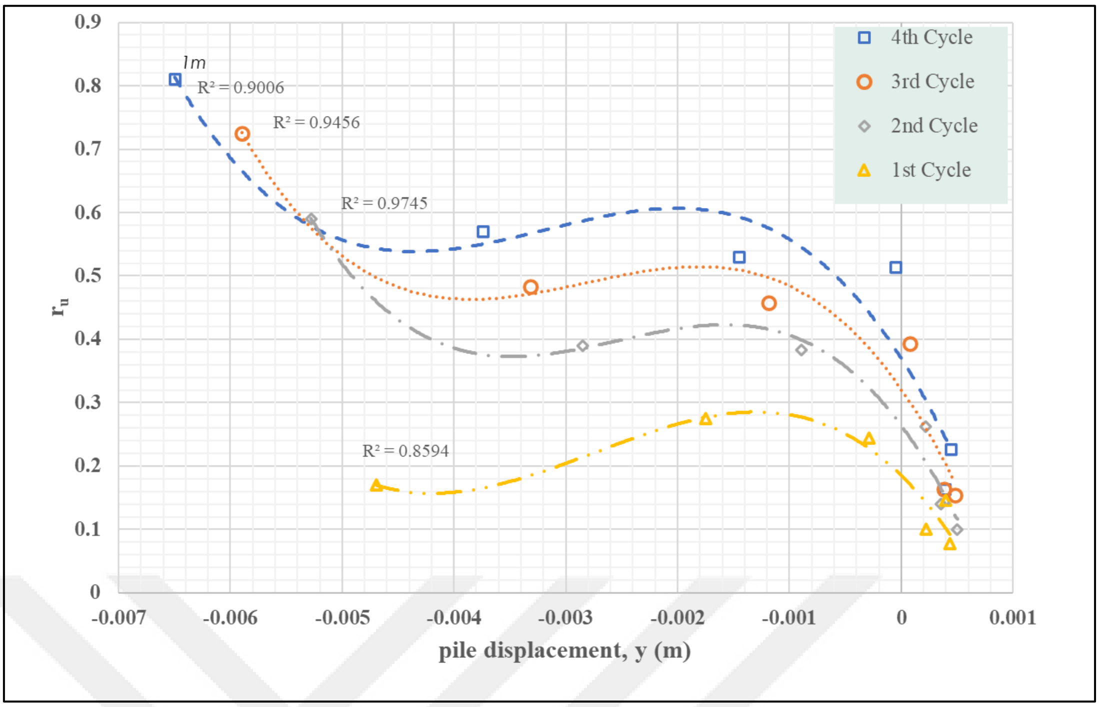

Figure 4.24 Soil resistance versus pile displacement at 5 meters depth under the cyclic loading with an amplitude 100 kPa and loading frequency is 1Hz

4th Cycle	$r = -10^7 \cdot y^3 - 101.1 \cdot 10^2 \cdot y^2 - 278.09 \cdot y + 0.3701$
3rd Cycle	$r = -10^7 \cdot y^3 - 103.489 \cdot 10^2 \cdot y^2 - 254.36 \cdot y + 0.321$
2nd Cycle	$r = -10^7 \cdot y^3 - 109.556 \cdot 10^2 \cdot y^2 - 237.61 \cdot y + 0.2641$
1st Cycle	$r = -10^7 \cdot y^3 - 86.817 \cdot 10^3 \cdot y^2 - 171.91 \cdot y + 0.1854$

Figure 4.25 Soil resistance versus pile displacement path due to loading amplitudes

4.2 Results of Kinematic Soil-Pile Interaction Analyses

The dynamic forces applied to the pile by the soil surrounding the pile and the inertial loads caused by the superstructure affect the pile foundation behavior under earthquake loads. Considering the internal forces arising in a pile, inertia loads are effective from the beginning of the pile to a depth of 15~20B, while kinematic loads dominate the behavior at deeper depths. The exception is when the pile head is rigidly attached to the foundation, or the pile passes through soil-rock formations with a contrasting stiffness.

When evaluated in terms of soil behavior, it is expected that the stress distribution occurring in the soil due to inertial loads or just due to the presence of the pile itself causes a change in excess pore water pressure, and the effective stress state in the immediate vicinity of the pile is expected to differ as compared with the free field soil state. This aspect of soil-pile interaction was studied by a series of numerical analyses where the soil was again represented by the UBC3D-PLM constitutive model. A harmonic motion was defined at the base of the model, and parametric analyses were made. Inertial loads are generated through the lumped mass placed at the pile head (Figure 4.26). Several types of analyses were performed at this stage of the research. These analyses consist of free field and free field plus pile cases as given in Table 4.3.

In these analyses, the earthquake acceleration was applied to the entire model base for two seconds with the dynamic surface displacement method. The frequency of the displacement applied at an amplitude of 0.15g was set to 1 hertz. In the analysis called Type-2, the lumped mass was modeled as a 120x120 volume element in cube geometry, and the desired weight was defined. In the Type-2.1 analysis, the analysis was repeated by increasing the superstructure weight. In these analyses, the pile is modeled by maintaining its normal weight and normal stiffness. In Type-3, while maintaining the pile stiffness, the pile weight was reduced to 10% of the actual weight, and the methodology was repeated. In Type-3.1, the superstructure load was preserved, and the pile was modeled at 10% weight and reduced flexibility (30% of Type 3 for instance). In Type-4, only the effect of the stiffness of the pile on the soil behavior was examined by means of kinematic analysis (i.e. no inertial loads). In Type-4.1, the superstructure load was removed, and the pile was modeled at 10% weight and reduced flexibility (30% of Type 3 for instance).The results of these analyses are discussed in the following sections.

Table 4.3 Kinematic interaction analyses schedule

Analyses Schedule of Kinematic Interaction					
Name	**Lumped Mass**	**Pile**	**Amplitude**	**Frequency**	**Loading Type**
Type-1	-	-	0.15g	1 Hz	Free-Field
Type-2	10194 kg	Pile	0.15g	1 Hz	Dynamic
Type-2.1	78290 kg	Pile	0.15g	1 Hz	Dynamic
Type-3	10194 kg	Pile (%10 Pile Weight)	0.15g	1 Hz	Dynamic
Type-3.1	10194 kg	Pile (%10 Pile Weight & %30 Pile Rigidity)	0.15g	1 Hz	Dynamic
Type-4	No Mass	Pile (%10 Pile Weight)	0.15g	1 Hz	Dynamic
Type-4.1	No Mass	Pile (%10 Pile Weight & %30 Pile Rigidity)	0.15g	1 Hz	Dynamic

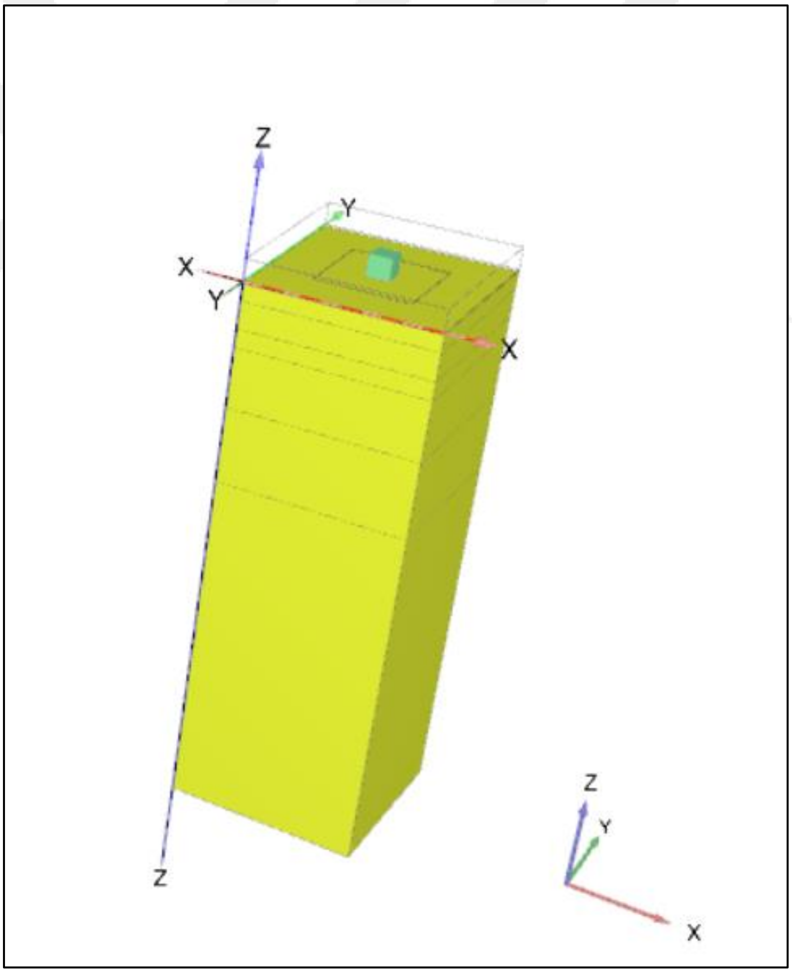

Figure 4.26 Kinematic analyses lumped mass modelling for 3d finite element analyses

The $r_{u,\sigma v'}$ state parameter from the analyses were read at the end of the 1 and 2 cycles to determine the trend in the active and passive regions of the pile separately for along the pile length. The graphs expressing the excess pore water pressure developments obtained and given in Figure 4.27.

After the inertial interaction analysis, the effect of inertia and the presence of pile on the excess pore water pressure was investigated when the cyclic loading was given from the bottom of the 3D model. The studies have observed that the movement approaches liquefaction as the number of cycles increases. In Figure 4.27, it is seen that the inertial loads relative to the free field and the presence of the pile increase the excess pore water pressure.

Figure 4.28 shows that as the pile head mass increases, the excess pore water pressure increases in the regions close to the surface and does not differ much in the depths because inertial loads are effective in areas near the ground surface. In addition, free-field and pile displacements are also compared and presented at the points where the pile is located (Figure 4.29).

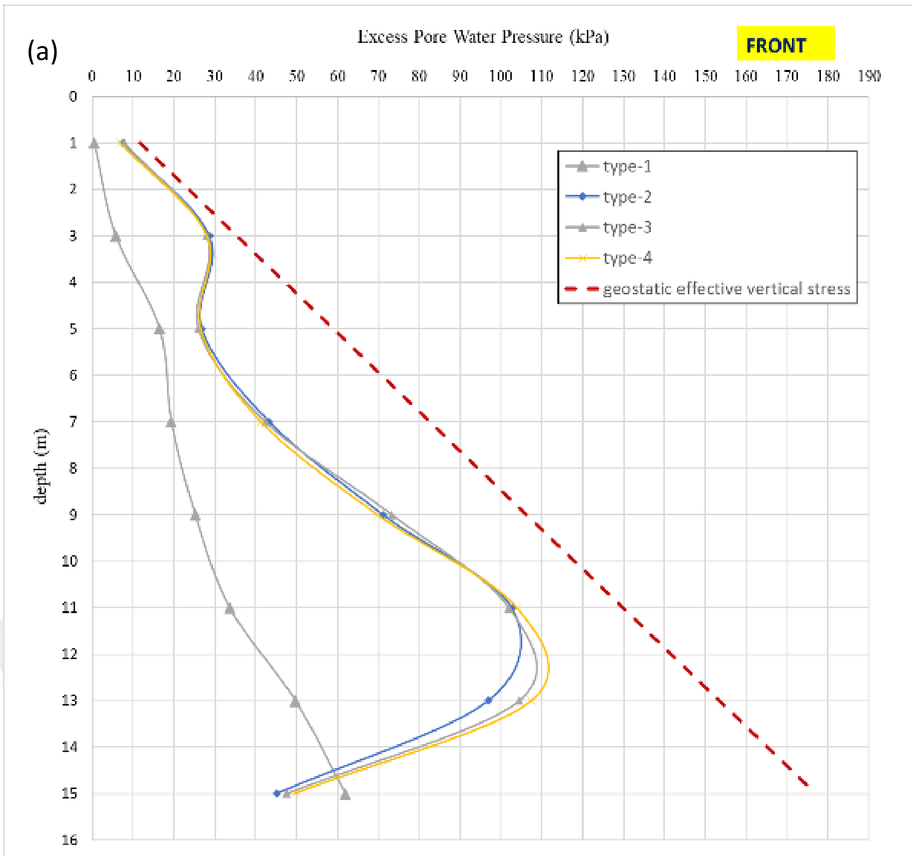

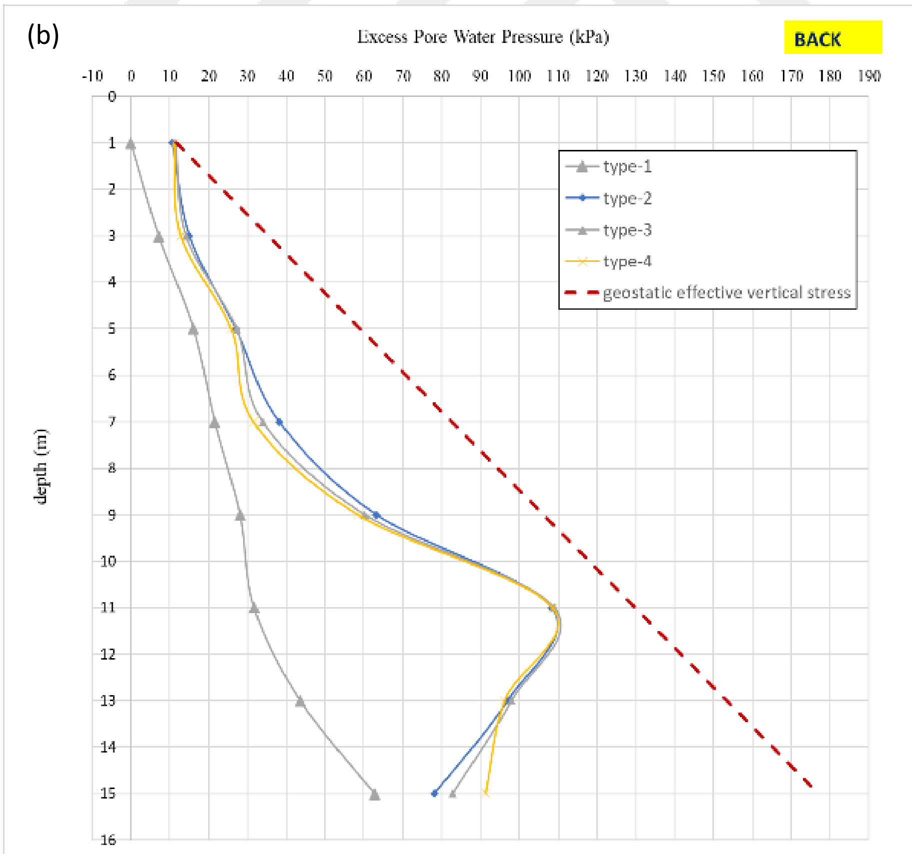

Figure 4.27 Excess pore water pressure regime across the depth at 2s, (a) adjacent to the pile-front side, (b) adjacent to the pile-back side

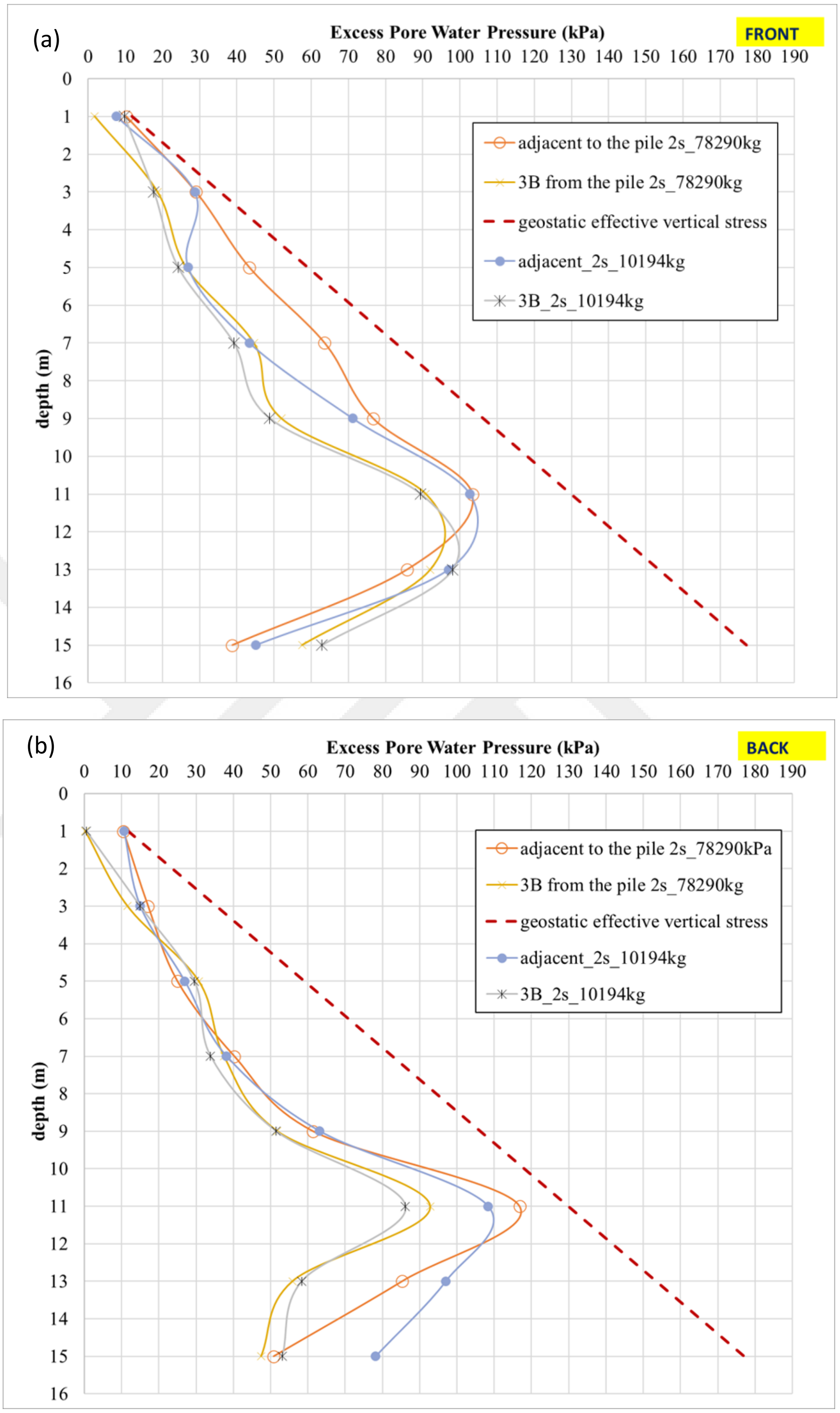

Figure 4.28 Excess pore pressure regime change due to superstructure weight at the end of 2 cycle (a) front of the pile (b) back of the pile

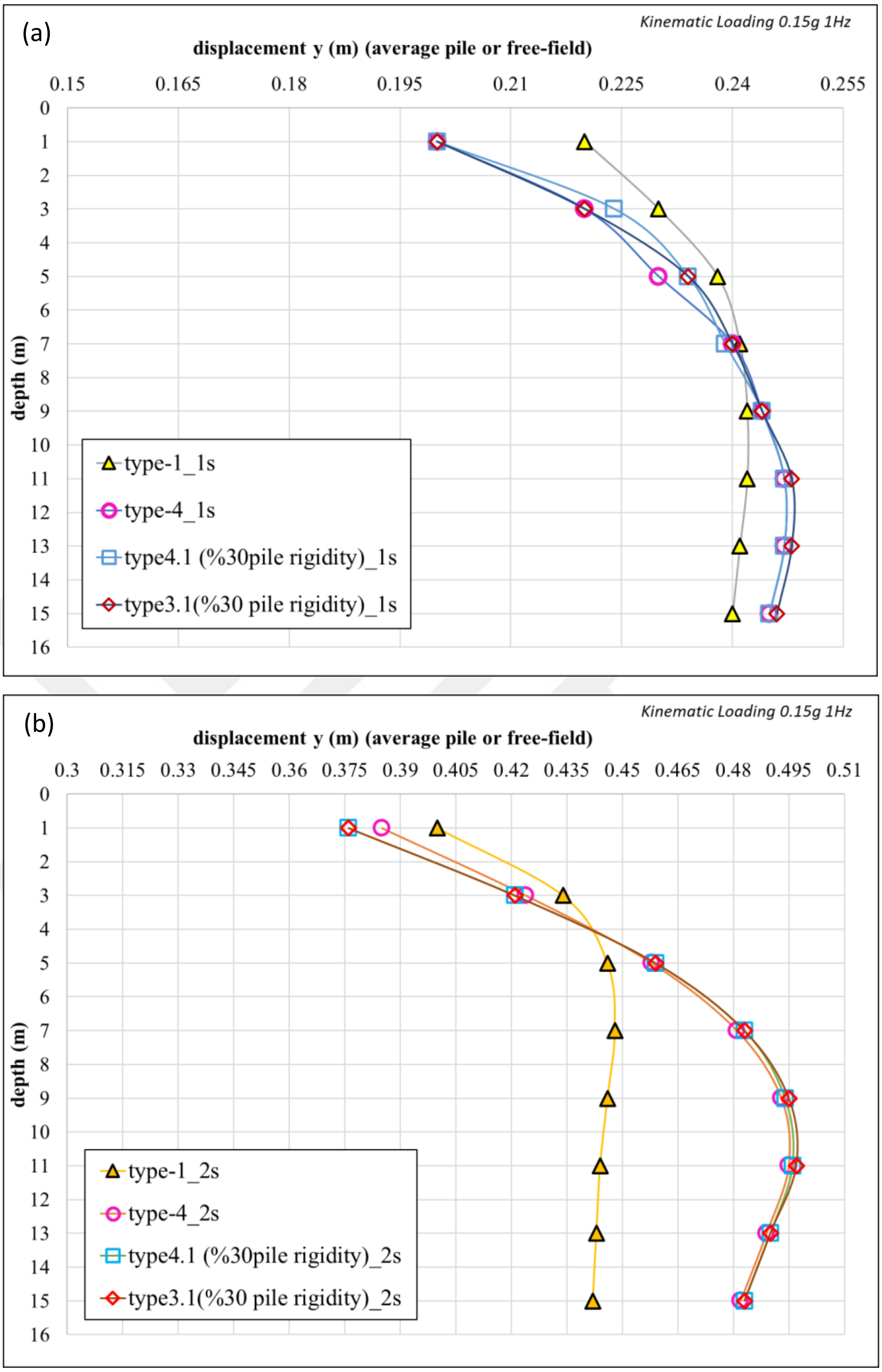

Figure 4.29 Comparison of presence the pile, presence the lumped mass and free-field displacements at the end of (a) 1s and (b) 2s

4.3 Discussions

Results of the above given inertial and kinematic analyses are discussed and interpreted as in the following:

1. In general, soil behavior differs between the initial loading phase and the subsequent unloading and reloading phases. During initial loading, the ground in front of the pile is in passive condition, while the ground behind the pile is in active. As the passive region compresses, the active region loosens.

2. Because the strength has already been reduced during unloading, the active soil zone liquefies quickly. This behavior is generally valid for all depths. During unloading, the stiffness of the soil decreases significantly, and the load-displacement curve follows a nearly horizontal path.

3. Excess pore water pressure decreases during initial loading and unloading since dilatation occurs in the passive soil zone. The decrease in soil resistance at 3m level is less as compared with 1m and 5m. This may be attributed to the fact that dilatation and consequent strength gain is prominent at this depth.

4. Excess pore water pressure development increases with increasing dynamic load amplitude at the pile head. During unloading and reloading, soil resistance is significantly reduced. However, the relationship between the load increment and pore water pressure increase is not directly proportional. Because of soil dilatation, excess pore water pressure development may decrease as the load amplitude increases.

5. Achieved results show that lateral load-displacement curve (p-y) for inertial loading conditions may be idealized as in the following figure (Fig.30). The unloading and reloading sections of the curve pose little stiffness and therefore may be idealized with a line parallel to the displacement axis. It is thought that results of monotonic undrained pile section analyses are in fair agreement with those of dynamic three-dimensional analyses.

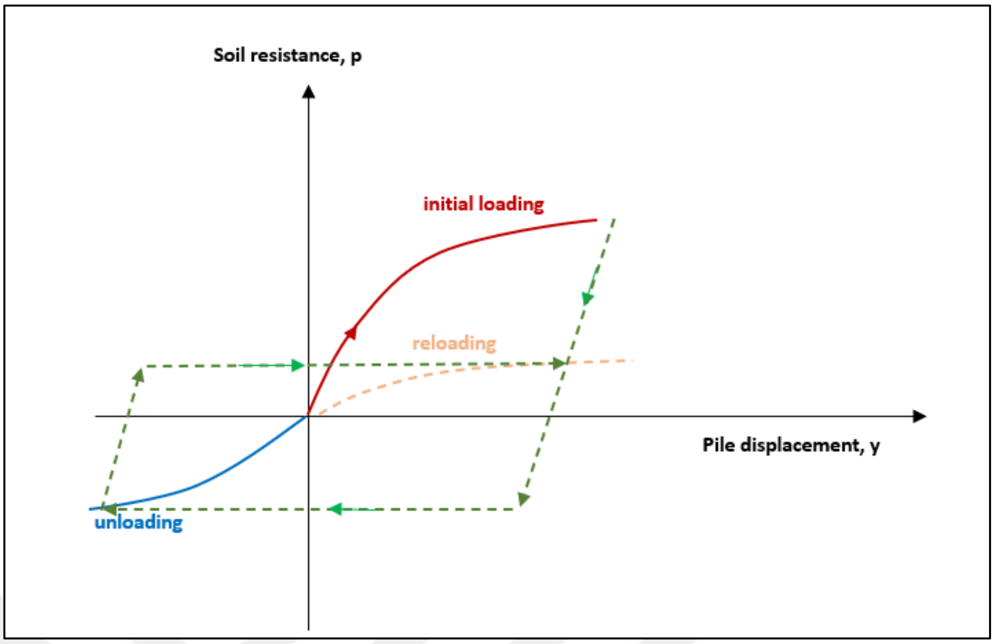

Figure 4.30. Idealized lateral load-displacement curve for piles under inertial dynamic loads

6. The relationships obtained as a result of the analyses can be tested for situations such as different loading frequencies, increasing the number of cycles, and different soil properties and charts can be created by expanding them. The given model can allow the generation of dynamic load-displacement curves for undrained conditions and the derivation of backbone curves for the case where springs are defined to represent the ground by three-dimensional modeling of the superstructure and foundation, which is a common analysis method placed in earthquake codes.

7. Presence of inertial loading has found to be not so influential on excess pore pressure generation with depth as compared with free field case.

8. Influence of the pile on excess pore water pressure quickly diminishes with the horizontal distance for a particular depth. Loading intensity affects the amount of induced pore pressures.

9. The gap between the pile and free field displacements gradually develops as dynamic loading progresses.

CHAPTER FIVE

CONCLUSIONS AND RECOMMENDATIONS

5.1 Conclusions

Finite element analyses results presented herein show that UBC3D-PLM model can be utilized in soil-pile interaction research that targets excess pore pressure accumulation in very loose sandy soils if care is spent on the established numerical model since UBC model may be quite sensitive to boundary value problems.

Pile section analyses are found to be applicable to the inertial cyclic loading cases. Full pile length and pile section analyses yielded similar but not the same results. Although spatial redistribution of excess pore water pressure can be handled in pile section model, high gradients parallel to the pile surface along the interface cannot be handled for the time being. As a result of this, generated excess pore water pressures are less and soil strength reduction is not that sharp in 3D full pile length model. Both full length and pile section models showed that high pressure gradients take place at the soil-pile interface and dilative response occurs at larger loading amplitudes. Presented p′-q plots and p-y curves belong to a case where soil depth is 3m below the model surface.

Achieved results show that presence of pile is quite important on excess pore water pressure generation. This consideration is valid both for dynamic head loading and dynamic loading applied at the base of the model.

Computed dynamic load-displacement curves indicate that the unloading and reloading sections pose very little stiffness and soil resistance greatly decreases as the soil zone that has been in active condition during initial loading at the back of the pile is loaded. This zone does not develop passive resistance unless dilatation and consequent strength gain as a result of excess pore water dissipation takes place.

A clear trend was observed when the excess pore pressure ratio and pile displacement were correlated with the curve fitting method. The investigations revealed that the excess pore pressure ratio could be expressed in terms of pile displacement.

Although the research conducted within the scope of this thesis provided an insight regarding influence of inertial loading on excess pore water pressure development, further research is recommended on the subject as in the following:

1. Dynamic analyses shall be enhanced for larger number of cycles to study dilatation and degradation mechanisms around the pile.

2. A lateral load-displacement curve model may be developed by modelling the excess pore water pressure generation around the pile.

3. Influence of pile flexibility on induced pore pressures may be studied by decreasing pile stiffness in dynamic analyses.

4. Model tests may be performed on small scale and a database may be formed by compiling available dynamic test data in the literature.

5. The excess pore pressure ratio-pile displacement relationships may be repeated for the increased number of cycles, different soil profiles, and different loading frequencies.

REFERENCES

Abdoun T., Dobry R., Zimmie T.F., & Zeghal M. (2005). Centrifuge research of countermeasures to protect pile foundations aganist liquefaction-induced lateral spreading. *Journal of Earthquake Engineering*, *9*(1), 105-125.

Abdrabbo F.M., & Gaaver K.E. (2012). Simplified analysis of laterally loaded pile groups. *Alexandria Engineering Journal*, *51*(2), 121-127.

American Petroleum Institute, (2000). Recommended practice for planning, designing and constructing fixed offshore platforms (Standard), *API*, Washington, D.C.

Aydınoğlu M.N. (2011). Zayıf zeminlerde yapılan binalarda dinamik yapı-kazık-zemin etkileşimi için uygulamaya yönelik bir hesap yöntemi. *Boğaziçi Üniversitesi Kandilli Rasathanesi ve Deprem Araştırma Enstitüsü Deprem Mühendisliği Anadilim Dalı Raporu*, İstanbul, 1.

Berrill, J., & Yasuda, S. (2002). Liquefaction and piled foundations: some issues. *Journal of Earthquake Engineering, 6*(S1), 1-41.

Bhattacharya S., & Bolton M. (2004). Buckling of piles during earthquake liquefaction. *13th World Conference on Earthquake Engineering*, Vancouver, B.C., Canada.

Bhattacharya S., Adhikari S., & Alexander N.A. (2009). A simplified method for unified buckling and free vibration analysis of pile-supported structures in seismically liquefiable soils. *Soil Dynamics and Earthquake Engineering, 29*(8), 1220–1235.

Boulanger R.W., Curras C.J., Kutter B.L., Wilson B.W., & Abghari A. (1998). Seismic soil-pile-structure interaction experiments and analyses. *Journal of Geotechnical and Geoenvironmental Engineering*, *125*(9), 750-759.

Bowen H.J., & Cubrinovski M. (2008). Effective stress analysis of piles in liquefiable soil; A case study of a bridge foundation. *Bulletin of The New Zealand Society for Earthquake Engineering, 41*(4).

Brown D., Morrison C., & Reese L.C. (1988). Lateral load behaviour of pile group in sand. *Journal of Geotechnical Engineering*, *114*(11), 1261-1276.

Brown D.A., Reese L.C., & O’Neill M.W. (1987). Cyclic lateral loading of a large-scale pile group. *Journal of Geotechnical Engineering*, *113*(11), 1326-1343.

Budkowska B.B. & Elmarakbi A. (2001). The assessment of shear effect of soil in analysis of laterally loaded models of the piles. *Mechanics and Computation*, *1,* 755-762.

Chenaf N. & Chazelas J.L. (2008). The Kinematic and Inertial Soil-Pile Interactions: Centrifuge Modelling. *3rd International Workshop of Young Doctors in Geomechanics*, 65-68.

China. Ministry of Construction of the People. (2001). Code for seismic design of buildings, *China Architecture & Building Press*.

Cubrinovski M., Ishihara K., & Furukawazono K. (1999). Analysis of Full-Scale Tests on Piles in Deposits Subjected to Liquefaction. *2nd International Conference on Earthquake Geotechnical Engineering*, Lisbon, Portugal.

Cubrinovski M., Kokusho T., & Ishihara K. (2006). Interpretation from large-scale table tests on piles undergoing lateral spreading in liquefied soils. *Soil Dynamics and Earthquake Engineering, 26*(2-4), 275-286.

Dash S.R. & Bhattacharya S. (2007). Criteria for design of piled foundations ın seismically liquefiable deposits. *4 th International Conference on Earthquake Geotechnical Engineering*, Thessaloniki, Greece, 1724.

Dash S.R., Govindaraju L., & Bhattacharya S. (2009). A case study of damages of the Kandla Port and Customs Office tower supported on a mat-pile foundation in liquefied soils under the 2001 Bhuj Earthquake. *Soil Dynamics and Earthquake Engineering, 29*(2), 333–346.

Dobry R. & Liu L. (1994). Centrifuge Modelling of Soil Liquefaction. *Earthquake Engineering 10. World Conference*, Rotterdam, 6801-6809.

Dutta S.C. & Roy R. (2002). A critical review on idealization and modeling for interaction among soil-foundation-structure system. *Computers and Structures, 80*(20-21), 1579-1594.

Erdoğan D., Altun S., Sezer A. & Özden G. (2007). Kinematik zemin-kazık etkileşiminin winkler temeline oturan kiriş yöntemi ile analizi. *Zemin Mekaniği ve Temel Mühendisliği 1. Özel Konulu Sempozyumu*, İstanbul.

Fan C. C., & Long J. H. (2005). Assessment of existing methods for predicting soil response of laterally loaded piles in sand. *Computers and Geotechnics, 32*(4), 274-289.

Fayyazi M.S., Taiebat M., Finn W.D.L., & Ventura C.E. (2012). Evaluation of p-multiplier method for performance-based design of piles groups. *Second*

International Conference on Performance-Based Design in Earthquake Geotechnical Engineering, Taormina, Italy.

Finn W.D.L., Yoshida N., & Lee M.K. (2000) DESRA-2C, dynamic effective stress analysis of soil deposits with liquefaction beneath an impermeable layer with energy transmitting boundary. Department of Civil Engineering, University of British Columbia, Vancouver.

Finn W. D. L. & Fujita N. (2002). Piles in liquefiable soils: seismic analysis and design issues. *Soil Dynamics and Earthquake Engineering, 22*(9-12), 731-742.

Finn W.D.L. & Fujita N. (2002). Piles in liquefiable soils: seismic analysis and design issues. *Soil Dynamics and Earthquake Engineering, 22*(9-12), 731-742.

Fukuoka M. (1966). Damage to civil engineering structures. *Soils and Foundations, 6*(2), 45-52.

Ghosh B., Mian J., & Lubkowski Z.A. (2012). Design of Piles in Liquefiable Soil: A Review of Design Codes and Methodologies. *The 15th World Conference on Earthquake Engineering*, Lisbon.

Hamada M., Yasuda S., Isoyama R., & Emoto K. (1986) Study on liquefaction induced permanent ground displacements. *Report for the development of earthquake prediction*, Tokyo Japan.

Hamada M., & O'Rourke T. D. (1992). Case studies of liquefaction and lifeline performance during past earthquakes. *Japanese Case Studies. Technical Rep. NCEER-92*(1), pp.1-28.

Horikoshi K., Tateishi A., & Ohtsu H. (2000). Detailed Investigation of Piles damaged by Hyogo-ken Nambu Earthquake. *12th World Conference on Earthquake Engineering*, 2477.

Humar J.L., Bagchi A., & Xia H. (1998). Frequency domain analysis of soil-structure interaction. *Computer and Structures, 66*(2-3), 337-351.

Hwang J., Kim C., Chung C., & Kim M. (2006). Viscous fluid characteristics of liquefied soils and behaviour of piles subjected to flow of liquefied soils. *Soil Dynamics and Earthquake Engineering, 26*(2-4), 313-323.

Ishihara K. (1996). Soil behaviour in earthquake geotechnics, *Oxford Science Publications.*

Ishihara K. (1997). Terzaghi Oration: Geotechnical Aspects of the 1995 Kobe Earthquake. *Proceedings of Fourteenth International Conference on Soil Mechanics and Foundation Engineering*, 2047-2073.

Ishihara K. (1997). Terzaghi oration: Geotechnical aspects of the 1995 Kobe earthquake. *In Proceedings of The International Conference on Soil Mechanics and Foundation Engineering-International Society for Soil Mechanics and Foundation Engineering, 4*, 2047-2074.

Ishihara K. & Cubrinovski M. (1998). Performance of large-diameter piles subjected to lateral spreading of liquefied deposits. *13th Southeast Asian Geotechnical Conference*, Taipei.

Klar A., Baker R. and Frydam S. (2004). Seismic soil-pile interaction in liquefiable soil. *Soil Dynamics and Earthquake Engineering, 24*(8), 551-564.

Kramer S. L. (1996*). Geotechnical Earthquake Engineering*, PrenticeHall, Englewood Cliffs, N. J., 653.

Kramer S. L. & Elgamal A. W. (2001). Modeling soil liquefaction hazards for performance-based earthquake engineering. *PEER Report 2001/*13.

Kuribayashi E., & Tatsuoka F. (1975). Brief review of liquefaction during earthquakes in Japan. *Soils and Foundations*, *15*(4), 81-92.

Liyanapathirana D.S. & Poulos H.G. (2002). A numerical model for dynamic soil liquefaction analysis. *Soil Dynamics and Earthquake Engineering*, *22*(9-12), 1007-1015.

Liyanapathirana D.S., & Poulos H.G. (2003). A pseudo static approach for seismic analysis of piles in liquefying soil. *Journal of Geotechnical and Geo-environmental Engineering*, *131*(12), 1480-1487.

Maheshwari B.K., Truman K. Z., El Naggar M.H., & Gould P. L. (2004). Three-dimensional nonlinear analysis for seismic soil-pile-structure interaction. *Soil Dynamics and Earthquake Engineering, 24*(4), 343–356.

Martin G.R., & Chen C.Y. (2005). Response of piles due to lateral slope movement. *Computers and Structures, 83*(8-9), 588-598.

Masing G. (1926). Eigenspannungen und verfestigung beim messing. *Proc. 2nd International Congress of Applied Mechanics*, Zurich, Swisse.

Matsuzawa H., Ishibashi I., & Kawamura M. (1985). Dynamic soil and water pressures of submerged soils. *Journal of Geotechnical Engineering*, *111*(10), 1161-1176.

Mogami T., & Kubo K. (1953). The behaviour of soil during vibration. *Proceedings of the third international conference on Soil Mechanics and Foundation Engineering, 1*, 152- 155.

Mokhtar A-S.A., Abdel-Motaal M.A., & Wahidy M.M. (2014). Lateral displacement and pile instability due to soil liquefaction using numerical model. *Ain Shams Engineering Journal*, *5*(4), 1019-1032.

Murchison J. M., & O'Neill M. W. (1984). Evaluation of p-y relationships in cohesionless soils. *ASCE, In Analysis and design of pile foundations*, 174-191.

Nanjyo A. et al. (I998). Ground deformation of reclaimed lands and damage of bridge foundations due to Hyogoken-Nambu earthquake, *Proc. of the Symposium on Flow and Permanent Deformation of Ground and Earth Structure during Earthquake*, Japanese Geotechnical Society, 281-286.

O’Rourke T. D., & Hamada M. (1992). Case Studies of Liquefaction and Lifeline Performance During Past Earthquakes: Volume 2, United States Case Studies. *National Center for Earthquake Engineering Research*, State University of New York, Buffalo, NY.

Olson S.M., & Stark T.D. (2002). Liquefied strength ratio from liquefaction flow failure case histories. *Canadian Geotechnical Journal, 39*(3), 629-647.

Özener Tohumcu P. (2007). *Investigation of liquefaction and postliquefaction behavior of layered sands during earthquakes by means of model tests* [Doctoral dissertation]. Yıldız Technical University, Istanbul.

Rahmani A., & Pak A. (2012). Dynamic behaviour of pile foundations under cyclic loading in liquefiable soils. *Computers and Geotechnics, 40,* 114-126.

Ramberg W., & Osgood W. R. (1943). Description of stress-strain curves by three parameters. *NACA-TN-902*.

. Reese L. C., Cox W. R., & Koop F. D. (1974). Analysis of laterally loaded piles in sand. *In Offshore Technology Conference.*

Rollins K.M., Gerber T.M., Lane J.D., & Ashford S.A. (2005). Lateral resistance of a full-scale pile group in liquefied sand. *Journal of the Geotechnical and Geo-environmental Engineering Division*, *131*(1), 115-125.

S. Jefferies M., & Been K. (2016), Soil liquefaction: a critical state approach, 2nd edition.

Schnabel P. B. (1972). SHAKE: A computer program for earthquake response analysis of horizontally layered sites. *EERC Report 72*-12, University of California, Berkeley.

Seed H. B. (1987). Design problems in soil liquefaction. *Journal of Geotechnical Engineering*, *113*(8), 827-845.

Seed H. B., Wong R. T., Idriss, I. M., & Tokimatsu, K. (1984). Moduli and damping factors for dynamic analysis of cohesionless soils, *EERC 84*-14. University of California, Berkeley.

Shanker K., Basudhar P.K., & Patra N.R. (2007). Buckling of piles under liquefied soil conditions. *Geotechnical and Geological Engineering*, *25*(3), 303-313.

Feng T. G., & Zhang L. M. (2013). Experimental study on the effect of vibration frequency on dynamic characteristics of saturated sand soil. *Journal of Water Resources and Architectural Engineering 3,* 11-14.

Takahashi A., & Takemura, J. (2005). Liquefaction-induced large displacement of pile supported wharf. *Soil Dynamics and Earthquake Engineering, 25(11),* 811-825.

Tang L., Ling X., Xu P., Gao X., & Wang D. (2009). Shake table test of soil-pile groups-bridge structure interaction in liquefiable ground. *Earthquake Engineering and Engineering Vibration*, *9*(1), 39-50.

Thavaraj T., & Finn W. L. (2000). A program for dynamic analysis of a single pile using a Winkler model and p-y curves. *Anabuki Chair of Foundation Geodynamics*, Kagawa University, Japan.

Tokimatsu K., & Asaka Y. (1998). Effects of liquefaction-induced ground displacements on pile performance in the 1995 Hyogoken-Nambu earthquake. *Special Issue of Soil and Foundations*, *38*, 163-177.

Tokimatsu K., & Asaka Y. (1998). Effects of liquefaction-induced ground displacements on pile performance in the 1995 Hyogoken-Nambu earthquake. *Soils and Foundations*, *38*, pp.163-177.

Tokimatsu K., Suzuki H., & Sato M. (2005). Effects of inertial and kinematic interaction on seismic behaviour of pile with embedded foundation. *Soil Dynamics and Earthquake Engineering*, *25*(7-10), 753-762.

Unutmaz B., & Çetin K.Ö. (2007). Sismik zemin sıvılaşmasında zemin-yapı-deprem etkileşimi. *Altıncı Ulusal Deprem Mühendisliği Konferansı*, İstanbul.

Uzuoka R., Sento N., Kazama M., Zhang F., Yashima A., & Oka F. (2007). Three-dimensional numerical simulation of earthquake damage to group-piles in a liquefied ground. *Soil Dynamics and Earthquake Engineering*, *27*(5), 395-413.

Wei X., Wang Q., & Wang J. (2008). Damage patterns and failure mechanisms of bridge pile foundation under earthquake. *The 14th World Conference on Earthquake Engineering*, Beijing, China.

Wolf T. K., Rasmussen K. L., Hansen M., Roessen H. R., & Ibsen L. B. (2013). Assessment of p-y curves from numerical methods for a non-slender monopile in cohesionless soil, *024*, Department of Civil Engineering, Aalborg University. DCE Technical Memorandum.

Gu X. Y. (2000). Review and prospect of marine engineering geology. *Journal of Engineering Geology*, *8*(1), 40-45.

Guo Y. & He L. (2009). Effect of vibration frequency on liquefaction strength of saturated sand soil. *Journal of disaster prevention and mitigation engine, 29*(6), 618-623

Youd T. L. & Hoose S. N. (1978). Historic ground failures in northern California triggered by earthquakes. *US Government Printing Office*, *993.*